12-2015

Photochemistry of a Series of Weakly Coupled Dinuclear Ruthenium(II) Complexes

Latisha Michelle Puckett
University of Arkansas, Fayetteville

Photochemistry of a Series of Weakly Coupled Dinuclear Ruthenium(II) Complexes

A dissertation submitted in partial fulfillment
of the requirements for the degree of
Doctor of Philosophy in Chemistry

By

Latisha Puckett
University of Arkansas
Bachelor of Science in Chemistry, 2010

December 2015
University of Arkansas

This dissertation is approved for recommendation to the Graduate Council.

_____
Dr. Bill Durham
Dissertation Director

_____
Dr. Jingyi Chen
Committee Member

_____
Dr. Ryan Tian
Committee Member

_____
Dr. Colin Heyes
Committee Member

Abstract

An improved synthetic method was developed for symmetric ruthenium(II) polypyridine complexes with the form $L_2Ru(diphen)RuL_2$. The scope of the reaction was investigated in regards to the ligands, bridging ligands, and starting materials. Several ligands were successful in the synthesis, including 2,2'-bipyridine (bpy), 4,4'-dimethyl-2,2'-dipyridyl (dmb), 1,10-phenanthroline (phen), 4,7-diphenyl-1,10-phenanthroline (dpphen), and 3,4,7,8-tetramethyl-1,10-phenanthroline (tmphen). Ligands that did not react to form symmetric dimeric complexes were 2,2'-bipyrazine, bpz, and 2,2'-bipyrimidine, bpm.

Dpp, 2,3-bis(2-pyridyl)-pyrazine, effectively replaced diphen as the bridging ligand to produce $(phen)_2Ru(dpp)Ru(phen)_2^{4+}$. However, replacing the $[Ru(CO)_2Cl_2]_n$ with $Ru(DMSO)_4Cl_2$ did not prove successful. The newly developed synthesis was also applied to the synthesis of monomeric complexes with the form $Ru(phen)L_2$ for comparison. The spectroscopic and electrochemical data collected for the dimeric complexes was similar to the data for the monomeric complexes indicating that the dimers are weakly coupled.

The photochemistry of the complexes was then studied to confirm that the dimers were weakly coupled. UV-vis tracking of the reaction of $(phen)_2Ru(diphen)Ru(phen)_2^{4+}$ implied a photosubstitution reaction took place in which a phen ligand was replaced by bromines. Several failed attempts were made to replace the bromines with a ligand that would allow the complex to be analyzed via ESI-MS. The photosubstitution products were never identified.

The photoredox reactions for the complexes were investigated as well. The effect of the oxidative quencher Fe^{3+} on the excited lifetimes of the complexes was analyzed. The k_q values found for $Ru(bpy)_3^{2+}$, $Ru(phen)(bpy)_2^{2+}$, and $(bpy)_2Ru(diphen)Ru(bpy)_2^{4+}$ were all comparable. This supports the classification of the dimeric complexes used in this study as weakly coupled.

The back reaction that follows the quenching reaction and the yield of the oxidized ruthenium complexes were studied. The determined k_{back} values for both quenchers, Fe^{3+} and Cu^{2+}, were in the expected range and similar among both the monomers and dimers. This suggests that the dimeric complexes are weakly coupled.

Acknowledgments

I would like to thank my committee for their guidance during my career as a graduate student. I would especially like to thank Dr. Bill Durham for his guidance, advice, and most importantly, even giving me the chance to work in his research lab.

Dedication

This dissertation is dedicated to Mark and Kadence. I would also like to dedicate it to Meme and Pa.

Table of Contents

Abbreviations

bpy — 2,2’-bipyridine

bpm — 2,2’-bipyrimidine

bpz — 2,2’-bipyrazine

$CDCl_3$ — chloroform-d

CD_3CN — acetonitrile-d_3

Cl-phen — 5-chloro-1,10-phenanthroline

cm — centimeter/s

CV — cyclic voltammetry

diphen — 5,5’-Bi-1,10-phenanthroline

dmb — 4,4’-dimethyl-2,2’-dipyridine

DMF — *N*,*N*-dimethylformamide

dpp — 2,3-Bis(2-pyridyl)-pyrazine

dpphen — 4,7-diphenyl-1,10-phenanthroline

en — ethylenediamine

ESI-MS — electrospray ionization mass spectrometry

g — gram/s

HCl — hydrochloric acid

HCOOH — formic acid

H_2O — water

HOMO — highest occupied molecular orbital

hr — hour/s

IR — infrared spectroscopy

IVCT — intervalence charge transfer

KCN — potassium cyanide

LMCT — ligand-to-metal charge transfer

LUMO — lowest unoccupied molecular orbital

M — molarity

Me_3NO — trimethylamine *N*-oxide

min — minute/s

mL — milliter/s

MLCT — metal-to-ligand charge transfer

MMCT — metal-to-metal charge transfer

mmol — millimol/s

mol — moles

m/z — mass to charge ratio

NH_4OH — ammonium hydroxide

NH_4PF_6 — ammonium hexafluorophosphate

Ni — nickel

$NiCl_2 \cdot 6H_2O$ — nickelous chloride hexahydrate

NMR — nuclear magnetic resonance spectroscopy

phen — 1,10-phenanthroline

PPh_3 — triphenylphosphine

RBF — round bottom flask

RSD - relative standard deviation

RT — room temperature

$RuCl_3$ — ruthenium(III) chloride

SCE — saturated calomel electrode

TBAI — tetrabutylammonium iodide

TGS — triglycine sulfate

tmphen — 3,4,7,8-tetramethyl-1,10-phenanthroline

UV-vis — ultraviolet-visible

v:v — volume to volume

1.1 Introduction

The conversion of solar energy into electricity and the reactions involved in biological respiration may seem to be completely unrelated, but to many inorganic chemists they share many common features. One such feature is the ruthenium(II) complex, $Ru(bpy)_3^{2+}$. This complex has played a central role in these areas of research as well as many others for over four decades (Amouyal, 1995), (Creutz and Sutin, 1975) (Grätzel, 2003), (Millett and Durham, 2002). The fascination with this complex stems from a unique combination of properties. The complex is remarkably stable. For example, it shows no reaction after refluxing in concentrated hydrobromic acid for several hours. The corresponding Ru(I) and Ru(III) complexes retain the bipyridyl coordination sphere, which is rare among transition metal complexes. The complex is brightly colored and has a long-lived excited state capable of undergoing redox reactions with other reagents in solution. The complex is also amenable to a plethora of structural modifications (Krause and Krause, 1980), (Horváth and Stevenson, 1993), (De Cola, et al. 1990).

The long lived excited state is the feature that is the key to its utility in a variety of applications. Specifically, absorption of light results in the formation of the excited state which exists long enough to react with a potential oxidizing agent to produce $Ru(bpy)_3^{3+}$ and the reduced oxidant. At this point, the energy from the light is stored as chemical energy in these redox products. The light can be from the sun, and the redox properties can be harnessed to form a battery. There are many technical issues to resolve before the system can actually be used on a commercial scale, but the basic reactions are well known. The early stages of photosynthesis are very analogous although ruthenium is not part of the chemistry.

Similar chemistry can be used to study the basic reactions involved in respiration. In this case, a short laser pulse is used to create the excited state in a few nanoseconds, and any reaction

slower than 50 nanoseconds can be readily monitored by measuring absorbance changes that follow the laser pulse. The technique is called laser flash photolysis. Fortunately, many of the proteins in the respiratory chain show absorption changes that are diagnostic for each reaction. These reactions are oxidation/reduction reactions, and ruthenium complexes have been developed that have allowed detailed analysis of the reactions of cytochrome c (Bechtold, et al., 1986), cytochrome c oxidase (Zaslavsky and Gennis, 2000), (Durham and Millett 2012), and the bc1 complex (Havens, et al., 2011), which are three of the four major proteins in the respiratory chain.

The development of ruthenium complexes for these investigation lead to a series of complexes containing two ruthenium centers. Among the restrictions that were followed during the development was a need to maintain a long excited lifetime. Two of the complexes that continue to be heavily used are $(bpy)_2Ru(diphen)Ru(bpy)_2^{4+}$, where bpy = 2,2'-bipyridine and diphen = 5,5'-bi-1,10-phenanthroline, and $(bpy)_2Ru(qpy)Ru(bpy)_2^{4+}$, where qpy = 2,2':5',5":2",2"'- quaterpyridine (Ahmed, 2010), (Barthram, et al, 1998), (Halpin, et al, 2009). These complexes are shown in Figure 1.1.1.

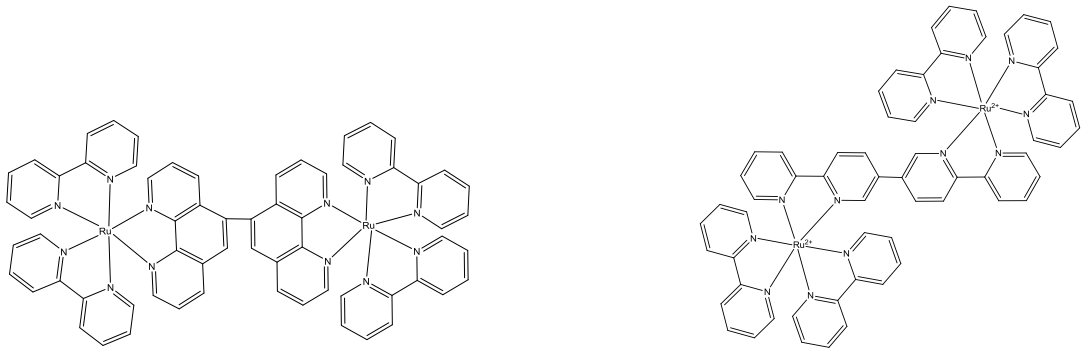

Figure 1.1.1. Structure for $(bpy)_2Ru(diphen)Ru(bpy)_2^{4+}$ (left) and $(bpy)_2Ru(qpy)Ru(bpy)_2^{4+}$ (right).

These complexes have excited state lifetimes that are equal to or greater than the corresponding mononuclear complexes. This is very surprising given the fact that the two ruthenium containing subunits are linked together through a single covalent bond. Such a linkage should have provided a pathway for rapid decay of the excited state via electron or energy transfer from one ruthenium center to the other. Subsequent studies suggest that the two ruthenium centers are very weakly coupled, and any type of deactivation pathway would be too slow to alter the lifetime (Njabon, 2013).

The suggestions are convincing, but a more detailed study of the consequences is required. This is the subject of this thesis. Specifically, the following will describe a method of synthesizing homonuclear dimeric complexes which is efficient and does not suffer from the production of unwanted monomeric complexes that are spectroscopically similar to the dimeric complexes. This is particularly important because many of the potential mononuclear side products have properties that are nearly identical to the dimeric complexes and would make any detailed spectroscopic study impossible.

This thesis will also describe an investigation of the excited-state redox properties of the complexes. This was accomplished primarily through a series of quenching studies using Fe^{3+} and Cu^{2+}. One specific question was of particular interest. Is it possible for the dimeric complexes to undergo a pseudo-two photon reaction resulting in both halves of the dimer in excited states? Furthermore, is it possible to oxidize or reduce both of the ruthenium centers photochemically?

1.2 Ground and Excited State Chemistry of Ruthenium

$Ru(bpy)_3^{2+}$ has been intensely studied and is commonly used as the starting point when studying the excited states of other ruthenium polypyridine complexes. The complex is low spin

with a d^6 electron configuration, and has D_3 symmetry in the ground state. The bipyridines have both σ-donor orbitals on the nitrogen atoms and delocalized π-donor orbitals and π*-acceptor orbitals on the aromatic rings (Horváth and Stevenson, 1993). A simplified molecular orbital diagram for $Ru(bpy)_3^{2+}$ is shown in Figure 1.2.1.

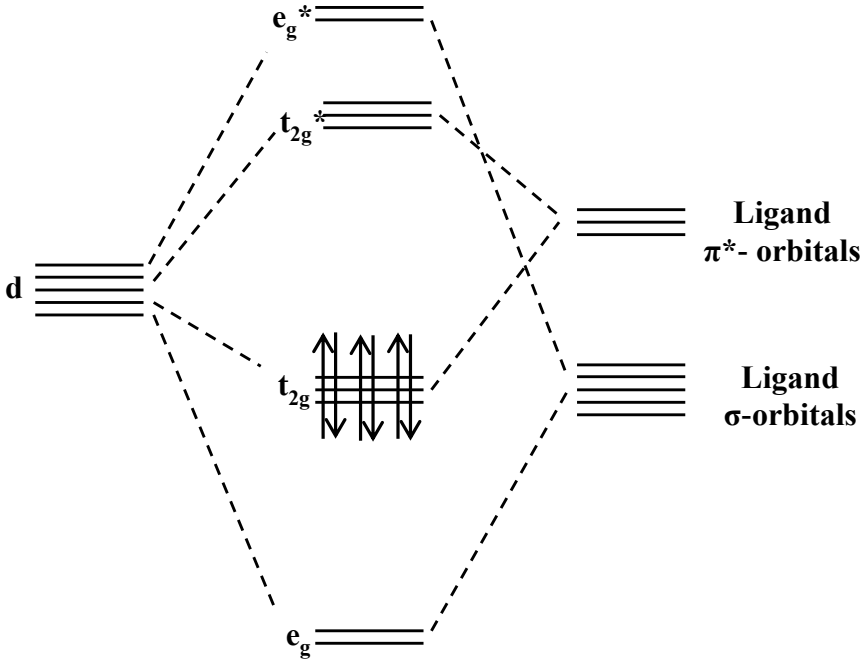

Figure 1.2.1. Simplified molecular orbital diagram of $Ru(bpy)_3^{2+}$.

As can be seen from Figure 1.2.1, the HOMO in $Ru(bpy)_3^{2+}$ is a set of three degenerate orbitals, labeled t_{2g}, formed by the combination of three metal centered d-orbitals and π* orbitals on the bipyridine ligands. The LUMO, labeled t_{2g}*, is formally the antibonding equivalent and is formed through the same combination. The molecular orbitals labeled e_g* are very close in energy to the t_{2g}* and are formed through a sigma interaction between the remaining d-orbitals and nitrogen lone pairs.

Solutions of $Ru(bpy)_3^{2+}$ exhibit a moderately strong absorbance band at 452 nm (ε = 14500 M^{-1} cm^{-1}) and another strong band at 290 nm. An absorbance spectrum for $Ru(bpy)_3^{2+}$ is shown in Figure 1.2.2. The band at 290 nm is commonly observed with bipyridine complexes,

and all evidence indicates that it is a ligand-centered transition. The band at 452 nm is responsible for the strong orange-red color of the solutions. It is described as a metal to ligand charge transfer band (MLCT) and corresponds to a transition from the t_{2g} orbital to the t_{2g}* orbital. The band has some structure indicating that it is due to more than one electronic transition consistent with splitting of the electronic states associated with this electronic transition. The MLCT description derives from the fact that the HOMO is primarily metal in character and the LUMO is primarily ligand based. Electronic transitions to the e_g* orbitals are expected to have energies slightly higher than the MLCT transitions. However, these transitions, sometimes referred to as d-d transitions, are formally forbidden and are expected to be very weak (Paris and Brandt, 1959), (Barigelletti, et al, 1987), (Treadway, et al., 1996), (Felix, et al., 1980).

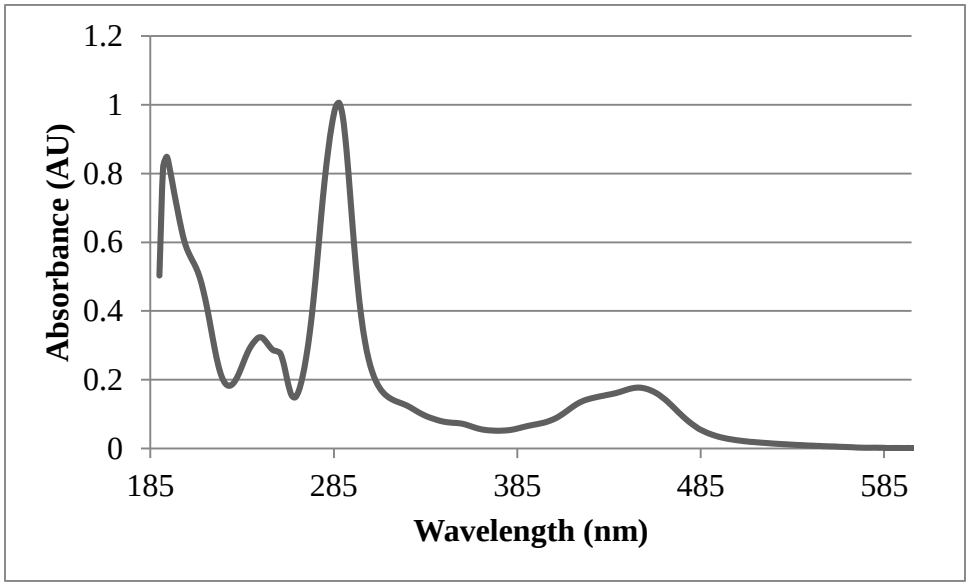

Figure 1.2.2. Absorbance spectrum for $Ru(bpy)_3^{2+}$.

Figure 1.2.3 is a commonly used Jablonski diagram which provides a graphical representation of the states and associated transitions for $Ru(bpy)_3^{2+}$.

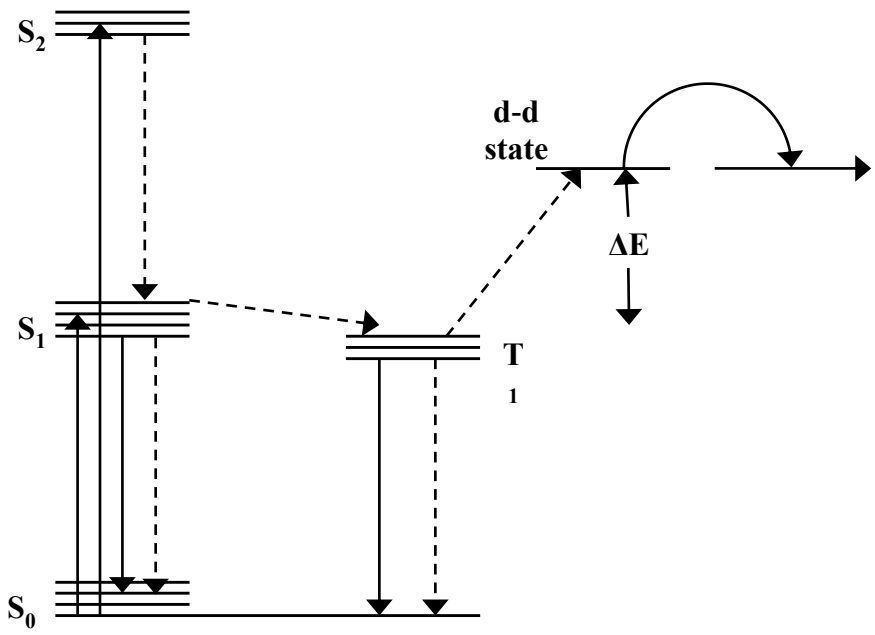

Figure 1.2.3. Jablonski energy diagram for $Ru(bpy)_3^{2+}$.

Since $Ru(bpy)_3^{2+}$ is low spin and diamagnetic it has no unpaired electrons in the ground state and is therefore labeled as a singlet state S_0. Upon absorption of a photon, the complex is excited to any of the available the singlet excited states, S_1, S_2 …indicated by the solid lines with arrows up. For the purpose of this discussion, S_1 can be viewed as the collection of states associated with the HOMO to LUMO transitions. These states relax rapidly, and direct spectroscopic investigations of these states are very sparse. Direct excitation to the triplet state, T_1, is spin forbidden; however, experimentally it has been shown that the intersystem crossing to the triplet state (dashed line between S_1 and T_1) occurs with nearly 100% efficiency. $Ru(bpy)_3^{2+}$ exhibits an emission centered at approximately 600 nm in aqueous solution at room temperature. This emission corresponds to the T_1 to S_0 transition, and the rate of decay corresponds to an excited state lifetime of the T_1 state of approximately 600 nsec at room temperature in aqueous solution.

Investigations of the rate of decay of the emission as a function of temperature reveal the following relation:

$$k_{obs} = k_{nr} + k_r + Ae^{(\Delta E/RT)}$$

The value for the radiative and non-radiative rate constants, $k_{nr} + k_r = 6.0 \times 10^5$ sec^{-1}. In order to fit the temperature dependence an additional state was required. This state appears to be in thermal equilibrium with T_1 and very rapidly decays non-radiatively with $A = 4.0 \times 10^{14}$ sec^{-1}, and ΔE = 50 kJ/mol (Allsopp et al., 1978). This state has been interpreted as a d-d state based on the temperature dependence of the photosubstitution reactions of $Ru(bpy)_3^{2+}$ and is responsible for the relatively low quantum yield for emission (Van Houten and Watts, 1975).

1.3 Photoredox Reactions of $Ru(bpy)_3^{2+}$

The relatively long excited state lifetime of the T_1 state allows ample opportunity for the complex to under reactions with other reagents in solution. The vast majority of the studies to date have focused on the photoredox reactions that $Ru(bpy)_3^{2+}$can undergo. This type of reaction can be explained by taking into account the fact that ruthenium is a d^6 metal and has a full t_{2g} orbital. The T_1 state is formed by promoting an electron from the t_{2g} orbital to a t_{2g}* orbital. This results in a hole in the t_{2g} orbital (the metal) and an electron in the t_{2g}* orbital (the ligand) (Roundhill, 1994) and radically changes the redox properties of the complex. This is illustrated in Figure 1.2.1, which is located in the previous section. The standard reduction potential for $Ru(bpy)_3^{2+/3+}$ is +1.29 V. The potential for $Ru(bpy)_3^{2+/3+}$* is -0.81 V (Creutz and Sutin, 1976).

In the ground state $Ru(bpy)_3^{2+}$ shows no tendency toward oxidation or reduction. Once the complex is excited, however, it is possible for $Ru(bpy)_3^{2+}$* to be reduced by accepting an electron into the t_{2g} orbital. It is also possible for the $Ru(bpy)_3^{2+}$* complex to be oxidized by

donating the electron residing in the π* orbital. This is described in Equations 1 and 2, where Q is the species interacting with the $Ru(bpy)_3^{2+}$* complex, commonly called a quencher.

$$Ru(bpy)_3^{2+}* + Q \rightarrow Ru(bpy)_3^{3+} + Q^- \quad (1)$$

$$Ru(bpy)_3^{2+}* + Q \rightarrow Ru(bpy)_3^{+} + Q^+ \quad (2)$$

The excited state complex is oxidized in Equation 1 to $Ru(bpy)_3^{3+}$, i.e., oxidatively quenched. Equation 2 shows the excited state complex being reduced to $Ru(bpy)_3^{+}$, i.e., reductively quenched.

1.4 Charge Transfer States Based Applications

Many applications based on the charge transfer states of inorganic complexes have been developed over the years. One such application is solar energy conversion (O'Donnell, et al., 2013), (Grätzel, 2003). Michael Grätzel is one of the leading researchers in dye-sensitized solar cells. The major components of a dye-sensitized solar cell are the mesoporous oxide wide band semiconductor and the charge transfer sensitizer. TiO_2 is a commonly used semiconductor in the cells. The TiO_2 is then covered with a layer of the dye, which contains the charge transfer sensitizer. The sensitizer absorbs sunlight, undergoes photoexcitation, and the charge is then transferred into the conduction band of the TiO_2. The charge is carried through the conduction band to the charge collector. The dye is regenerated through electron donation from the analyte (Grätzel, 2003).

The determination of the best charge transfer sensitizer to use has been a major area of study. Organic molecules often do not have broad absorbance bands, so inorganic complexes became promising candidates for charge transfer sensitizers. In order to be an optimal charge

transfer sensitizer, the complex must meet several criteria. These criteria include a broad range of absorbance, the ability to bond to carboxylate or phosphate groups in order to be anchored to the semiconductor surface, transferring the electron to the semiconductor with a quantum yield of unity, have a redox potential large enough to be regenerated by the solvent, and have an excited state energy level that matches the lower level of the conduction band (Grätzel, 2003).

While many different inorganic complexes have been studied for use as a charge transfer sensitizer (Wenger, 2009), a ruthenium based complex has become the standard. The complex *cis*-$RuL_2(NCS)_2$, where L= 2,2'-bipyridyl-4,4'-dicarboxylic acid, meets the above outlined criteria for an optimized charge transfer sensitizer and is shown in Figure 1.4.1 (Nazeeruddin et al., 1993), (Fan, et al., 2009), (Schwarz, et al., 2000).

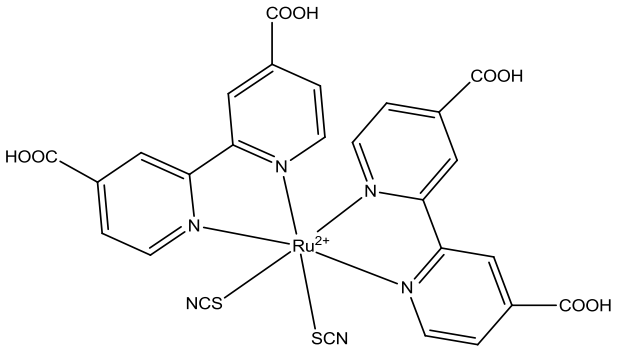

Figure 1.4.1. Structure of $RuL_2(NCS)_2$, where L= 2,2'-bipyridyl-4,4'-dicarboxylic acid.

The maximum absorbance of the complex is at 380 nm and 518 nm. This absorption is attributed to MLCT during which an electron is photoexcited from the metal to a π^* orbital of the carboxylated bipyridyl ligand. The carboxylate acts as the anchor to the semiconductor allowing the electron to then be transferred into the conduction band of the semiconductor (Grätzel, 2003). After years of intense research in the field, the ruthenium complex found by Nazeeruddin et al. is still considered the standard for charge transfer sensitizers.

Another application that takes advantage of charge transfer in inorganic complexes is their use as photoredox initiators for the study of electron transfer in proteins. Ruthenium(II) polypyridine complexes are popular choices for photoredox initiators. The unique properties mentioned previously apply in this application as well (Durham and Millett, 2012). In addition, the redox properties of the ruthenium complexes can be changed by simply changing the ligands. Cytochrome *c* oxidase (Zaslavsky et al., 1998), cytochrome *bc*1 (Sadoski et al., 2000), cytochrome *c* (Meade et al., 1989), and cytochrome b_5 (Scott, et al., 1993) are a few of the proteins chosen for electron transfer studies. In a specific study of electron transfer in cytochrome *c*, a derivative of $Ru(bpy)_3^{2+}$ is covalently bound to the protein of study. The bonding occurs between a cysteine attached to the cytochrome *c* and α-bromodimethylbipyridine ligand on the ruthenium complex. This is illustrated in Figure 1.4.2 (Durham and Millett, 2012).

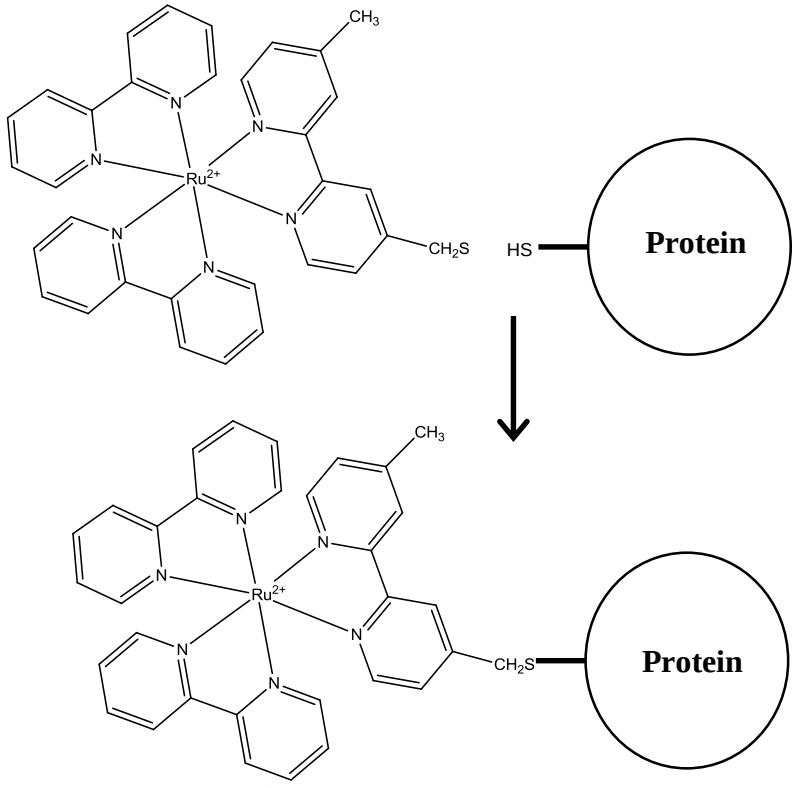

Figure 1.4.2. A derivative of $Ru(bpy)_3^{2+}$ covalently bonded to a cysteine on the protein of study.

A short laser pulse excites the ruthenium complex, and the Ru^{2+}* MLCT excited state is formed. This excited state can then transfer an electron to become oxidized, which in turn reduces the heme iron. The ruthenium photoredox initiator is regenerated by a solution phase donor that reduces Ru^{3+} back to Ru^{2+}. This process is shown in scheme 1.4.1. Later studies using dimeric ruthenium(II) polypyridine complexes with a 4+ charge showed improved yields while using lower concentrations of the complex (Durham and Millett, 2012).

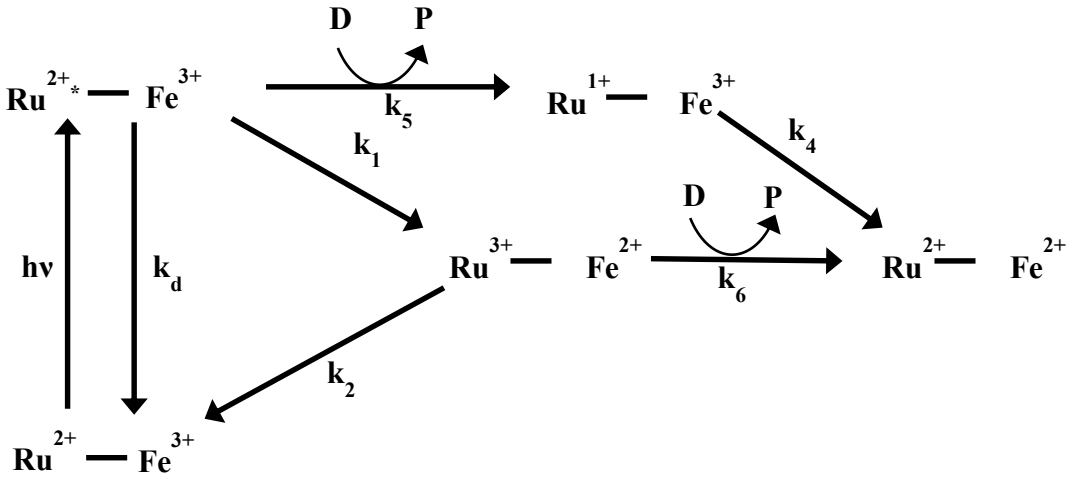

Scheme 1.4.1. Pathways of photochemical reduction reaction of heme in cytochrome *c*.

A third application that relies on the charge transfer state of inorganic complexes is their use as catalysts in several different types of organic transformation reactions. Recently visible light photoredox catalysis has become a major area of study in organic chemistry (Prier et al., 2013). Ruthenium complexes are well suited for use as photoredox catalysts. Moreover, they absorb energy in the visible light region, so electron transfer can be initiated with visible light. Upon excitation, the inorganic complexes are able to transfer an electron to the organic substrate in a single-electron process (Prier et al., 2013). This differs from the traditional oxidants or reductants, which provide two electrons by way of an oxygen atom transfer process.

Monomeric ruthenium(II) polypyridine complexes are often used as photoredox catalysts. The redox potentials of the complexes can be tuned by attaching various ligands to the ruthenium center. Numerous types of reactions can be carried out using the ruthenium complexes as photoredox catalysts. One such example is the intermolecular [3+2] cycloaddition of cyclopropylamines with olefins (Maity et al., 2012).

$Ru(bpz)_3^{2+}$, seen in Figure 1.4.3, was chosen as the photocatalyst in this organic transformation reaction. A feasible catalytic cycle was proposed by the group, which starts with the excitation of the ruthenium complex with visible light to become Ru^{2+}* through MLCT. The photoexcited state of ruthenium then oxidizes the cyclopropylamine to form a nitrogen radical cation and Ru^{1+}. The ring associated with the nitrogen radical cation opens and creates a β-carbon radical iminium ion. The ion then adds to the olefin to establish a stable radical and create a cyclopentane ring associated with the nitrogen radical cation. Ru^{1+} reduces the compound, and the cycle is complete (Maity et al., 2012).

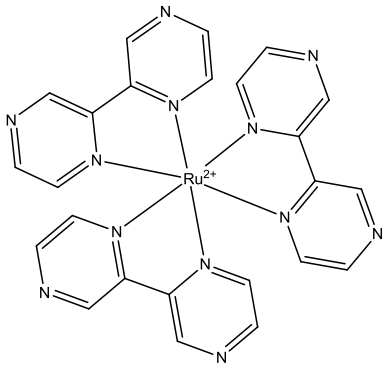

Figure 1.4.3. Structure of $Ru(bpz)_3^{2+}$.

1.5 Photosubstitution Reactions of $Ru(bpy)_3^{2+}$

In addition to the photoredox reactions described above $Ru(bpy)_3^{2+}$ undergoes a photosubstitution reaction in which bipyridine is replaced by water. In acidic aqueous solution the quantum yield for the process is less than 0.001. Although the quantum yield is small, this

reaction will degrade the complex in time when used in some of the applications described above (Van Houten and Watts, 1978).

In solvents with very low dielectric constants, such as dichloromethane, loss of bipyridine is followed by incorporation of the anions, such as chloride or bromide, that are present in the solution as counterions. In these solvents, the complex is present as an ion-pair formed with the counterions. Energetics of the reaction favors loss of the uncharged bipyridine over charge separation, and the quantum yield can be 0.02 or higher (Durham, et al., 1980).

Photosubstitution in inorganic complexes generally results from the population of e_g* orbitals, which are formally antibonding with respect to the ligands. Direct population of this orbital from the ground state is Laporte forbidden and masked by the charge transfer transition. In addition, it was noted above that the quantum yield for population of the triplet state is 1 following absorption into any band. Thus population of states corresponding to population of the e_g* orbital must occur through the T_1 excited state. Currently, population of the e_g* orbital is thought to occur by way of a thermal equilibrium with the T_1 state as indicated in the Jablonski diagram shown in Figure 1.2.3 (Durham, et al., 1982). Some investigators have pointed out that the rate of decay of the thermally populated state is too fast to be consistent with an equilibrium process.

1.6 Electronic Coupling in Dimeric Complexes

The presence of more than one metal center in the same complex introduces at least one important new feature, namely the electronic coupling between metal centers. The electronic coupling is a measure of how much the presence of one metal center impacts the other metal center. For example, in a dimer a favorable interaction could result in a lowering of the redox potentials of the two metal centers or a lowering of the absorption energies. The lowering in

energy is a result of the formation of a molecular orbital that combines a small amount of the metal center orbitals with or without bridging ligand orbitals. There is likewise formation of an unfavorable combination, but this is normally not populated. These interactions can be very large or very, very small (D'Alessandro, et al, 2001), (Nelson, 2000), (D'alessandro and Keene, 2006), (Kreitner, et al, 2014), (Wang, et al, 1998), (De Cola, et al., 1990).

In order to classify the degree of electronic coupling between the metal centers, three classes have been designated. A complex is designated as Class I when the electronic coupling is very weak and the two metal centers behave completely independently. Class II complexes belong to an intermediate class with moderate to weak coupling. These complexes show an intervalence charge transfer band (IVCT) in the visible or IR region of the spectrum. This band corresponds to a transfer of an electron from one metal center to the other. The energy and band shape provides direct information about the magnitude of the electronic coupling. In Class III complexes, the metal centers are strongly coupled, and the metal centers cannot be treated separately (Emeléus and Sharpe, 1968). Oxidation in these cases, for example, can only be viewed as removing an electron from the pair of metals and not one or the other. Iron-sulfur proteins are Class III and contain redox centers composed of four iron atoms and four sulfur atoms with the valence electrons completely delocalized over the entire set of eight atoms. Class III complexes can also show an IVCT band.

The Creutz- Taube ion, $(NH_3)_5Ru(pyrazine)Ru(NH_3)_5^{5+}$, first reported in the 1970s (Creutz and Taube, 1973) is a Class III complex. The complex exhibits a narrow, intense IVCT band in the near IR region (Petrov et al., 1994) and has been extensively studied because of the insights it can provide about the interaction of the metal centers.

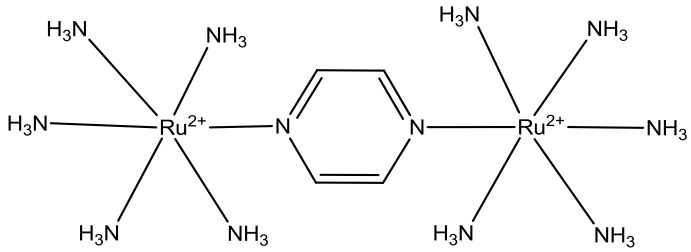

Figure 1.6.1. The structure of the Creutz-Taube ion.

These classes can also be characterized numerically based on a parameter, α, which is called the mixing coefficient. It is related to the magnitude of the interaction of the orbitals containing the valence electrons. Class I complexes are characterized by $\alpha \sim 0$, in Class II complexes $0 < \alpha < 0.707$ and in Class III $\alpha > 0.707$ (Miessler and Tarr, 2004).

1.7 Prior Investigations of $(bpy)_2Ru(diphen)Ru(bpy)_2^{4+}$

Prior to this work the synthesis of $(bpy)_2Ru(diphen)Ru(bpy)_2^{4+}$ $(dmb)_2Ru(diphen)Ru(dmb)_2^{4+}$, where dmb = 4,4'-dimethyl-2,2'-bipyridine, and $(dmb)_2Ru(diphen)Ru(bpy)_2^{4+}$ was investigated (Njabon, 2013). The structures of $(dmb)_2Ru(diphen)Ru(dmb)_2^{4+}$ and $(dmb)_2Ru(diphen)Ru(bpy)_2^{4+}$ are seen in Figures 1.7.1 and 1.7.2, respectively. $(bpy)_2Ru(diphen)Ru(bpy)_2^{4+}$ can be seen in Figure 1.1.1.

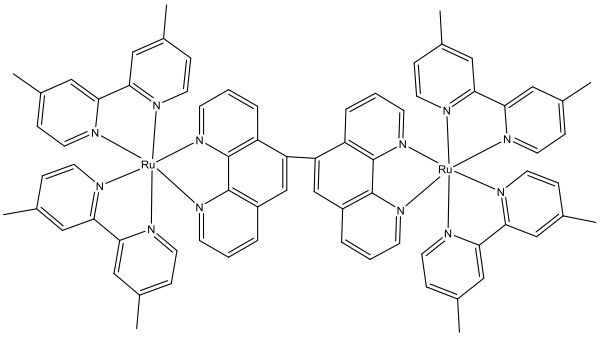

Figure 1.7.1. Structure for $(dmb)_2Ru(diphen)Ru(dmb)_2^{4+}$.

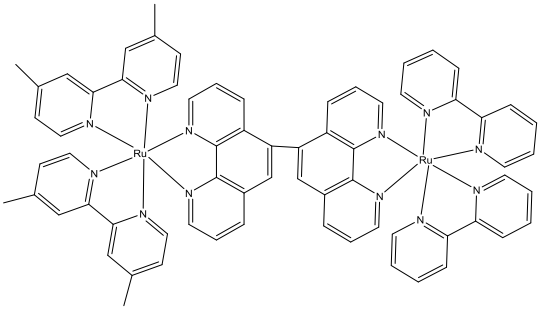

Figure 1.7.2. Structure for $(dmb)_2Ru(diphen)Ru(bpy)_2^{4+}$.

The electrochemistry of $(bpy)_2Ru(diphen)Ru(bpy)_2^{4+}$ was thoroughly investigated using cyclic voltammetry. For example, the $E_{1/2}$ for the oxidation of $(bpy)_2Ru(diphen)Ru(bpy)_2^{4+}$ is 1.30 V versus SCE in acetonitrile containing 0.1 M tetrabutylammonium hexafluorophosphate. The $E_{1/2}$ for the oxidation of $(dmb)_2Ru(diphen)Ru(dmb)_2^{4+}$ is 1.190 V versus SCE. In both cases, the complexes are well behaved and show reversible electrochemistry with a peak to peak separation of approximately 60 mV. The difference in potentials of these two complexes is expected based on previous studies and is attributed to the electron donating properties of the methyl substituents.

The cyclic voltammogram for the mixed dimer $(dmb)_2Ru(diphen)Ru(bpy)_2^{4+}$ is shown in Figure 1.7.3 (Njabon, 2013). It clearly indicates that the metal centers are present in a 1:1 ratio, and the metal centers have the same oxidation potentials as the corresponding homonuclear dimers after correction for the reference electrode potential. The result supports the view that the complexes are essentially independent of each other with little or no electronic coupling, i.e., Class I.

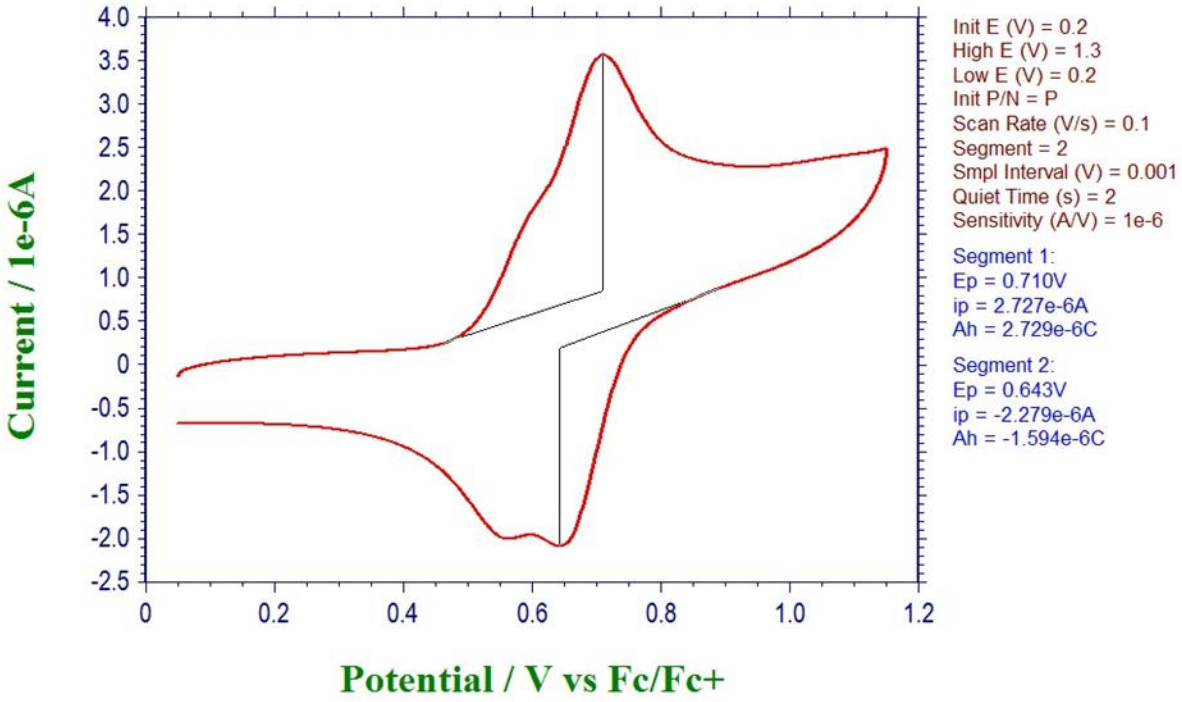

Figure 1.7.3. Cyclic voltammogram for $(dmb)_2Ru(diphen)Ru(bpy)_2^{4+}$ (Njabon, 2013).

Spectroscopic studies were also performed using the three complexes. Emission measurements were taken at either 77 K in a frozen glass or at room temperature. The solvent used was a 4:1 (v:v) ratio of EtOH/MeOH. The emission spectra collected at 77 K for the dimeric complexes are all similar in shape to the analogous monomeric complexes. Figure 1.7.4 shows the emission spectra for the complexes at 77 K (Njabon, 2013).

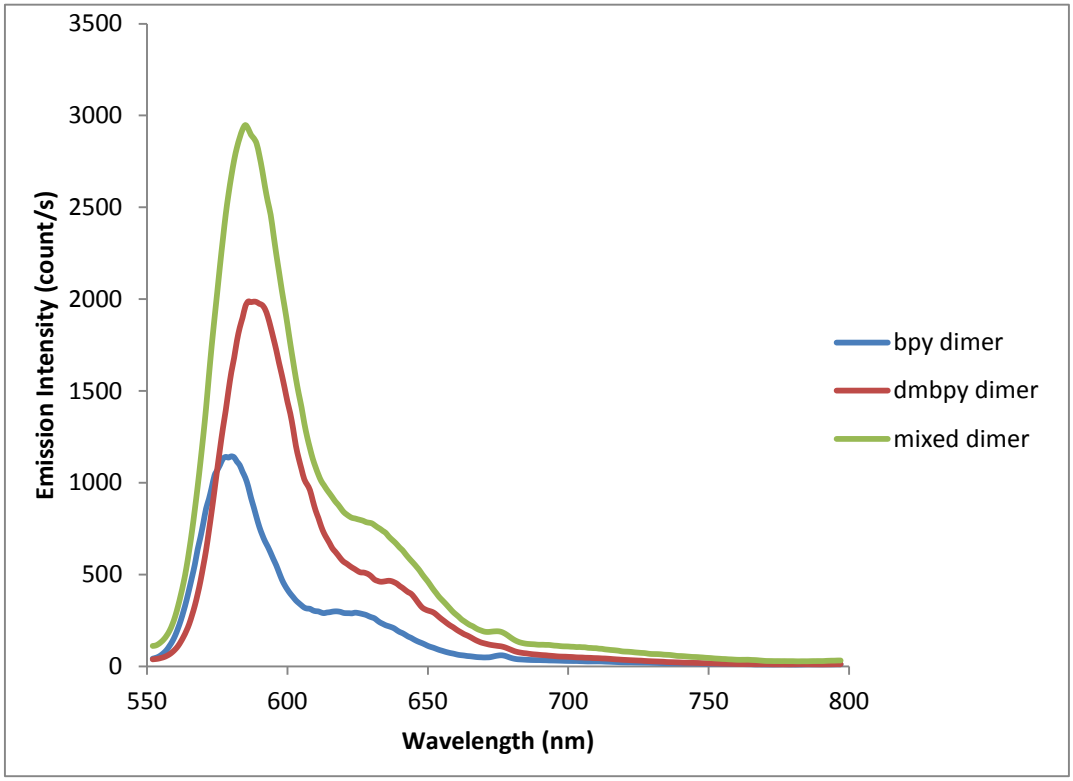

Figure 1.7.4. Emission spectra of $(bpy)_2Ru(diphen)Ru(bpy)_2^{4+}$, $(dmb)_2Ru(diphen)Ru(dmb)_2^{4+}$, and $(dmb)_2Ru(diphen)Ru(bpy)_2^{4+}$ at 77 K (Njabon, 2013).

When the spectra of $(bpy)_2Ru(diphen)Ru(bpy)_2^{4+}$ and $(dmb)_2Ru(diphen)Ru(dmb)_2^{4+}$ were added together, the resulting spectra was virtually superimposable with the experimentally obtained $(dmb)_2Ru(diphen)Ru(bpy)_2^{4+}$ spectrum. This leads to the conclusion that the ruthenium metal centers emit independently at the experimental temperature (Njabon, 2013). This finding supports the classification of $(bpy)_2Ru(diphen)Ru(bpy)_2^{4+}$ as a class I complex.

Emission spectra were also collected at room temperature. It was observed that $(bpy)_2Ru(diphen)Ru(bpy)_2^{4+}$ emitted at 606 nm and $(dmb)_2Ru(diphen)Ru(dmb)_2^{4+}$ emitted at 629 nm. The asymmetric dimer $(dmb)_2Ru(diphen)Ru(bpy)_2^{4+}$ emitted between these values at 618 nm which is consistent with emission from both ruthenium centers acting independently.

The temperature dependence of the excited state lifetimes provides more detailed information about the excited state energy manifold. A comparison of data obtained with

$(bpy)_2Ru(diphen)Ru(bpy)_2^{4+}$ and data available in the literature for $Ru(bpy)_2(phen)^{2+}$ is shown in Figure 1.7.5. The best fit parameters are $k_{nr} + k_r = 6.0 \times 10^5$ sec^{-1}, $A = 4.0 \times 10^{14}$ sec^{-1}, and ΔE = 50 kJ/mol (Allsopp et al., 1978).

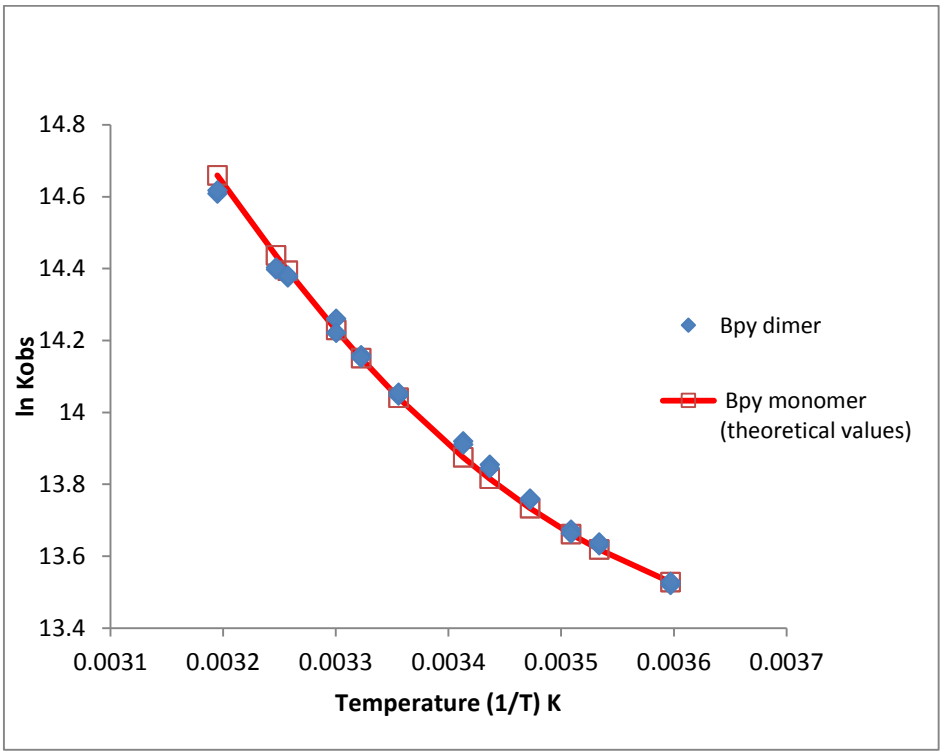

Figure 1.7.5. Plot showing the temperature dependence of the excited state decay for $(bpy)_2Ru(diphen)Ru(bpy)_2^{4+}$ compared to theoretical $Ru(bpy)_3^{2+}$ values from the literature (Njabon, 2013), (Allsopp et al. 1978).

As can be seen from Figure 1.7.5, the temperature dependence of the lifetime values for the dimeric complex corresponds to the values for the monomeric complex. This, once again, indicates that the ruthenium centers are acting as independent units and strongly supports the classification of $(bpy)_2Ru(diphen)Ru(bpy)_2^{4+}$ as a class I complex.

After investigation of the spectroscopic and excited state properties of $(bpy)_2Ru(diphen)Ru(bpy)_2^{4+}$, it was concluded that the complex was class I and that there was no electronic coupling between the ruthenium metal centers. This was contrary to what was first believed based on what was known about the structure of $(bpy)_2Ru(diphen)Ru(bpy)_2^{4+}$,

specifically the fact that the two phenanthroline subunits of diphen are coupled by a single covalent bond which should provide for a strong complex – complex interaction. These findings suggested that the diphen bridging ligand was having a much larger impact on the coupling than expected.

Previous studies have indicated that the angular orientation of the bridging ligand can affect the electronic coupling (Benniston, et al., 2004), (Benniston, et al., 2006). Calculations reveal that free rotation around the 5.5' bond is severely restricted as shown in Figure 1.7.6.

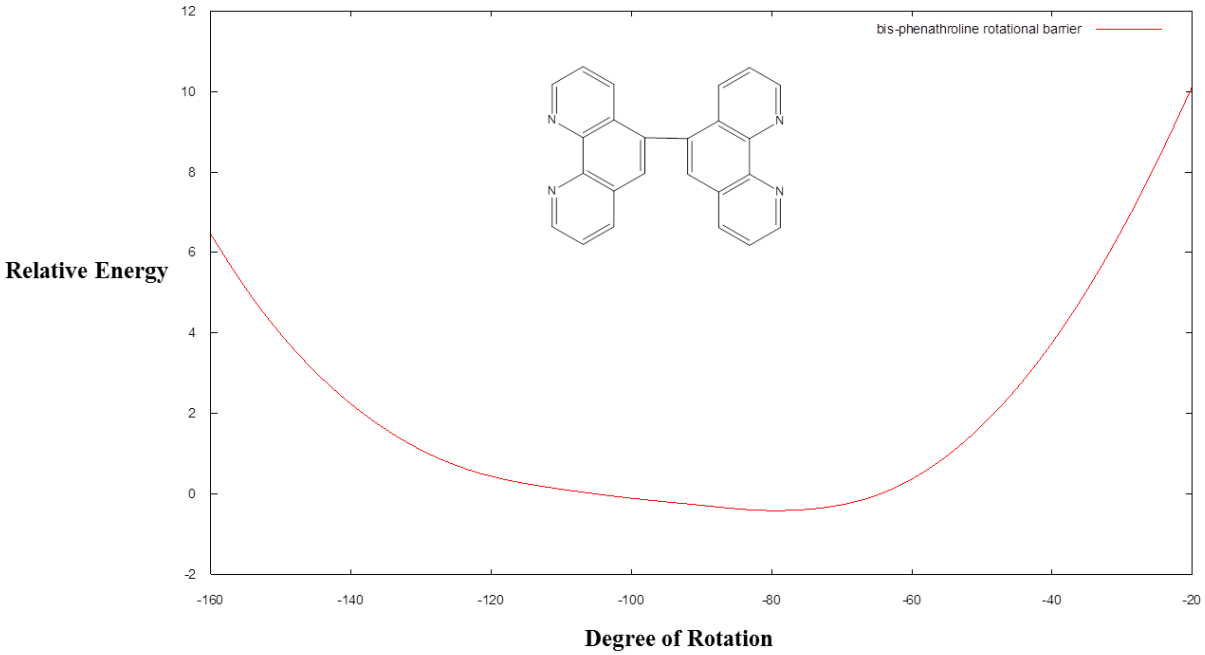

Figure 1.7.6. Plot of the degree of rotation about the 5,5' covalent bond in the free diphen ligand versus the relative energy.

Based on these calculations, it is believed that the orthogonal orientation of the diphen bridging ligand is a major reason the ruthenium(II) dimeric complexes are weakly coupled. The two phenanthroline subunits cannot freely rotate around the 5,5' covalent bond, which connects the units. The calculations performed on the free diphen ligand show that the two phenanthroline subunits have large barriers at 0° and 90° and have a torsion angle at about 40°. These findings

are supported by similar results for biphenyl in solution, which was found to have a dihedral angle of 37° ± 2° (Akiyama, et al., 1986).

1.8 Synthesis of Ruthenium(II) Dimeric Complexes

The literature describing the synthesis of ruthenium(II) polypyridine complexes is enormous, and thus many avenues are potentially available for the preparation of dimeric complexes. In fact, there are many reports in the literature describing synthetic routes to these complexes (Toyota, et al, 2005), (Treadway and Meyer, 1999), (Griffiths, et al., 2000). However, the current research problem requires a careful choice in order to avoid contamination with monomeric complexes. The target complexes are very weakly coupled and therefore are nearly identical in many respects to corresponding monomers. With this in mind, synthetic procedures which minimize the formation of closely related monomeric complexes were sought.

Synthesis of dimeric complexes can in general be performed in two different ways. In one method, appropriate monomeric complexes are synthesized, and these are then reacted with the bridging moiety to form the target dimer. In the other method, an appropriate precursor is reacted with the bridging moiety to form a dimer. This dimer is then reacted further with appropriate ligands to produce the target complex.

Examples of the first approach are common. For example, many start with $Ru(bpy)_2Cl_2$, which is readily prepared in large quantities. $Ru(bpy)_2Cl_2$ has been used for several decades and its chemistry is well understood. The complex can be reacted with a bridging ligand, L-L, and dimeric complexes formed through the following series of reactions. Previous work has shown, however, that this procedure is often complicated by the presence of small amounts of $Ru(bpy)_3^{2+}$ in the $Ru(bpy)_2Cl_2$, which will appear in the final product.

In the last decade, $[Ru(CO)_2Cl_2]_n$ has become a popular starting material for ruthenium complexes due to the ease of synthesis and its application in the synthesis of mixed ligand complexes. $[Ru(CO)_2Cl_2]_n$ can be prepared by heating $RuCl_3 \cdot 3H_2O$ in a solution of HCl and HCOOH. The product is recovered by simple evaporation to dryness (Anderson, 2007), (Aguirre et al., 2001). The product is poorly characterized because it is reactive and not soluble in most common solvents. The IR spectrum has been investigated and does provide some insight into the structure. An IR spectrum for the polymeric material is shown in Figure 1.8.1. Peaks are seen ~2027 cm^{-1}, ~2075 cm^{-1}, ~2088 cm^{-1}, and ~2139 cm^{-1}.

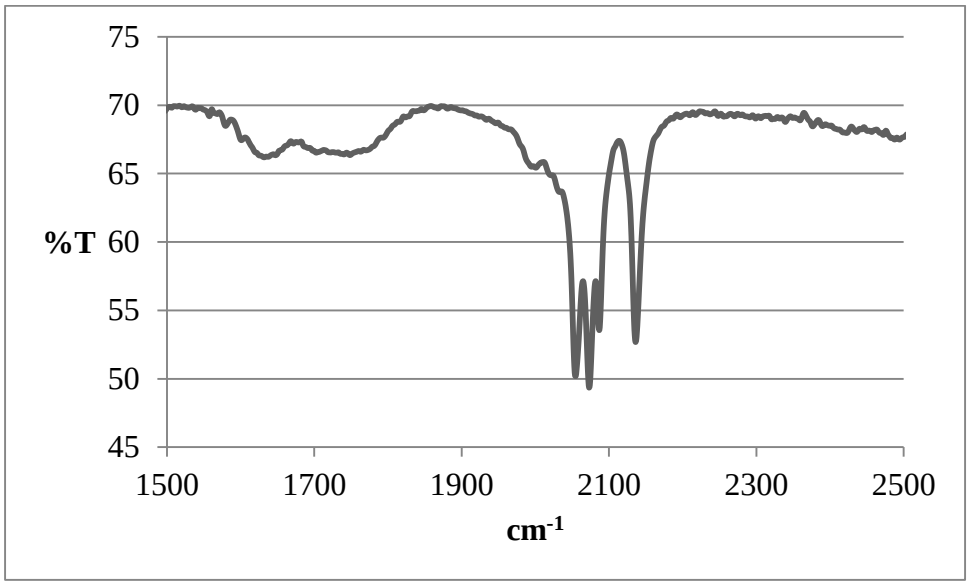

Figure 1.8.1. IR (KBr pellet) spectrum for $[Ru(CO)_2Cl_2]_n$.

The proposed structure is shown in Figure 1.8.2. The multiple carbonyl stretching peaks from 2027-2088 cm^{-1} indicate terminal *cis*-carbonyl groups (Spiccia et al, 2004), (Cleare and Griffith, 1969). The chlorides bridge the structure and exist in both the *trans* and *cis* geometry (Spiccia et al., 2004). The peak at ~2139 cm^{-1} is believed to be from an impurity, which is $[Ru(CO)_3Cl_2]_2$ (Spiccia et al, 2004), (Anderson et al., 1995). This impurity does not seem to affect the products of the reactions in which $[Ru(CO)_2Cl_2]_n$ is used as a precursor.

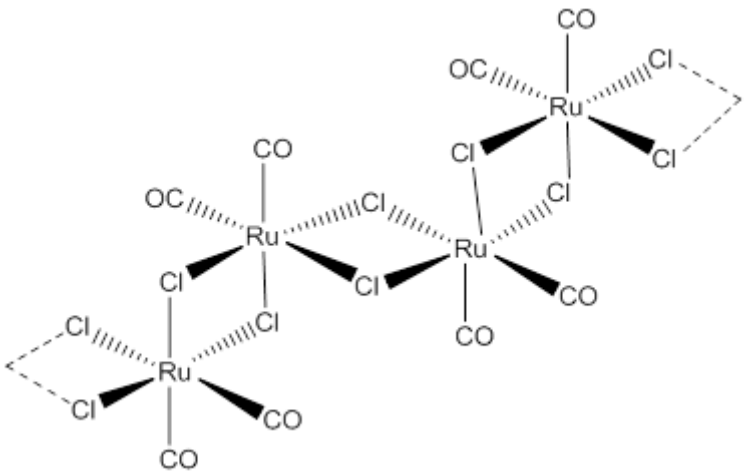

Figure 1.8.2. Proposed structure for polymeric $[Ru(CO)_2Cl_2]_n$.

$[Ru(CO)_2Cl_2]_n$ reacts readily with a chelating ligand under very mild conditions to yield complexes of the general formula $Ru(L)(CO)_2Cl_2$ (Spiccia, et al., 2004). Further reaction with chelating ligands requires some means of removing CO. Reaction with Me_3NO is perhaps the most common approach and results in the loss of CO in the form of CO_2 (Treadway and Meyer, 1999), (Spiccia, et al., 2004). Careful control of conditions and stoichiometry allow for the synthesis of complexes with the general formula $Ru(L)(L')COCl^+$ or $Ru(L)(L')_2^{+2}$. Use of $[Ru(CO)_2Cl_2]_n$ offers a variety of avenues to the target dimers that avoid the contamination problem described above.

There are very few reports in the literature describing the specific compounds of interest in the current work. The bridging ligand is typically prepared through a nickel(0) coupling reaction from chlorophenanthroline. This Ni(0) catalyzed coupling reaction has been used in organic syntheses for many years for coupling of aryl halides to produce biaryls (Iyoda, et al., 1990). This method occurs under mild conditions and provides good yields in many cases.

In 1993, Constable, et al. detailed a novel synthesis for coupling a ruthenium(II) polypyridine complex, which utilized a Ni(0) catalyzed coupling reaction. The general reaction is shown in scheme 1.8.1.

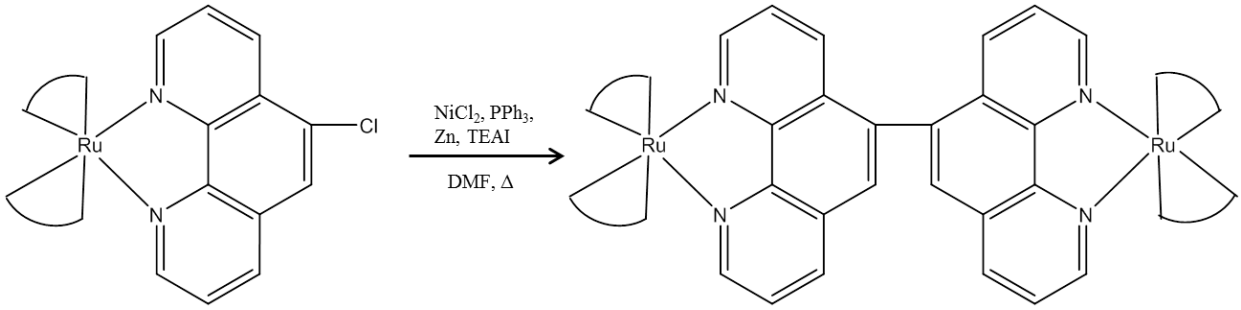

Scheme 1.8.1. A general Ni(0) catalyzed coupling reaction for a ruthenium dimeric complex.

In 2000, Fanni, et al., claiming to be the first, used a very similar Ni(0) catalyzed coupling reaction to couple a ruthenium(II) polypyridine complex. Since these two studies, the method has been used by numerous other groups.

2.1 Experimental

2.2 Materials

Ammonium hydroxide (NH_4OH) was purchased from Macron Chemicals. Tetrabutylammonium bromide and 2-pyrazinecarboxylic acid was purchased from TCI. Copper(II) acetate monohydrate, 2-methoxyethanol, triphenylphosphine (PPh_3), *N*,*N*-dimethylformamide (DMF), tetraethylammonium iodide, 4,7-diphenyl-1,10-phenanthroline 98+% (dpphen), 3,4,7,8-tetramethyl-1,10-phenanthroline 98+% (tmphen), 2,2'-bipyridyl 99% (bpy), and ammonium hexafluorophosphate (NH_4PF_6) were all purchased from Alfa Aesar. Ethanol was purchased from Koptec. Diethyl ether, hydrochloric acid (HCl), acetonitrile, and methanol were purchased from EMD. Ruthenium(III) chloride hydrate ($RuCl_3 \cdot XH_2O$) was purchased from Acros Organics. Formic acid (HCOOH) was purchased from Mallinckrodt Chemicals, and chloroform was purchased from BDH. The 5-chloro-1,10-phenanthroline (Cl-phen) and 1,10-phenanthroline (phen) were purchased from GFS Chemicals. Trimethylamine *N*-oxide (Me_3NO), 2,3-Bis(2-pyridyl)-pyrazine (dpp), and 4,4'-dimethyl-2,2'-dipyridyl (dmb) were purchased from Aldrich. Nickelous chloride hexahydrate ($NiCl_2 \cdot 6H_2O$) and potassium cyanide (KCN) were purchased from J.T. Baker. The zinc dust and ethylene glycol were purchased from Fisher Scientific. Acetonitrile-d_3 (CD_3CN) and chloroform-d ($CDCl_3$) were bought from Cambridge Isotope Laboratories, Inc.

$[Ru(phen)_3](PF_6)_2$ was synthesized using the microwave procedure for $[Ru(bpy)_3](PF_6)_2$ as detailed by Anderson in 2007. $[Ru(bpy)_3](PF_6)_2$ and $Ru(DMSO)_4Cl_2$ samples were synthesized by previous group members. Purity of $[Ru(bpy)_3](PF_6)_2$ was confirmed with ESI-MS, and the purity of $Ru(DMSO)_4Cl_2$ was confirmed with ^1H NMR spectroscopy. 2,2'-bipyrazine was synthesized as described by Anderson, which was based on procedures used by

Lafferty and Rillema (Anderson, 2007), **(**Lafferty and Case, 1967), (Rillema, et al., 1983). Purity was confirmed with NMR spectroscopy.

Elemental analysis was performed by Atlantic Microlab, Inc. in Norcross, GA.

2.3 Instrumentation and General Procedures

All electrospray ionization mass spectrometry (ESI-MS) experiments were performed using a Bruker Daltronics ultrOTOF -Q™ with a quadrupole mass filter. A flow rate of 3 mL/min was used. Acetonitrile was used as the solvent.

For ^{1}H NMR experiments, a Bruker 300 Ultra Shield™ NMR was used. CD_3CN or $CDCl_3$ were used as solvents. The Bruker TopSpin™ program was used to process the NMR spectra.

UV-visible spectrometry experiments were carried out using a Hewlett Packard 8453 spectrophotometer. A quartz cuvette with a 1 cm path length was used, and the data was transferred to Excel for analysis.

A CH Instruments Electrochemical workstation was used for the cyclic voltammetry experiments. The counter electrode used was a platinum wire, and reference electrode was a saturated calomel electrode (SCE). The working electrode was a platinum disk electrode with a 1 mm diameter, and the experiments were carried out in 0.1M tetrabutylammonium-hexafluorophospate in acetonitrile. Data was analyzed using Excel.

Infrared (IR) spectroscopy was performed using a Perkin Elmer Spectrum 100 FT-IR Spectrometer equipped with a triglycine sulfate (TGS) detector. Samples were prepared in potassium bromide and pressed into pellets. Spectra were recorded over the range of 450-4000 cm^{-1} with a 4 cm^{-1} resolution. Typically, 16 spectral scans were averaged to produce the final

spectrum. The spectra were processed using the Perkin Elmer Spectrum Express program and then transferred to Excel for analysis.

Microwave syntheses were carried out using a CEM Discover microwave synthesis system equipped with an Explorer auto sampler. A 10 mL microwave reaction vessel was used. The temperature was set at above 200 °C, and the pressure setting was 17 bar. The power was set at 200 watts, and the samples were irradiated for the times indicated. The samples were allowed to cool to room temperature before removing from the machine.

2.4 Photochemical Procedures

Photolysis experiments were done using one of two different lamps. One lamp was a 300 watt, 120 volt bulb "sunlamp" with no filtering. The second lamp was 1000 watt Xe bulb. The reaction solutions were irradiated with the select lamp for various times while being stirred. The solution was kept at room temperature. The reactions were monitored with UV-vis analysis.

Quenching experiments were carried out using a flash photolysis system of traditional design. The excitation laser was a PhaseR flash lamp pumped dye laser with LD490 dye which provided a 500 nsec pulse of 480 nm light. The probe beam, at 90^{o} relative to the laser excitation, was provided by a 100 watt tungsten lamp. A shutter protected the sample from irradiation by the probe prior to laser excitation. The sample was held in a 1 cm cuvette. After passing through the sample, the probe beam was passed through a monochromator and finally to a PMT detector. Transient absorbance changes were recorded on a LeCroy digital oscilloscope after passing through a summing amplifier which provided a variable offset potential. The transient absorbance changes were large and signal averaging was not required. Files collected with the digital oscilloscope were transferred to a PC for kinetic analysis.

All of the reported quenching studies were performed with solutions containing 0.5 M H_2SO_4, either 10 or 50 mM quencher and enough ruthenium complex to provide an absorbance of 0.28. Quenchers were $Cu(SO_4)$ or $Fe_2(SO_4)_3$. Experiments were performed with air saturated solutions and argon purged solutions. Typically the same solution was used, first air saturated then purged.

The rate of back reaction following the quenching event was assumed to be second order and analyzed using the relation

$$\frac{1}{A_t} - \frac{1}{A_0} = kt$$

where A_0 is the concentration of oxidized ruthenium complex at time = 0, A_t is the concentration of oxidized ruthenium complex at time = t, and k is the second-order rate constant. In practice, the equation was rewritten as follows:

$$Abs_t = Abs^0 - \left(\frac{1}{\frac{1}{\Delta Abs_0} - \frac{kt}{\epsilon b}} \right)$$

where Abs_t is the absorbance at time t, Abs^0 is the absorbance prior to excitation, ΔAbs_0 is the initial change in absorbance following excitation, ε is the extinction coefficient for the ruthenium complex, b is the path length, and k is the second-order rate constant. This form of the equation takes into account the fact that only a fraction of the ruthenium complex is oxidized by the laser pulse, and it converts the concentration units to absorbance.

The second order rate constant was obtained by fitting the data to calculated absorbance values. The procedure requires a three parameter fit, Abs^0, ΔAbs_0 and the second-order rate constant. The data was fit using either an Excel manual trial and error search to minimize the sum of the squares of the difference between the calculated values and the data or an automated

routine provided by GNOME Gnumeric. Both methods gave the same results when applied to the same data sets.

Quenching yields were calculated by comparison to the yield of the reaction of $Ru(bpy)_3^{2+}$ with Fe^{3+} which is known to have a yield of 100%. In practice, the maximum change in absorbance at 450 nm for a given complex was compared to the change in absorbance for $Ru(bpy)_3^{2+}$ for each concentration of quencher under the same solution conditions. The absorbance changes were obtained from the same data sets used for the determination of the rates of the back reaction described above. This procedure was used in the early experiments reported by Sutin, et al. (Hoselton, et al., 1978), (Lin, et al., 1976).

Lifetime data was collected using a system built around a QuantaRay DCR Nd:YAG. Solutions, held in 1 cm semimicro glass cuvettes, were made with 0.5 M H_2SO_4, 0-5 mM quencher, and enough ruthenium complex to bring the absorbance to ~0.08. The solutions were purged for 15 minutes with ultrahigh purity argon. After 15 minutes of purging the emission decay rates were constant and further purging had no effect up to 24 hrs. The emitted light was collected with a 25 x 150 mm double convex lens and focused on a monochromator set to 600 nm. The detector was a R928 PMT followed in close proximity with a Stanford Research Systems SR445 DC-300 MHz amplifier. Transient emissions signals were recorded on a LeCroy 6054 digital oscilloscope. Approximately 100 emission events at a rate of 10 Hz were recorded, averaged and save as the final data file. Signal levels were held, by turning the laser power to near the minimum required for lasing, at relatively low levels to avoid ringing in the coaxial cables. The emission data were analyzed as single exponential decays using a successive integration fitting routine followed by a Leven-Marquardt based linear fitting algorithm (Press et al., 1992). The relative standard deviation (RSD) for the slope of the line for each data set was

found by using the Excel "linest" function to first get the standard deviation. The value for the standard deviation was then divided by the slope to get the RSD.

2.5 Syntheses

5,5'-Bi-1,10-phenanthroline (Hu et al., 2001). $NiCl_2 \cdot 6H_2O$ (0.152 g, 1.17 mmol), PPh_3 (1.22 g, 4.65 mmol), and 10 mL dry DMF were placed in a 100 mL RBF. The solution was stirred and nitrogen purged for 30 min at 50°C (blue). Unpurified zinc dust (0.075 g, 1.15 mmol) was added to the solution. The solution was stirred under nitrogen atmosphere until it was dark red/brown. Cl-phen (0.248 g, 1.15 mmol) that was nitrogen purged in 5 mL of DMF was added to the RBF. The solution was then stirred under nitrogen overnight at 50 °C (dark green). The mixture was evaporated to dryness yielding a dark green solid. The dark green solid was then boiled in 40 mL of water for 2 hr. After boiling, the solution was cooled and filtered. Saturated NH_4PF_6 solution was added to the solution. A grey gummy precipitate was collected on a medium porosity fritted funnel, and then heated to reflux for 4 hr in a solution of KCN (0.750 g, 11.5 mmol) in 20 mL of a methanol and H_2O (19:1. v:v). The solution was allowed to cool and filtered. The white solid was washed with H_2O, ethanol, and then ether. The solid was dried in a desiccator. Yield: 49%. ^{1}H NMR (300 MHz, CD_3CN): δ 9.21 (q, 1H), 9.14 (q, 1H), 8.45 (q, 1H), 8.06 (s, 1H), 7.84 (q, 1H), 7.80 (q, 1H), 7.51 (q, 1H).

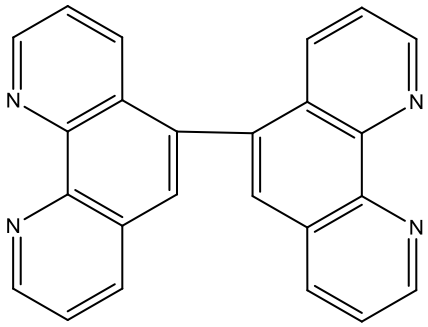

$[Ru(CO)_2Cl_2]_n$ (Anderson, 2007), (Aguirre et al., 2001). $RuCl_3 \cdot XH_2O$ (1.01 g, 3.86mmol) was placed in a 100 mL RBF, and 50 mL of a 1:1 (v:v) solution of concentrated HCl and HCOOH were added (brown). While stirring, the solution was heated to reflux for 24 hr under nitrogen. The yellow solution was then filtered. The filtrate was evaporated to dryness using a hotplate.

The product, a yellow solid, was used in subsequent procedures with no further purification. Yield: 81%.

$(CO)_2Cl_2Ru(diphen)Ru(CO)_2Cl_2$

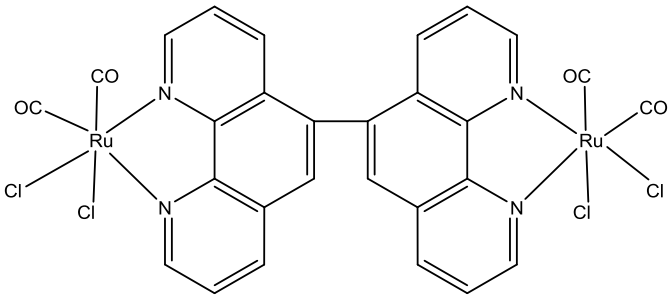

$[Ru(CO)_2Cl_2]_n$ (1.47 g, 6.45 mmol) was dissolved in 60 mL of hot 2-methoxyethanol. Diphen (0.462 g, 1.29 mmol) was dissolved in 35 mL of hot 2-methoxyethanol in a separate beaker. Both solutions were filtered before adding the diphen solution to the $[Ru(CO)_2Cl_2]_n$ solution (orange to deep red, almost instantly). The solution was boiled for 7 min and cooled. The solution was filtered using a medium porosity fritted funnel, and the solid was put in the desiccator to dry (yellow with orange surface layer). Yield: 39%.

$[(phen)_2Ru(diphen)Ru(phen)_2](PF_6)_4$

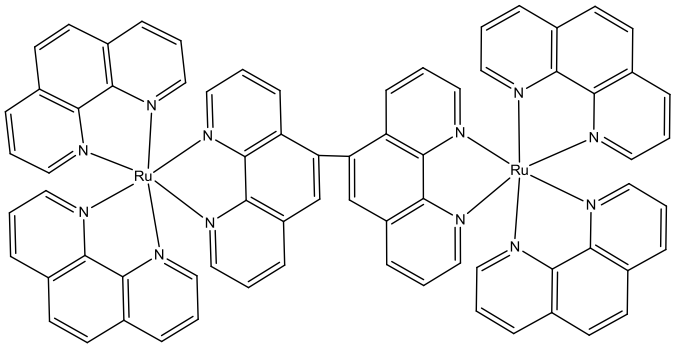

$(CO)_2Cl_2Ru(diphen)Ru(CO)_2Cl_2$ (0.200 g, 0.246 mmol), phen (0.426 g, 2.36 mmol), and Me_3NO (0.187 g, 2.49 mmol) were added to 70 mL of nitrogen purged 2-methoxyethanol (peach). The solution was heated to reflux for 2 hr (dark brown). After cooling, the solution was filtered. The solvent was removed via rotary evaporator, and 100 mL of water was added to dissolve the remaining oily substance. Saturated NH_4PF_6 aqueous solution was added to the solution. The precipitate was recovered by filtration through a medium porosity fritted funnel. Further purification was carried out by dissolving the orange solid in acetonitrile and dropping the solution into ether. The product was again collected using a medium porosity

fritted funnel. Yield: 88%. MS (ESI): m/z = 321.0 [M^{4+} - 4PF_6]/4 = 320.34). Anal. Calcd for $C_{72}H_{46}N_{12}Ru_2P_4F_{24}$: C, 46.46; H, 2.50; N, 9.03. Found: C, 42.00; H, 3.01; N, 9.28.

[(dpphen)$_2$Ru(diphen)Ru(dpphen)$_2$](PF$_6$)$_4$

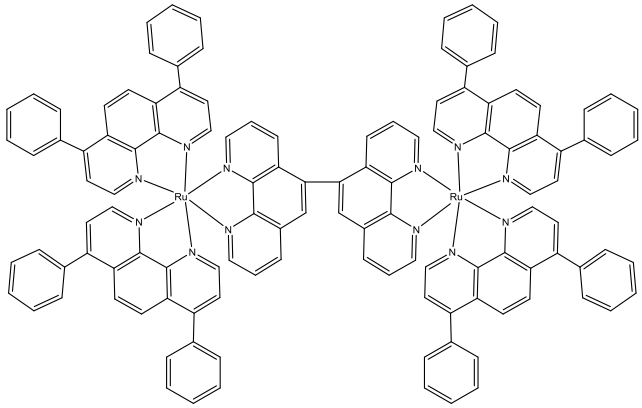

[(dpphen)$_2$Ru(diphen)Ru(dpphen)$_2$](PF$_6$)$_4$ was synthesized and purified using the procedure described above for [(phen)$_2$Ru(diphen)Ru(phen)$_2$](PF$_6$)$_4$. Yield: 55%. MS (ESI): m/z = 472.58 [M^{4+} - 4PF_6]/4 = 472.53). Anal. Calcd for $C_{120}H_{78}N_{12}Ru_2P_4F_{24}$: C, 58.30; H, 3.20; N, 6.80. Found: C, 57.22; H, 3.85; N, 7.85.

[(tmphen)$_2$Ru(diphen)Ru(tmphen)$_2$](PF$_6$)$_4$

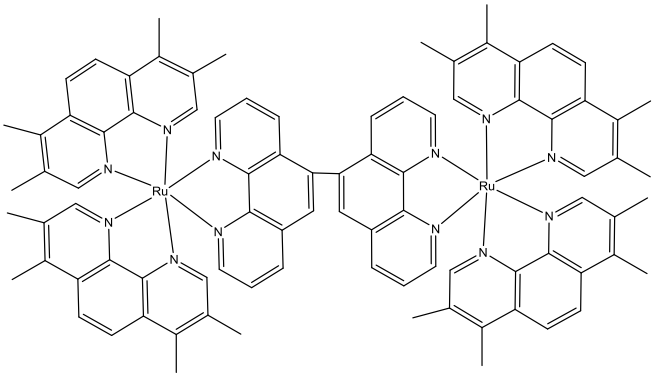

[(tmphen)$_2$Ru(diphen)Ru(tmphen)$_2$](PF$_6$)$_4$ was synthesized and purified using the procedure described above for [(phen)$_2$Ru(diphen)Ru(phen)$_2$](PF$_6$)$_4$. Yield: 71%. MS (ESI): m/z = 376.6 [M^{4+} - 4PF_6]/4 = 376.47).

[(bpy)$_2$Ru(diphen)Ru(bpy)$_2$](PF$_6$)$_4$

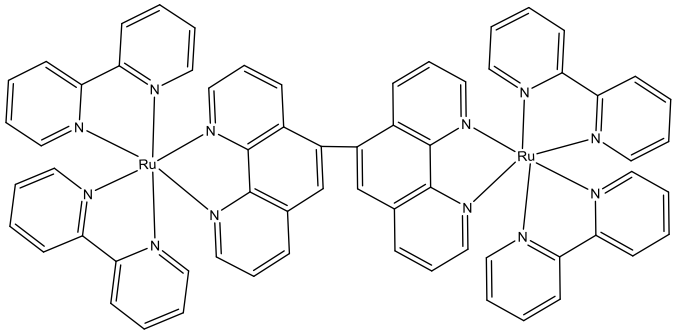

$(CO)_2Cl_2Ru(diphen)Ru(CO)_2Cl_2$ (0.0549 g, 0.067 mmol), bpy (0.0953g, 0.610 mmol), and Me_3NO (0.0470 g, 0.626 mmol) were dissolved in 20 mL of 2-methoxyethanol that had been nitrogen purged. The solution was heated for 1 hr, and additional

Me_3NO (0.0258 g, 0.343 mmol) was added. The solution was heated for 1 hr and cooled. It was then filtered. Most of the solvent was removed via rotavap, and the oily substance was then dissolved in H_2O. Saturated NH_4PF_6 solution was added, and the solution was filtered using a medium porosity fritted funnel to collect the solid (orange). The solid was then dissolved in acetonitrile, added drop-wise to diethyl ether, and filtered. Yield: 63%. MS (ESI): m/z = 296.52 [M^{4+} - $4PF_6$]/4 = 296.32).

[$(dmb)_2Ru(diphen)Ru(dmb)_2$]$(PF_6)_4$

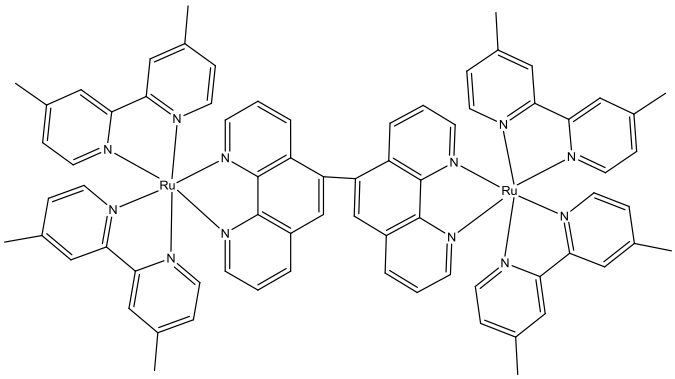

Synthesis and purification of [$(dmb)_2Ru(diphen)Ru(dmb)_2$]$(PF_6)_4$ was done using the same procedure reported for the synthesis of [$(bpy)_2Ru(diphen)Ru(bpy)_2$]$(PF_6)_4$. Yield: 84%. MS (ESI): m/z = 324.6 [M^{4+} - $4PF_6$]/4 = 324.38).

$Ru(CO)_2Cl_2$(phen) [$Ru(CO)_2Cl_2]_n$ (0.4657 g, 2.04 mmol) was dissolved in 60 mL of hot 2-methoxyethanol. Phen (0.4676 g, 2.59 mmol) was dissolved in 20 mL RT 2-methoxyethanol. The two solutions were mixed together and heated to a boil for 25 min. The solution was cooled and then filtered. A yellow solid was collected on a medium porosity fritted funnel. Most of the filtrate was evaporated using a rotary evaporator. The yellow solid was again collected on a medium porosity fritted funnel. Both yellow solids appeared to be identical based on the IR spectra which contained the two carbonyl bands expected for the complex. Yield: 59%

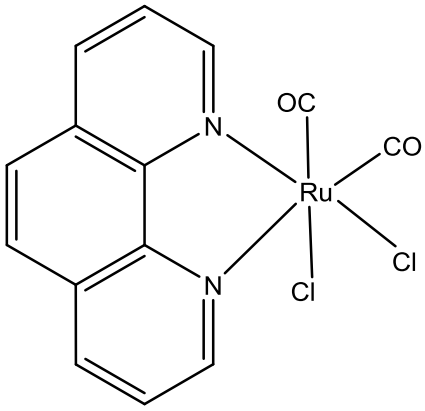

[Ru(phen)(dpphen)$_2$](PF$_6$)$_2$ $Ru(CO)_2Cl_2(phen)$ (0.1003 g, 0.246 mmol), Me_3NO (0.1301 g, 1.73 mmol), and dpphen (0.2473 g, 0.740 mmol) were added to 35 mL N-purged 2-methoxyethanol. The solution was heated to reflux under nitrogen for 2 hr. The solution was cooled, and most of the solvent was removed via a rotary evaporator. About 100 mL of DI H_2O was added to RBF. The solution was filtered before adding 10 mL of saturated NH_4PF_6 solution. The orange solid was filtered out using a medium porosity fritted funnel. To further purify the sample, the solid was dissolved in acetonitrile, added drop-wise to ether, and collected on a medium porosity fritted funnel. Yield: 77%

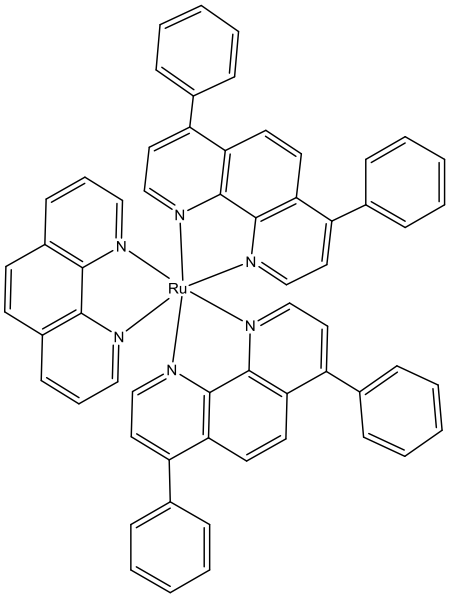

[Ru(phen)(tmphen)$_2$](PF$_6$)$_2$ $[Ru(phen)(tmphen)_2](PF_6)_2$ was synthesized and purified using the same procedure as that used for $[Ru(phen)(dpphen)_2](PF_6)_2$. Yield: 100%

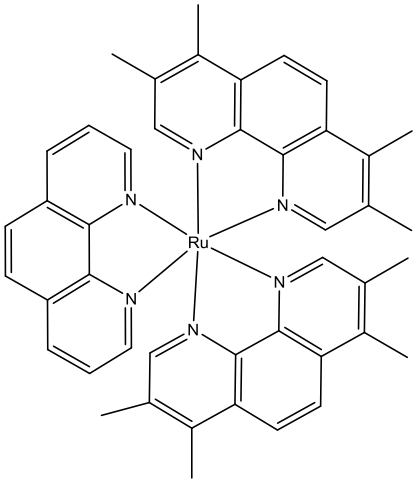

[Ru(phen)(bpy)$_2$](PF$_6$)$_2$ Ru(CO)$_2$Cl$_2$(phen) (0.1022 g, 0.250 mmol), bpy, (0.1167 g, 0.747 mmol), and Me_3NO (0.1127 g, 1.5 mmol) were added to 35 mL of N-purged 2-methoxyethanol. The solution was heated to reflux for 1 hr under nitrogen. At this point, additional Me_3NO (0.0580 g, 0.772 mmol) was added to the solution. The solution was heated for another 2.5 hr. The solution was cooled, and most of the solvent was evaporated on a rotary evaporator. About 100 mL of DI H_2O was added, and the solution was filtered. Approximately 10 mL of saturated NH_4PF_6 solution was added, and the orange solid was collected on a medium porosity fritted funnel. After dissolving the solid in acetonitrile and dropping the solution into ether, the solid was collected by a medium porosity fritted funnel. Yield: 34%

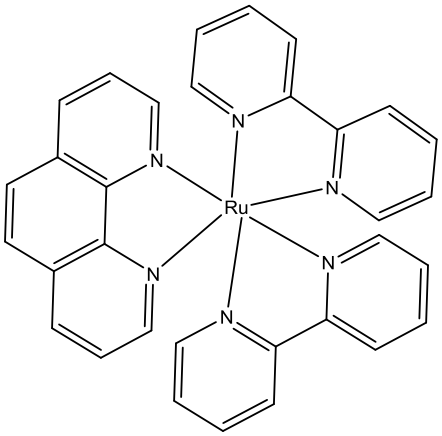

[Ru(phen)(dmb)$_2$](PF$_6$)$_2$ [Ru(phen)(dmb)$_2$](PF$_6$)$_2$ was synthesized and purfied using the same procedure as that used for [Ru(phen)(bpy)$_2$](PF$_6$)$_2$. Yield: 51%

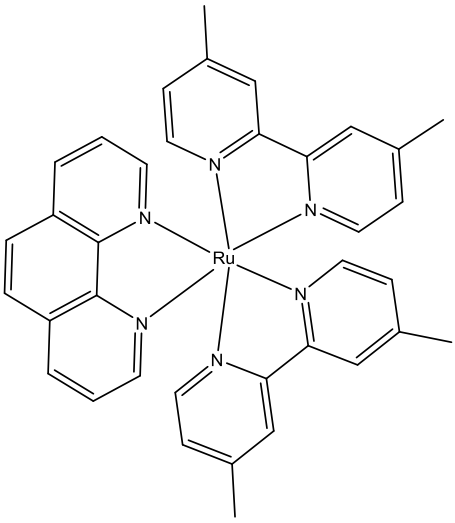

$(CO)_2Cl_2Ru(dpp)Ru(CO)_2Cl_2$ $[Ru(CO)_2Cl_2]_n$ (0.7370 g, 3.23 mmol) was dissolved in 30 mL of hot 2-methoxyethanol. Dpp (0.1535 g, 0.655 mmol) was dissolved in 30 mL of RT 2-methoxyethanol. The two solutions were filtered and then mixed together.

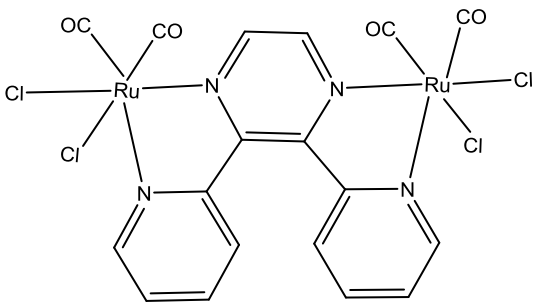

The solution was then heated to a boil for 20 min. The solution was allowed to cool, and then an olive green solid was filtered out using a medium porosity fritted funnel. Yield: 30%

$[(phen)_2Ru(dpp)Ru(phen)_2](PF_6)_4$ $(CO)_2Cl_2Ru(dpp)Ru(CO)_2Cl_2$ (0.1235 g, 0.178 mmol), phen (0.3533 g, 1.96 mmol), and Me_3NO (0.1540 g, 2.05 mmol) were dissolved in 35 mL of N-purged 2-methoxyethanol. The solution was heated to reflux under nitrogen for 1 hr. More Me_3NO (0.0797 g, 1.06 mmol) was added, and the solution was heated for an additional 1 hr. The solution was cooled and filtered. Most of the solvent was removed by using a rotary evaporator. DI H_2O (100 mL) was used to dissolve the remaining solvent. About 10 mL of saturated NH_4PF_6 solution was added. The brown precipitate was collected on a medium porosity fritted funnel. For further purification, the solid was dissolved in acetonitrile. The solution was added drop-wise to ether, and the solid was collected with a medium porosity fritted funnel. Yield: 89%

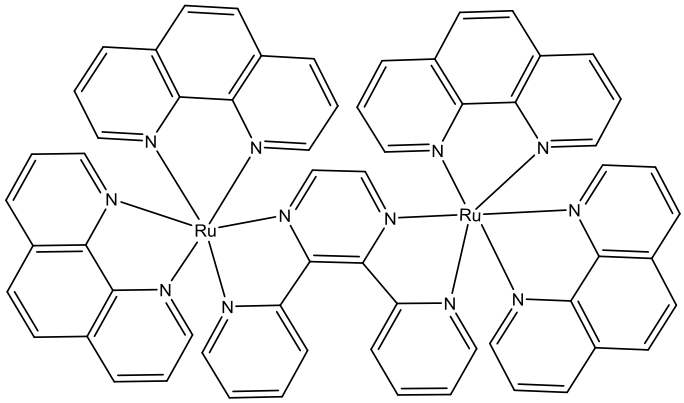

3.1 Results

3.2 Synthesis of Symmetric Ruthenium(II) Dimeric Complexes

A series of dimeric complexes with the general formulation $L_2Ru\text{-bridge-}RuL_2^{4+}$ was required for the investigations described in this work. The bridging ligand, diphen, appeared to be a key component contributing to the photochemical properties of interest and thus was the focus of the synthetic work. Preparation of the target complexes that were free from monomeric complexes was critically important and synthetic routes tailored to that end were developed.

As indicated, diphen was a focal point of this work, and it was prepared in better yield that previously reported using the following reactions. The product was characterized by ^1H NMR, and the aromatic region of the spectrum is shown in Figure 3.2.1. The relative chemical shifts and the splitting are consistent with the expected molecule reports found in the literature.

Figure 3.2.1. ^{1}H NMR spectrum for diphen showing the aromatic region. (300MHz, CD_3CN).

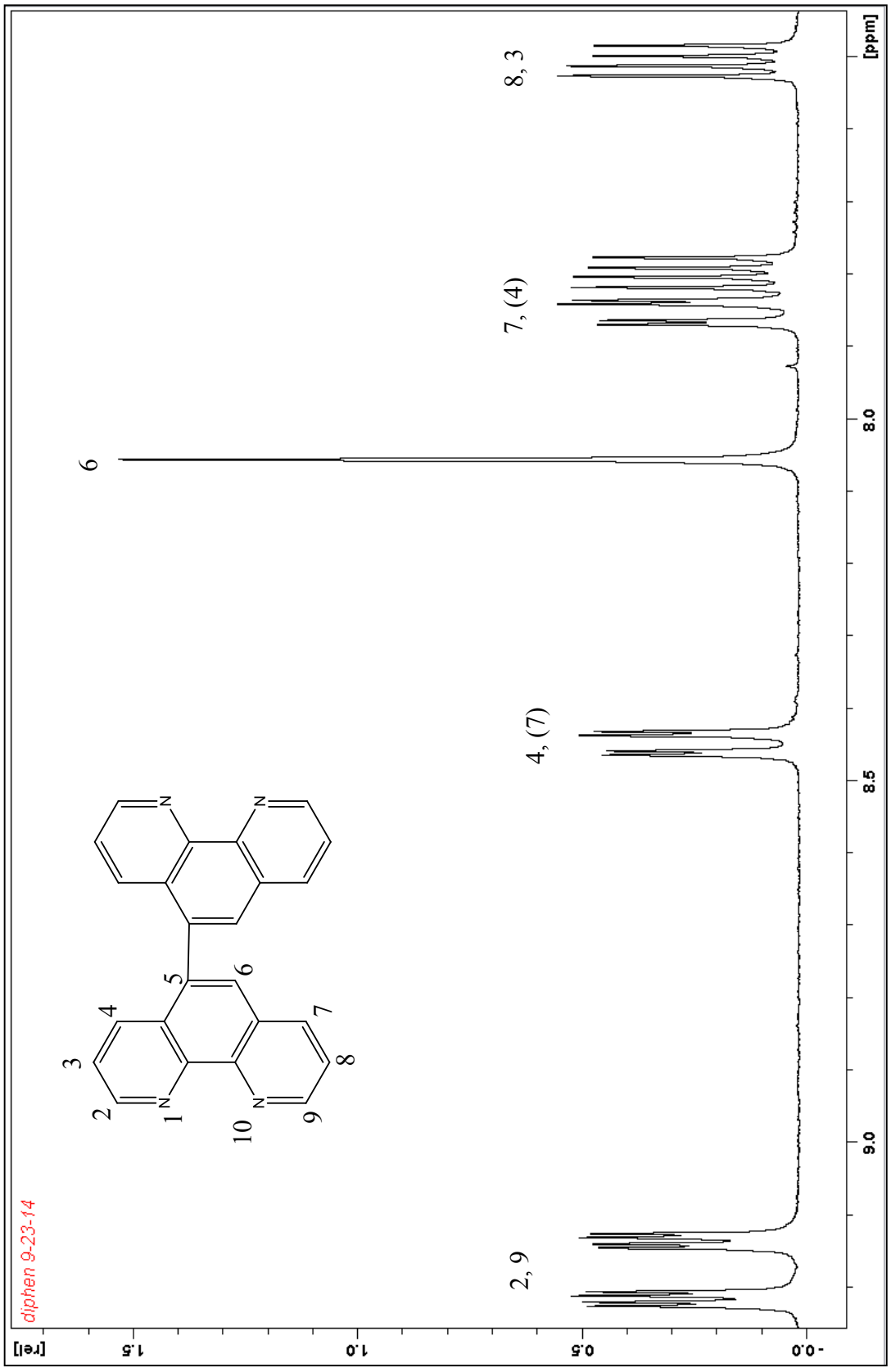
diphen 9-23-14
[rel]
1.5
1.0
0.5
0.0
9.0
8.5
8.0
[ppm]
2, 9
4, (7)
6
7, (4)
8, 3
N
N
N
N
1
2
3
4
5
6
7
8
9
10

The dimeric ruthenium complexes were prepared according to the following reactions.

$$[Ru(CO)_2CL_2]_n + \text{diphen} \xrightarrow[\Delta]{\text{2-methoxyethanol}} (CO)_2Cl_2Ru(\text{diphen})Ru(CO)_2Cl_2 \qquad \textbf{Eq1}$$

$$(CO)_2Cl_2Ru(\text{diphen})Ru(CO)_2Cl_2 + \text{Ligand} \xrightarrow[N_2,\ \Delta]{Me_3NO,\ \text{2-methoxyethanol}} L_2Ru(\text{diphen})RuL_2 \qquad \textbf{Eq2}$$

The trimethylamine N-oxide was used to remove the carbonyl groups through the formation of CO_2. The carbonyl containing intermediates obtained with these reactions were not sufficiently soluble in commonly used solvent to allow any spectral characterization. IR spectroscopy of the solid products, because of the presence of the strongly absorbing carbonyl stretching bands, proved invaluable in following the reactions. The IR spectrum of the starting material, $[Ru(CO)_2Cl_2]_n$ is shown in Figure 3.2.2. Four peaks due to CO stretching are seen at 2053 cm^{-1}, 2075 cm^{-1}, 2088 cm^{-1}, and 2138 cm^{-1}.

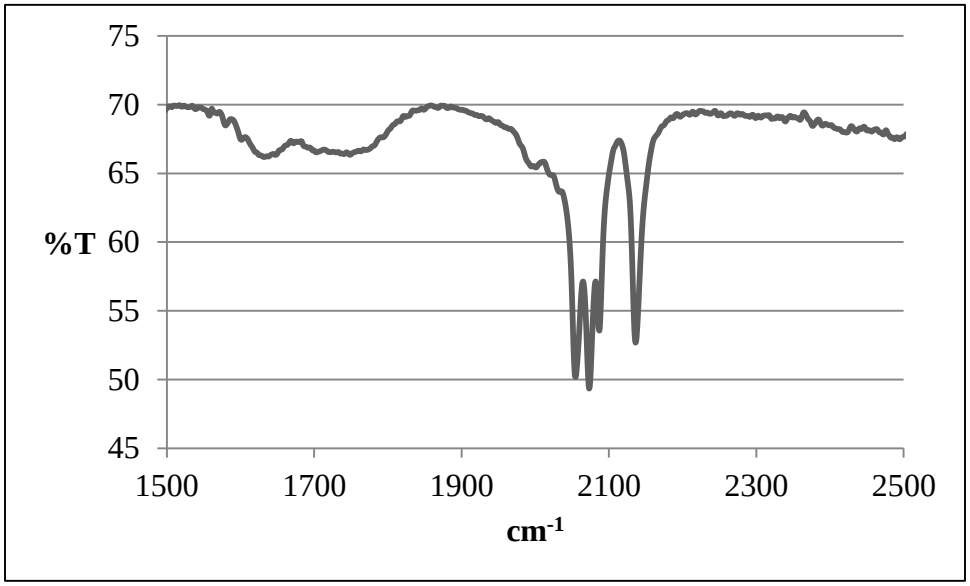

Figure 3.2.2. IR spectrum (KBr pellet) for $[Ru(CO)_2Cl_2]_n$ showing peaks due to CO stretching at 2053 cm^{-1}, 2075 cm^{-1}, 2088 cm^{-1}, and 2138 cm^{-1}.

$[Ru(CO)_2Cl_2]_n$ and diphen were reacted together to produce $(CO)_2Cl_2Ru(diphen)Ru(CO)_2Cl_2$. The IR spectra of $[Ru(CO)_2Cl_2]_n$ and $(CO)_2Cl_2Ru(diphen)Ru(CO)_2Cl_2$ are compared in Figure 3.2.3. Figure 3.2.3(b) shows 2 peaks at 1987 cm^{-1} and 2058 cm^{-1} from CO stretching in $(CO)_2Cl_2Ru(diphen)Ru(CO)_2Cl_2$ consistent with the expected symmetric and asymmetric stretching bands normally found in complexes containing 2 carbonyl groups in a cis geometry.

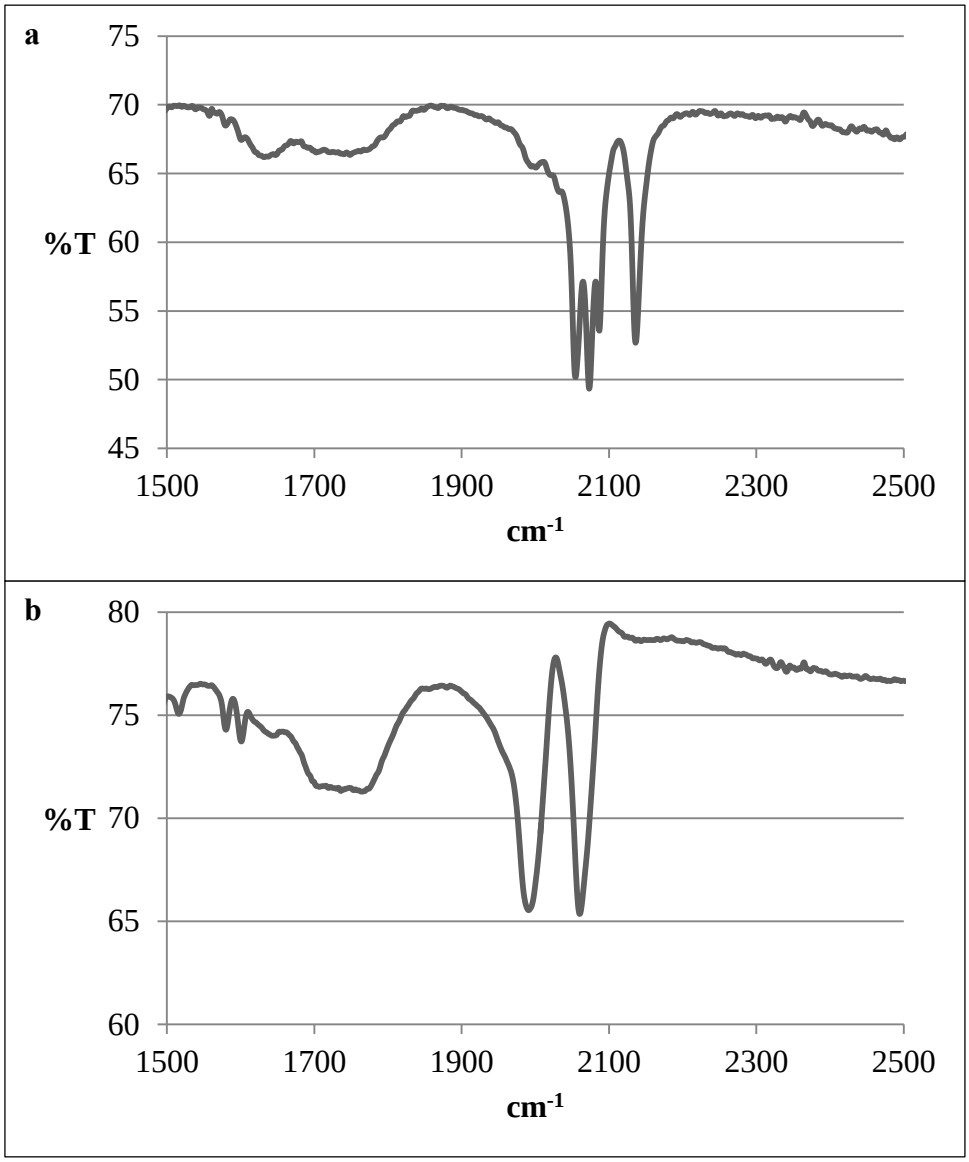

Figure 3.2.3. IR spectra comparison for (a) $[Ru(CO)_2Cl_2]_n$ and (b) $(CO)_2Cl_2Ru(diphen)Ru(CO)_2Cl_2$.

The first ligand chosen to react with $(CO)_2Cl_2Ru(diphen)Ru(CO)_2Cl_2$ was 1,10-phananthroline (phen). Spectroscopic and electrochemical techniques were utilized to characterize the expected product $[(phen)_2Ru(diphen)Ru(phen)_2](PF_6)_4$. IR confirmed the absence of peaks due to CO. The spectrum over the range expected for CO bands is shown in Figure 3.2.4.

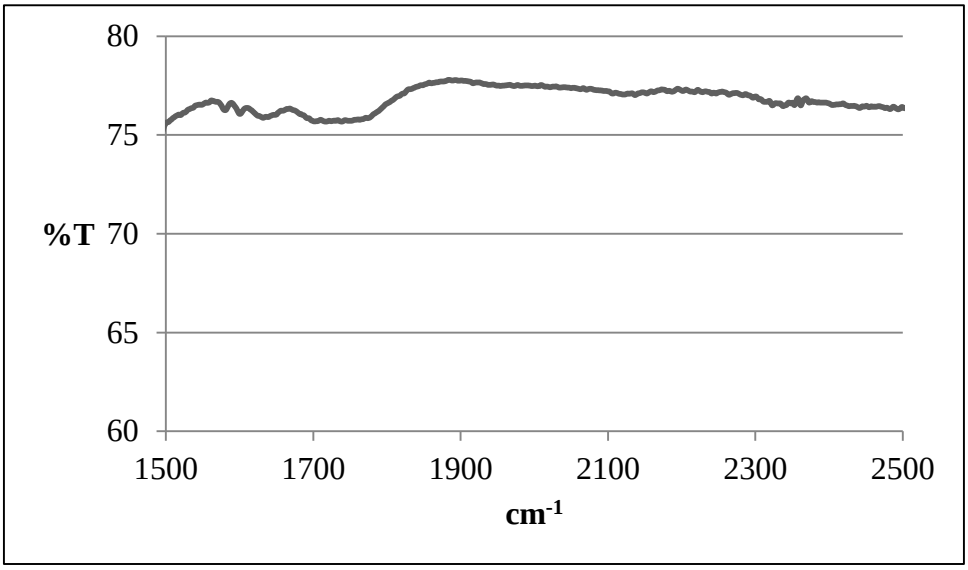

Figure 3.2.4. IR spectrum (KBr pellet) for $[(phen)_2Ru(diphen)Ru(phen)_2](PF_6)_4$ showing the absence of CO stretching peaks.

The UV-vis spectrum can be seen in Figure 3.2.5 showing a λ_{max} value of 448 nm. $Ru(phen)_3^{2+}$, a very analogous compound has a similar spectrum with maxima at 446 nm and 264 nm.

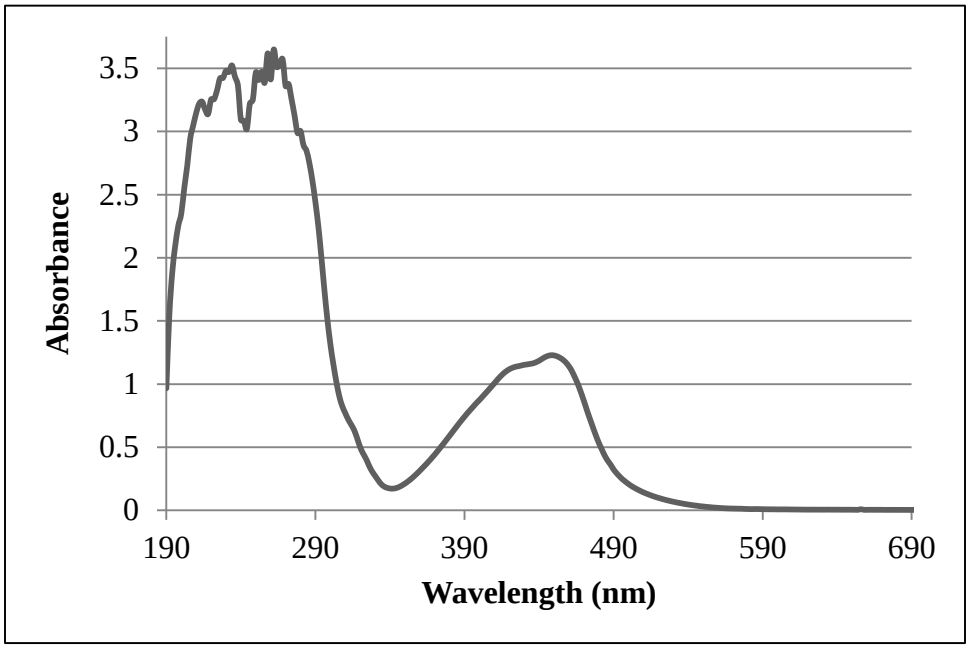

Figure 3.2.5. UV-Vis spectrum for $[(phen)_2Ru(diphen)Ru(phen)_2](PF_6)_4$ in acetonitrile.

Figure 3.2.6 shows the cyclic voltammogram of $[(phen)_2Ru(diphen)Ru(phen)_2](PF_6)_4$. The redox potential for the complex was found to be 1.308 V vs SCE which identical to $Ru(phen)_3^{2+}$ with a redox potential of 1.309 V vs SCE.

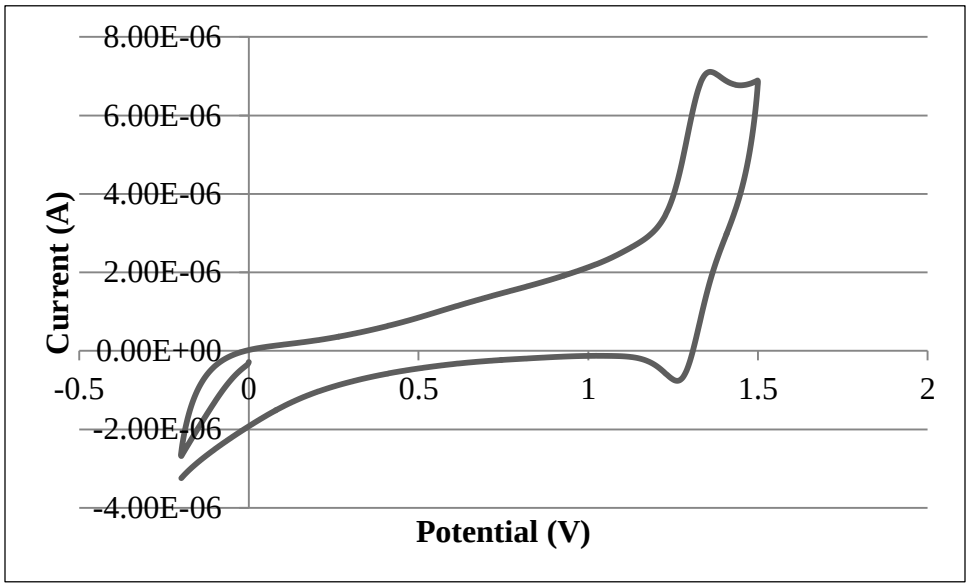

Figure 3.2.6. Cyclic voltammogram for $[(phen)_2Ru(diphen)Ru(phen)_2](PF_6)_4$. (0.1M $TBAPF_6$ in acetonitrile, SCE).

ESI-MS was also used to analyze the sample, and the spectra are shown in Figures 3.2.7 and 3.2.8. Ruthenium complexes exhibit a distinct isotope pattern with ESI-MS analysis. The isotope pattern for a complex with one ruthenium differs from the isotope pattern for a complex with two ruthenium centers. The expected peak for $(phen)_2Ru(diphen)Ru(phen)_2^{4+}$ is seen at 321.0 m/z. Other peaks seen are due to the ionization technique used. $(phen)_2Ru(diphen)Ru(phen)_2^{3+}$ is present, as indicated by peak 427.7 m/z. Additional peaks for 4^+ are seen at 338.8 and 358.0 m/z and at 452.0, 475.7, and 500.4 m/z for 3^+. These could indicate the further fragmentation of $(phen)_2Ru(diphen)Ru(phen)_2^{4+}$ and $(phen)_2Ru(diphen)Ru(phen)_2^{3+}$ due to collision-induced dissociation in the quadrupole system used. The peaks increase by ~70 g/mol compared to the previous peak. No evidence of monomeric ruthenium(II) complexes is seen.

Figure 3.2.7. Full ESI-MS spectrum for $[(phen)_2Ru(diphen)Ru(phen)_2](PF_6)_4$.

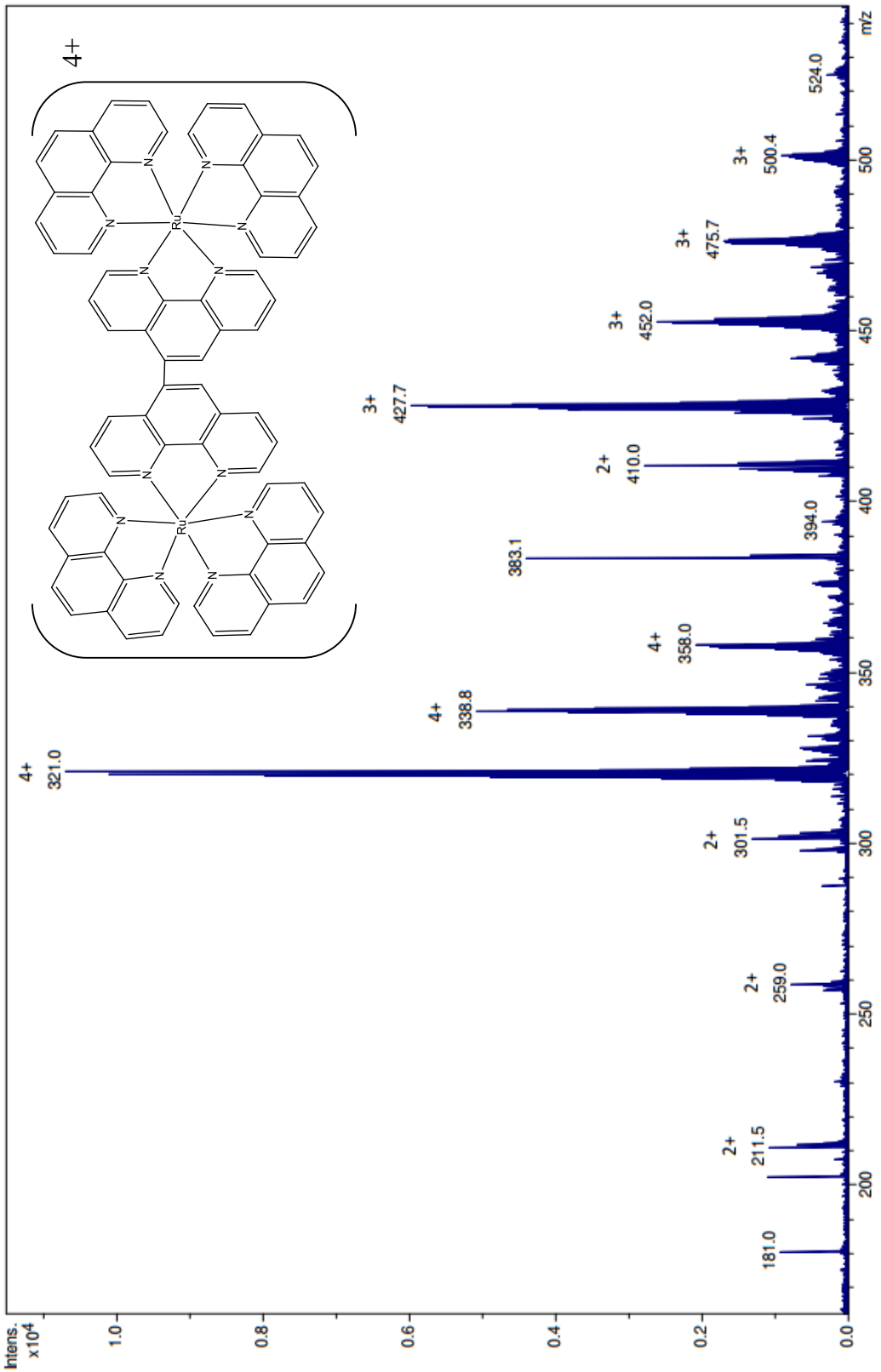
4+
Intens.
x10^4
1.0
0.8
0.6
0.4
0.2
0.0
m/z
200
250
300
350
400
450
500
4+
321.0
4+
338.8
4+
358.0
2+
259.0
2+
211.5
2+
301.5
181.0
383.1
394.0
2+
410.0
3+
427.7
3+
452.0
3+
475.7
3+
500.4
524.0

Figure 3.2.8. Enlarged portion of ESI-MS spectrum for $[(phen)_2Ru(diphen)Ru(phen)_2](PF_6)_4$.

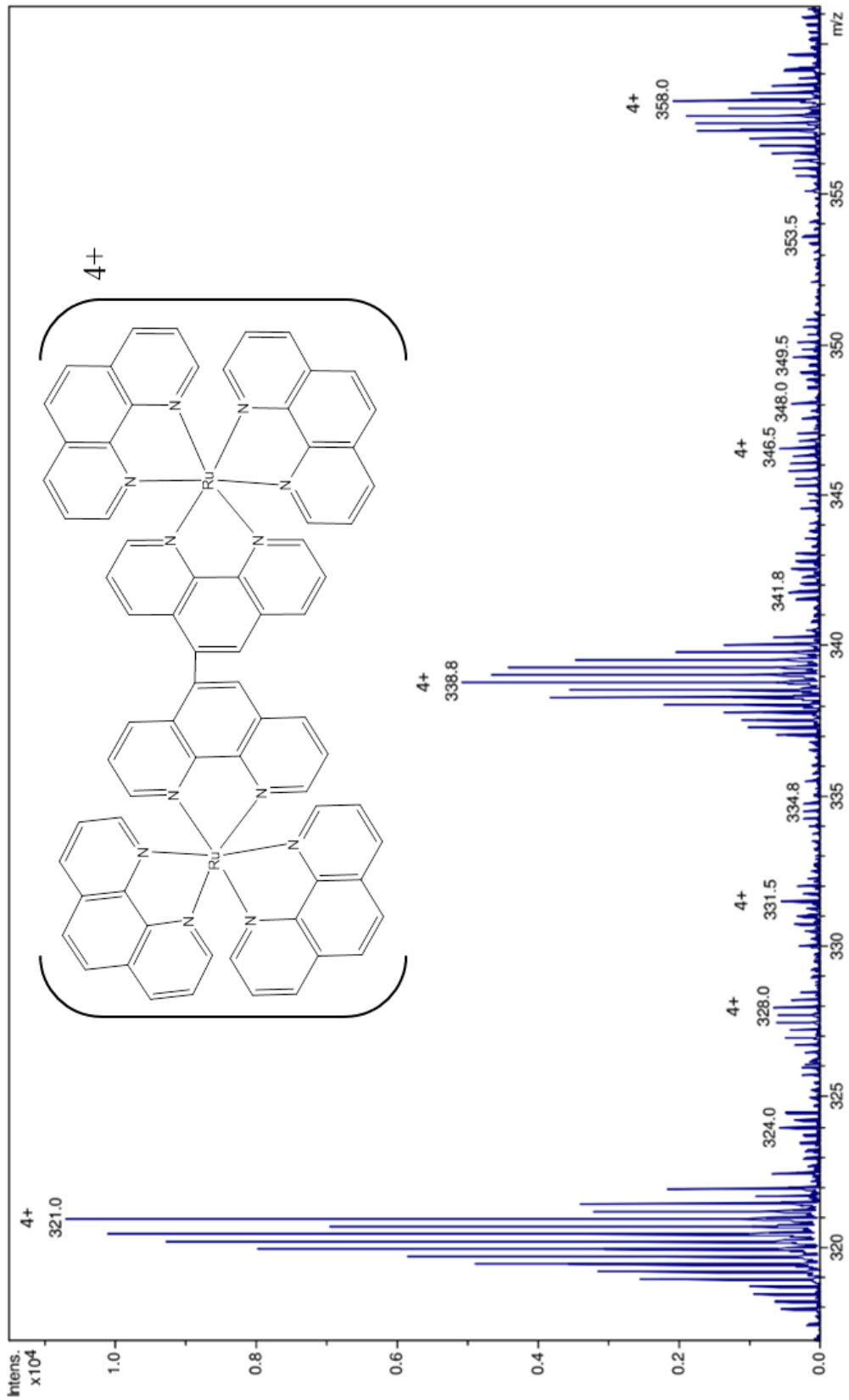
4+
Ru
Ru
Intens.
x10^4
1.0
0.8
0.6
0.4
0.2
0.0
4+
321.0
4+
324.0
4+
328.0
4+
331.5
334.8
4+
338.8
341.8
4+
346.5
348.0
349.5
353.5
4+
358.0
320
325
330
335
340
345
350
355
m/z

After the successful synthesis of $[(phen)_2Ru(diphen)Ru(phen)_2](PF_6)_4$, the additional dimeric complexes produced were $[(dpphen)_2Ru(diphen)Ru(dpphen)_2](PF_6)_4$, $[(tmphen)_2Ru(diphen)Ru(tmphen)_2](PF_6)_4$, $[(bpy)_2Ru(diphen)Ru(bpy)_2](PF_6)_4$, and $[(dmb)_2Ru(diphen)Ru(dmb)_2](PF_6)_4$. The IR spectra, UV-vis spectra, and the cyclic voltammogram collected for the additional dimeric complexes were all similar to the spectra and voltammogram shown above for $[(phen)_2Ru(diphen)Ru(phen)_2](PF_6)_4$. The spectroscopic and electrochemical data for the complexes are collected in Table 3.4.1.

The ESI-MS spectra for $[(dpphen)_2Ru(diphen)Ru(dpphen)_2](PF_6)_4$ are seen in Figures 3.2.9 and 3.2.10. The peak at 472.6 m/z is as expected for $(dpphen)_2Ru(diphen)Ru(dpphen)_2^{4+}$. The peak at 333.1 m/z is as expected for the dpphen free ligand.

The ESI-MS spectra for $[(tmphen)_2Ru(diphen)Ru(tmphen)_2](PF_6)_4$ are seen below in Figures 3.2.11 and 3.2.12. The peak at 376.4 m/z is as expected for $(tmphen)_2Ru(diphen)Ru(tmphen)_2]^+$, and the peak at 501.9 m/z is expected for $(tmphen)_2Ru(diphen)Ru(tmphen)_2^{3+}$. Other peaks seen are possibly additional fragmentation of the dimeric complex, such as the peak at 394.6 m/z, which differs by 72.62 g/mol from $(tmphen)_2Ru(diphen)Ru(tmphen)_2^{4+}$.

$[(dmb)_2Ru(diphen)Ru(dmb)_2](PF_6)_4$ ESI-MS spectra are seen in Figures 3.2.13 and 3.2.14. The peak expected for $(dmb)_2Ru(diphen)Ru(dmb)_2^{4+}$ is seen at 324.6 m/z. The peak at 433.1 m/z is the $(dmb)_2Ru(diphen)Ru(dmb)_2^{3+}$ peak. Additional peaks are due to further fragmentation of the complex.

Figures 3.2.15 and 3.2.16 show ESI-MS spectra for $[(bpy)_2Ru(diphen)Ru(bpy)_2](PF_6)_4$. $(bpy)_2Ru(diphen)Ru(bpy)_2^{4+}$ is expected at 296.5 m/z, and $(bpy)_2Ru(diphen)Ru(bpy)_2^{3+}$ is seen

as expected at 395.7 m/z. Other peaks are small in comparison, and possibly due to continued fragmentation of $(bpy)_2Ru(diphen)Ru(bpy)_2^{4+}$.

Figure 3.2.9. Full ESI-MS for $[(dpphen)_2Ru(diphen)Ru(dpphen)_2](PF_6)_4$.

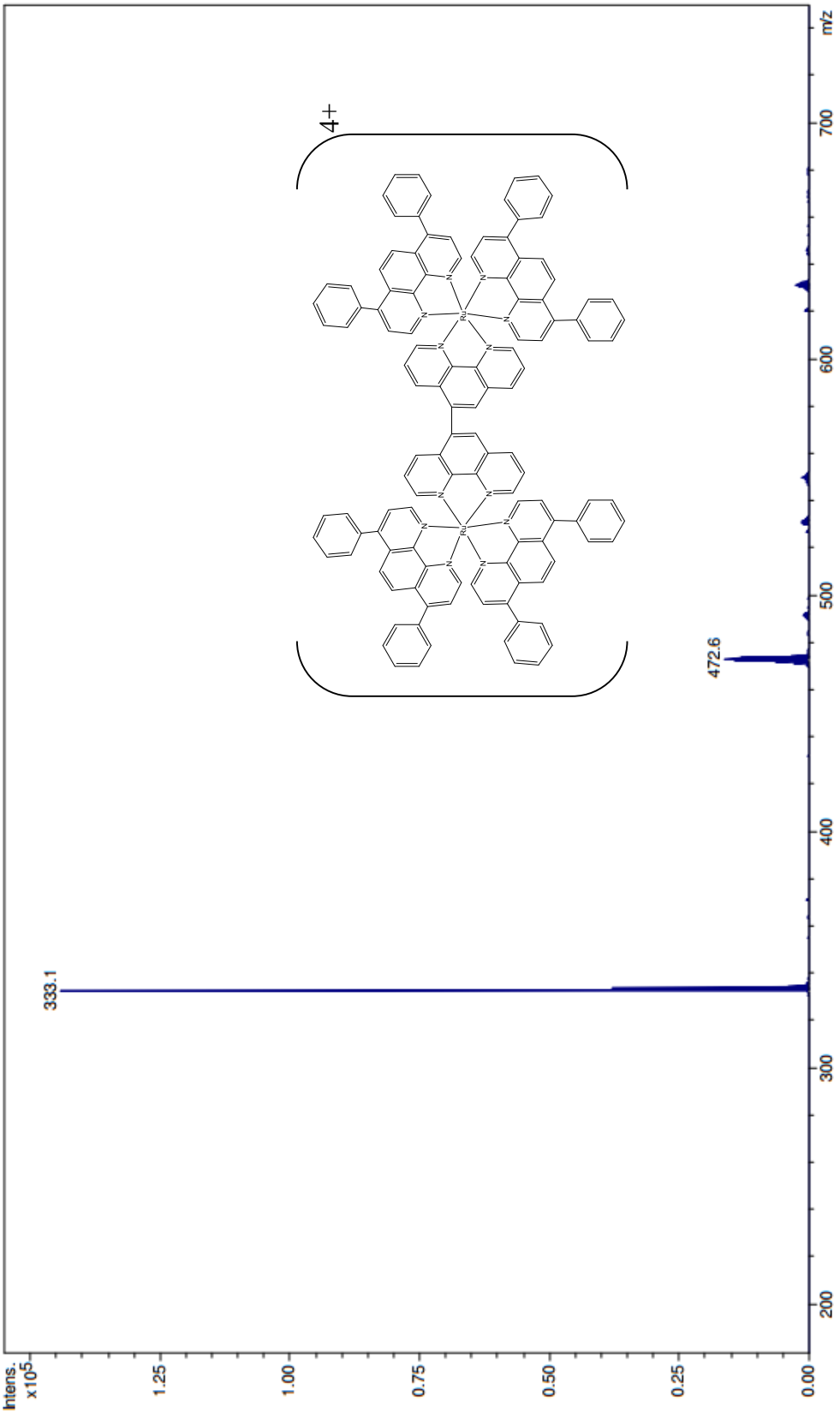
4+
333.1
472.6
Intens.
x10^5
1.25
1.00
0.75
0.50
0.25
0.00
200
300
400
500
600
700
m/z

Figure 3.2.10. Portion of ESI-MS spectrum for $[(dpphen)_2Ru(diphen)Ru(dpphen)_2](PF_6)_4$.

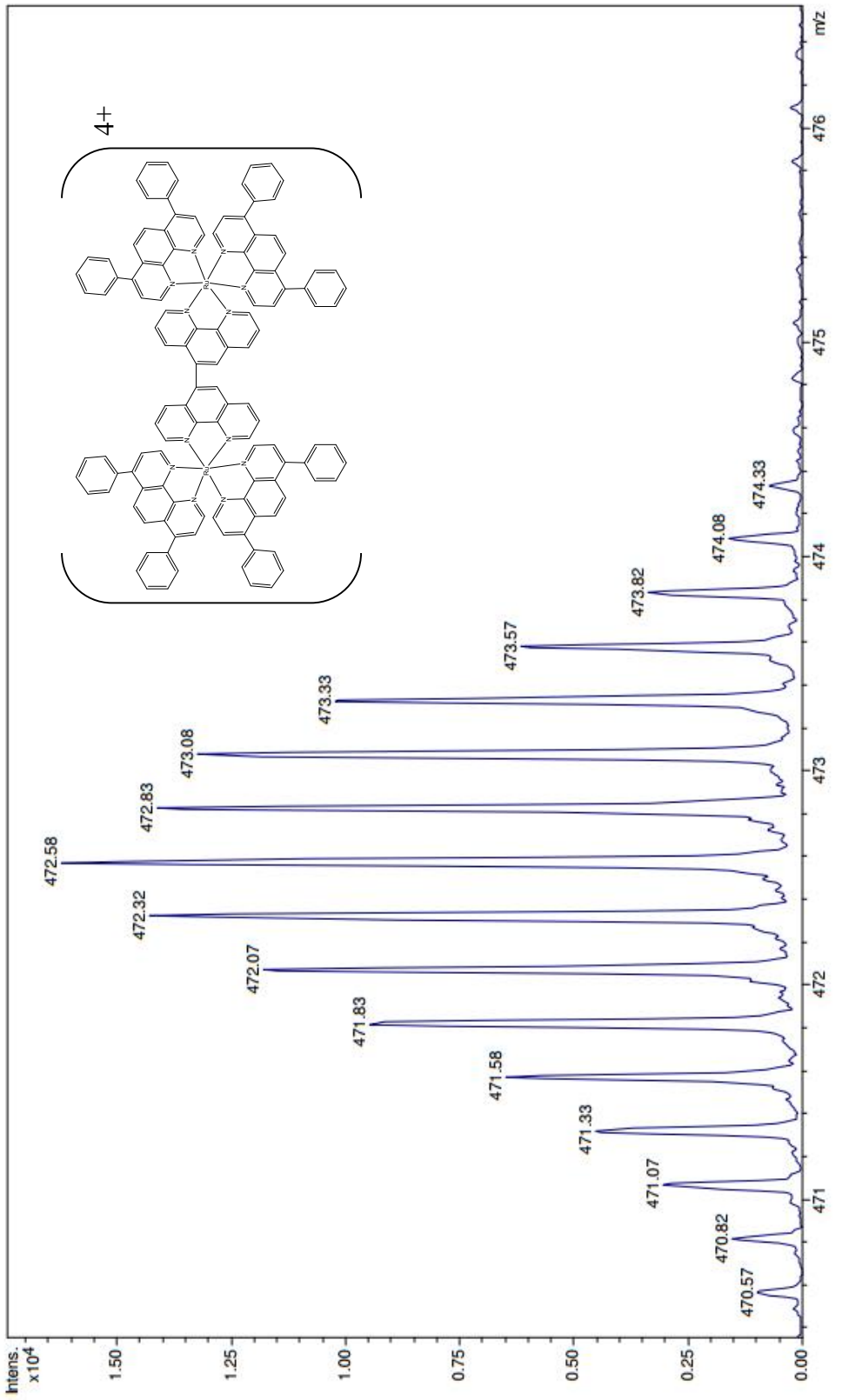
4+
Intens.
x10^4
1.50
1.25
1.00
0.75
0.50
0.25
0.00
470.57
470.82
471.07
471.33
471.58
471.83
472.07
472.32
472.58
472.83
473.08
473.33
473.57
473.82
474.08
474.33
471
472
473
474
475
476
m/z

Figure 3.2.11. Full ESI-MS for $[(tmphen)_2Ru(diphen)Ru(tmphen)_2](PF_6)_4$.

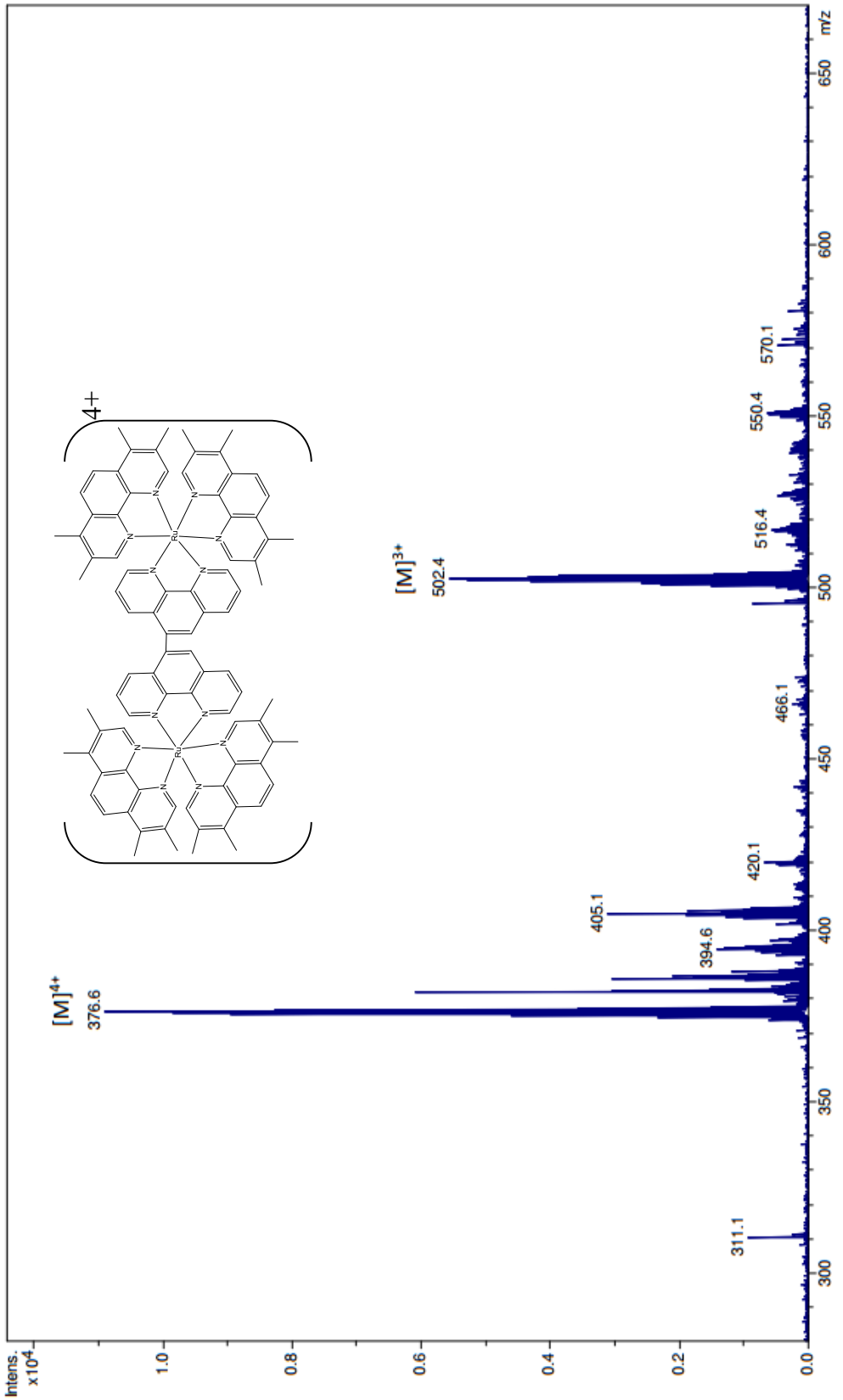
Intens.
x10^4
1.0
0.8
0.6
0.4
0.2
0.0
300
350
400
450
500
550
600
650
m/z
[M]4+
376.6
[M]3+
502.4
4+
311.1
394.6
405.1
420.1
466.1
516.4
550.4
570.1

Figure 3.2.12. Portion of ESI-MS spectrum of $[(tmphen)_2Ru(diphen)Ru(tmphen)_2](PF_6)_4$.

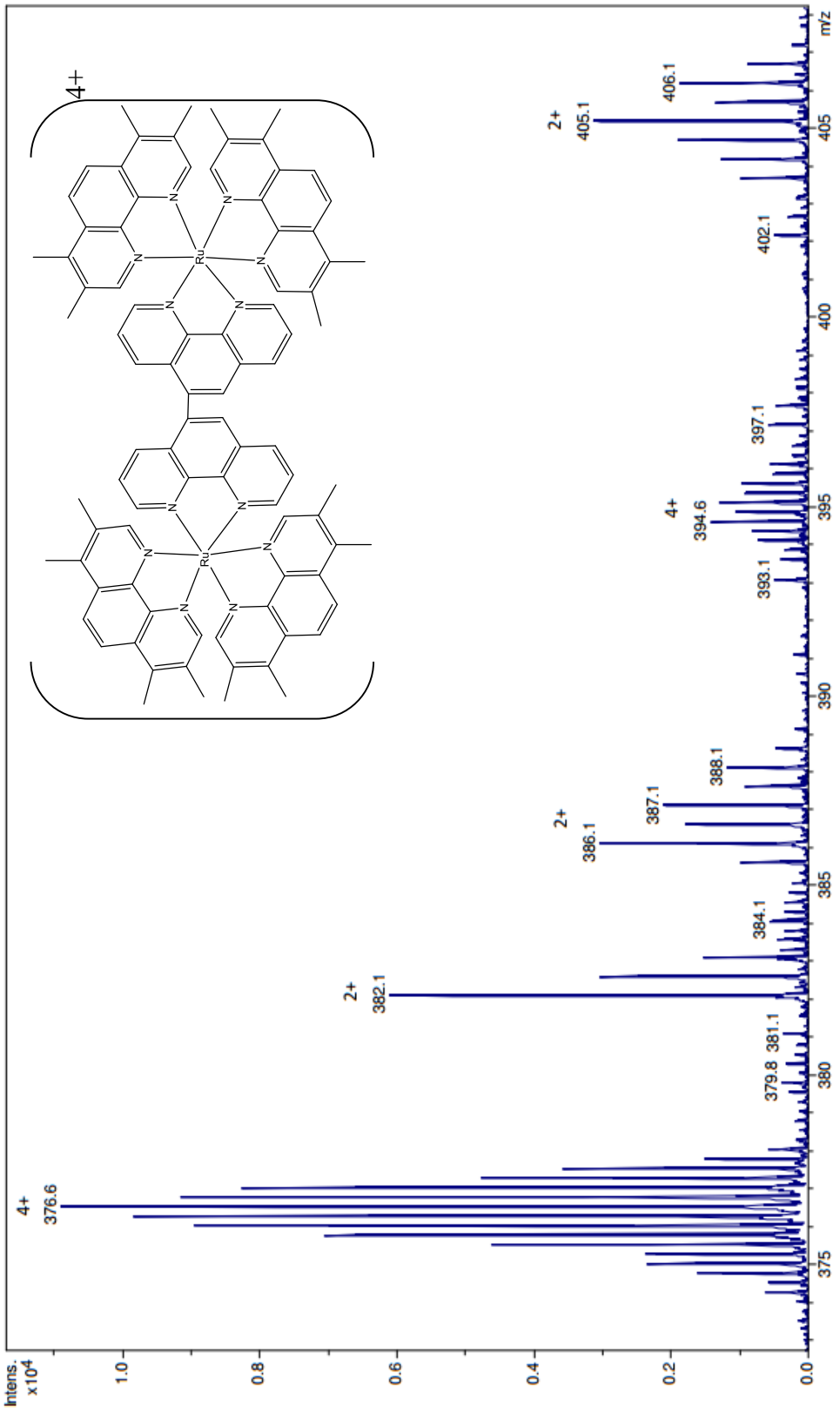
4+
Intens.
x10^4
1.0
0.8
0.6
0.4
0.2
0.0
4+
376.6
2+
382.1
2+
386.1
2+
405.1
4+
394.6
379.8
381.1
384.1
387.1
388.1
393.1
397.1
402.1
406.1
375
380
385
390
395
400
405
m/z

Figure 3.2.13. Full ESI-MS spectrum for $[(dmb)_2Ru(diphen)Ru(dmb)_2](PF_6)_4$.

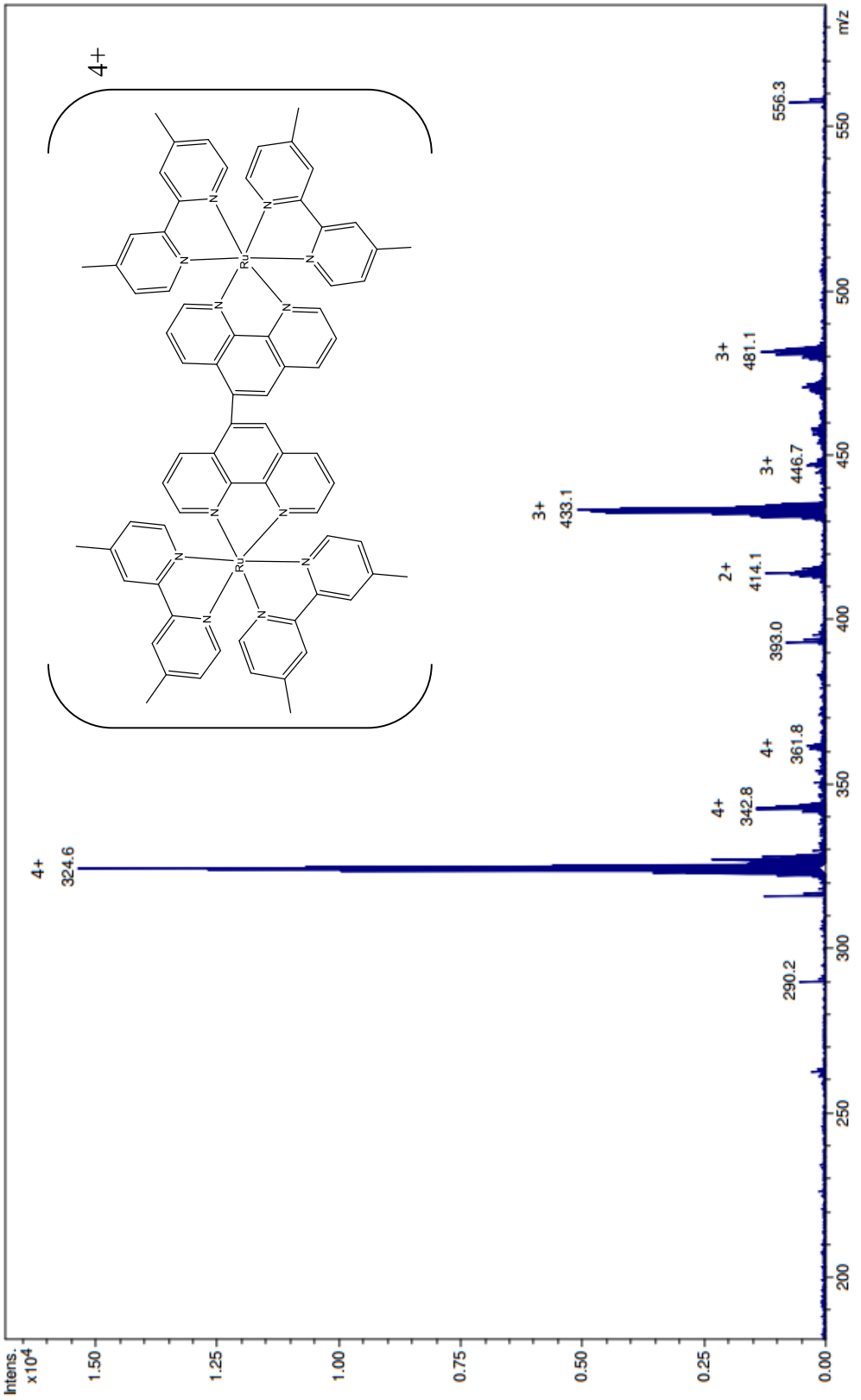
4+
Intens.
x10^4
1.50
1.25
1.00
0.75
0.50
0.25
0.00
200
250
300
350
400
450
500
550
m/z
4+
324.6
290.2
4+
342.8
4+
361.8
393.0
2+
414.1
3+
433.1
3+
446.7
3+
481.1
556.3

Figure 3.2.14. Portion of ESI-MS for $[(dmb)_2Ru(diphen)Ru(dmb)_2](PF_6)_4$.

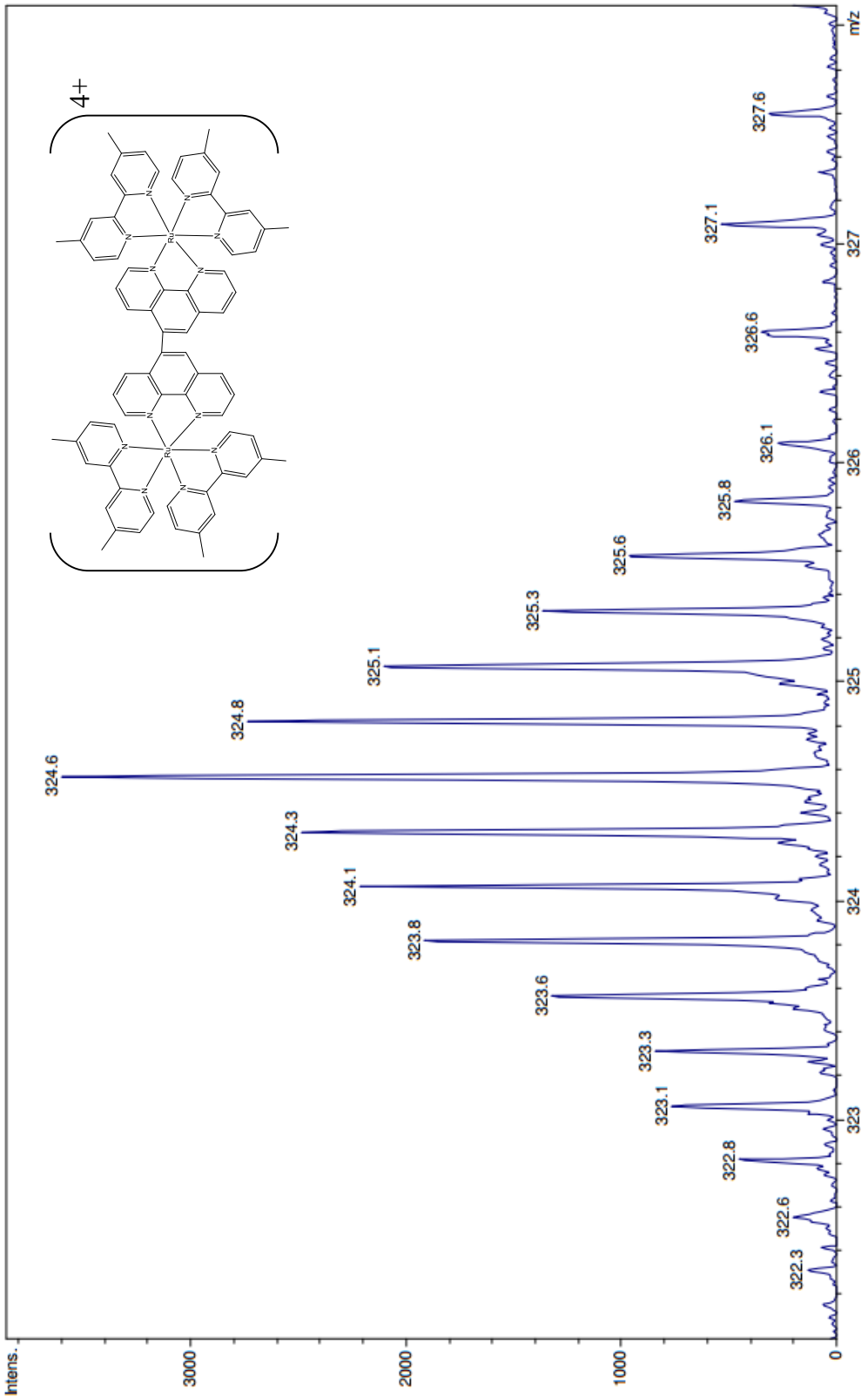
4+
Intens.
3000
2000
1000
0
322.3
322.6
322.8
323.1
323.3
323.6
323.8
324.1
324.3
324.6
324.8
325.1
325.3
325.6
325.8
326.1
326.6
327.1
327.6
323
324
325
326
327
m/z

Figure 3.2.15. Full ESI-MS spectrum showing the peaks for $[(bpy)_2Ru(diphen)Ru(bpy)_2](PF_6)_4$.

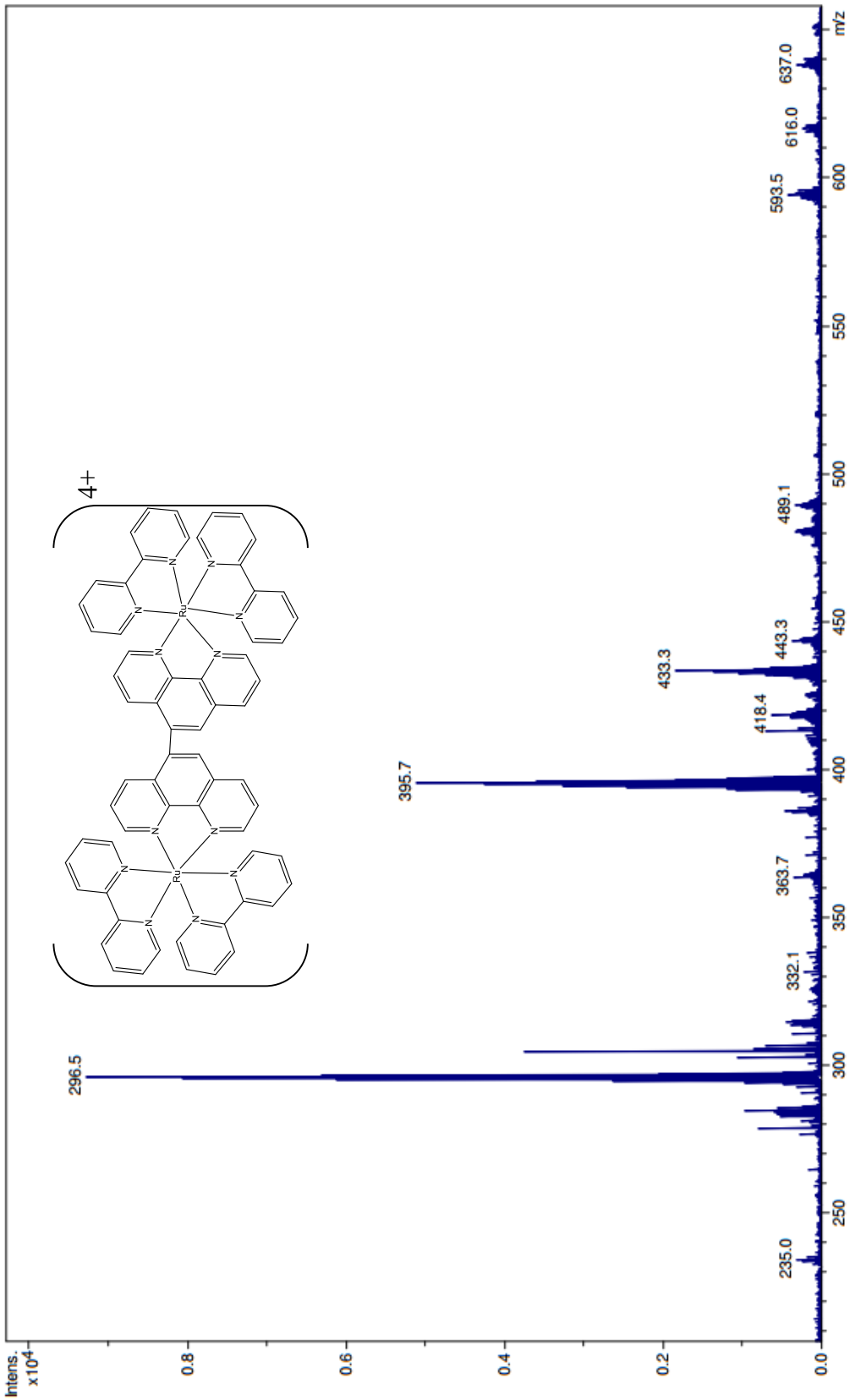
4+
Intens.
x10^4
0.0
0.2
0.4
0.6
0.8
m/z
235.0
250
296.5
300
332.1
350
363.7
395.7
400
418.4
433.3
443.3
450
489.1
500
550
593.5
600
616.0
637.0

Figure 3.2.16. Portion of ESI-MS spectrum for $[(bpy)_2Ru(diphen)Ru(bpy)_2](PF_6)_4$.

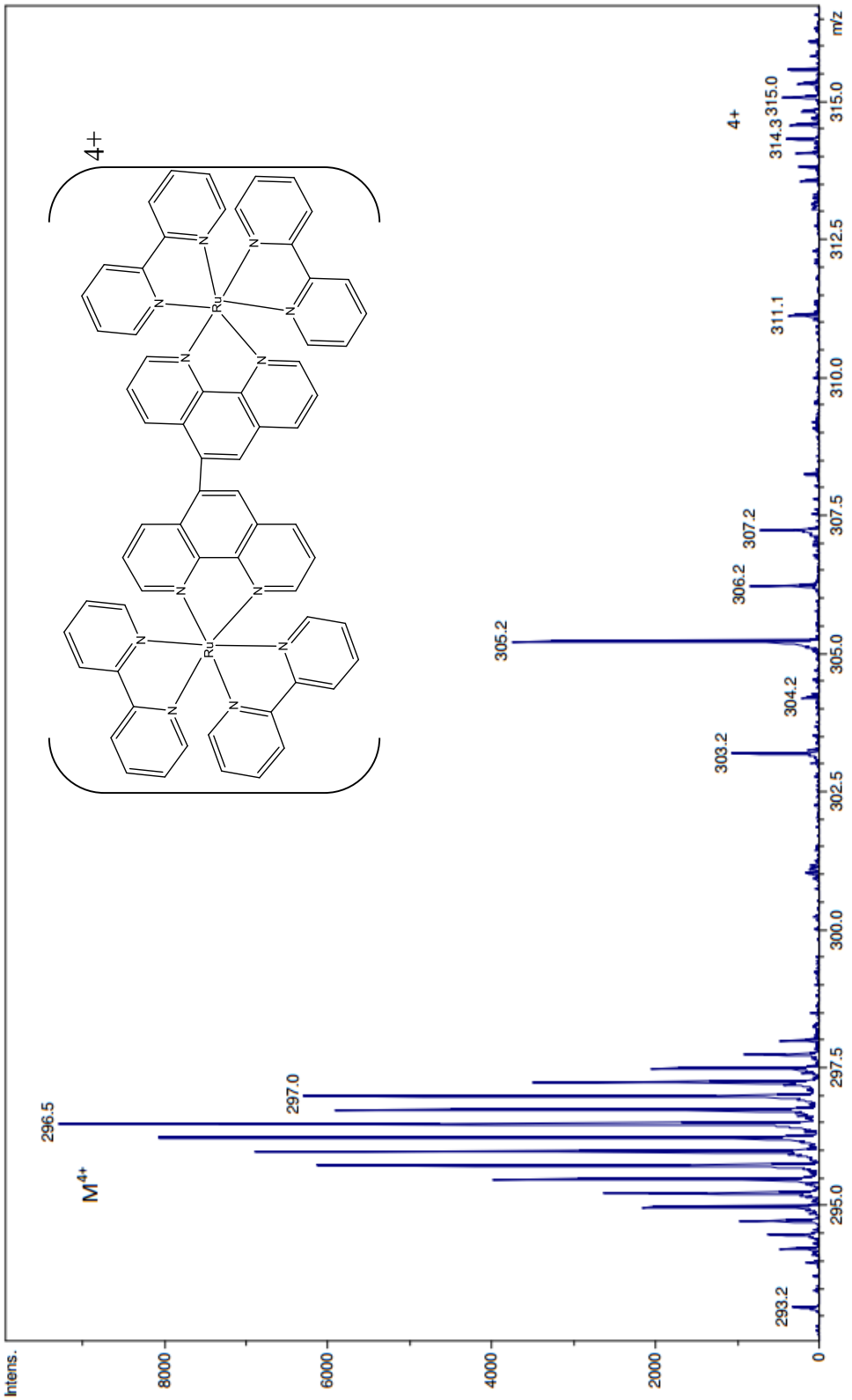
4+
Ru
Intens.
8000
6000
4000
2000
0
M4+
296.5
297.0
293.2
295.0
297.5
300.0
302.5
303.2
304.2
305.2
305.0
306.2
307.2
307.5
310.0
311.1
312.5
314.3
315.0
315.0
m/z

3.3 Investigation of Bridging Ligands in Improved Synthetic Route for Dimeric Ruthenium(II) Complexes

In order to test the generality of the procedure, a bridging ligand commonly used in the literature was examined. Dpp, 2,3-Bis(2-pyridyl)-pyrazine, was reacted with $[Ru(CO)_2Cl_2]_n$ to produce $(CO)_2Cl_2Ru(dpp)Ru(CO)_2Cl_2$. The IR spectrum was compared to the IR spectrum for $[Ru(CO)_2Cl_2]_n$. This is shown in Figure 3.3.1 below. Figure 3.3.1(b) shows 2 peaks at 2010 and 2065 cm^{-2} from CO stretching in $(CO)_2Cl_2Ru(dpp)Ru(CO)_2Cl_2$. These two peaks are consistent with the expected asymmetric and symmetric stretching bands typically seen in complexes containing two carbonyl groups.

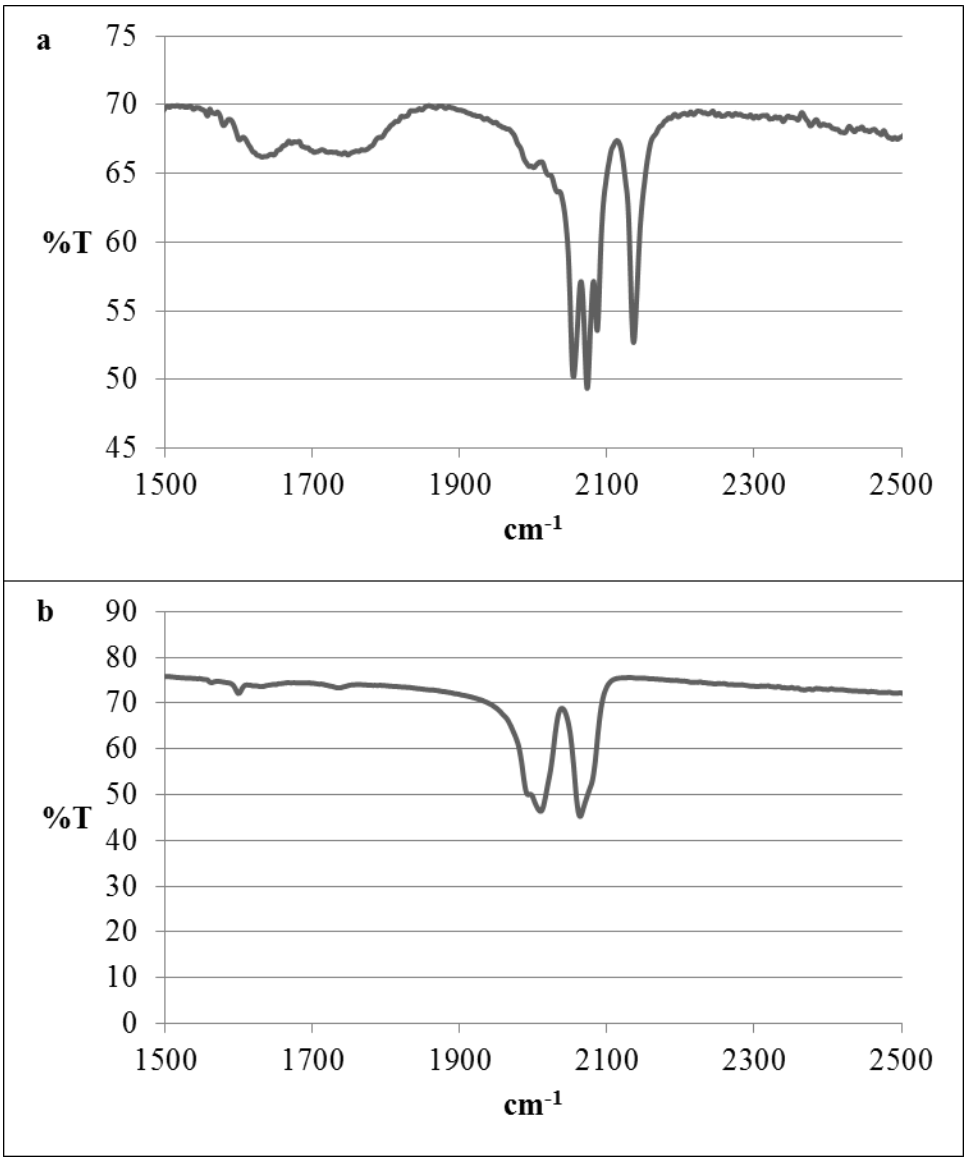

Figure 3.3.1. IR spectra (KBr pellet) comparison for $[Ru(CO)_2Cl_2]_n$ and $(CO)_2Cl_2Ru(dpp)Ru(CO)_2Cl_2$.

$(CO)_2Cl_2Ru(dpp)Ru(CO)_2Cl_2$ was then reacted with phen. The expected product, $[(phen)_2Ru(dpp)Ru(phen)_2](PF_6)_4$, was analyzed via spectroscopic and electrochemical techniques. IR analysis confirmed the absence of peaks due to CO. The spectrum in Figure 3.3.2 is over the range expected for CO bands.

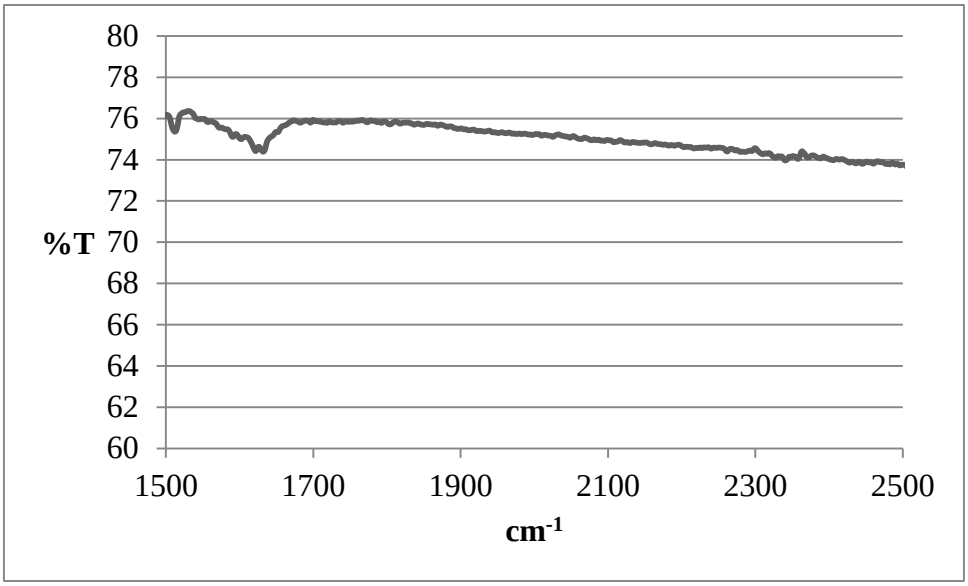

Figure 3.3.2. IR spectra (KBr pellet) for $[(phen)_2Ru(dpp)Ru(phen)_2](PF_6)_4$, which shows the absence of CO stretching peaks.

The λ_{max} value for $[(phen)_2Ru(dpp)Ru(phen)_2](PF_6)_4$ was at 446 nm, and can be seen in Figure 3.3.3. This value matches exactly with the λ_{max} value of the similar monomeric complex $Ru(phen)_3^{2+}$.

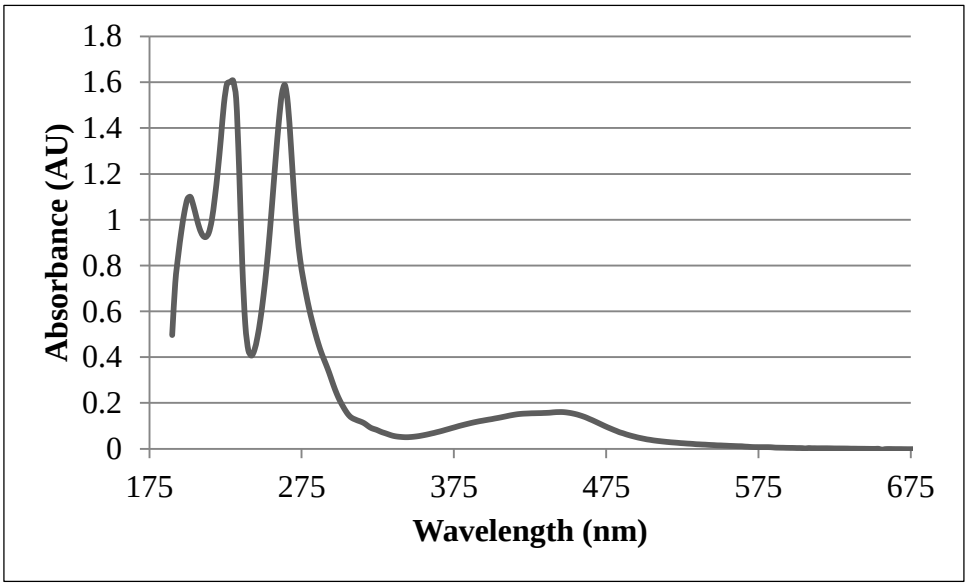

Figure 3.3.3. UV-vis spectrum for $[(phen)_2Ru(dpp)Ru(phen)_2](PF_6)_4$ in acetonitrile.

The cyclic voltammogram for $[(phen)_2Ru(dpp)Ru(phen)_2](PF_6)_4$ is Figure 3.3.4. The redox potential for the complex was found to be 1.304 V vs SCE. This value was very close to the redox potential of 1.309 V vs SCE for $Ru(phen)_3^{2+}$. It is also similar to an averaged redox potential for $(bpy)_2Ru(dpp)Ru(bpy)_2^{4+}$ reported in the literature, 1.34 V vs SCE, which was adjusted to SCE from Ag/AgCl reference electrode (Seneviratne, et al., 2002). Spectroscopic and electrochemical data can be seen in Table 3.4.1.

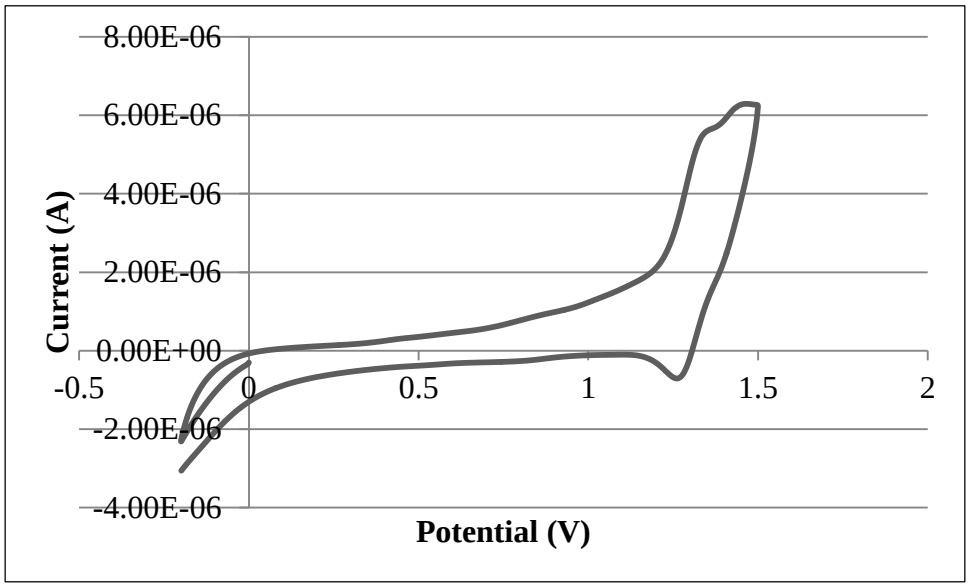

Figure 3.3.4. Cyclic Voltammogram for $[(phen)_2Ru(dpp)Ru(phen)_2](PF_6)_4$ (0.1M $TBAPF_6$ in acetonitrile, SCE).

3.4 Dimeric Complex Synthesis Applied to Monomeric Complexes

The same synthetic route used for the dimeric complexes was applied to the synthesis of monomeric ruthenium(II) complexes. $[Ru(CO)_2Cl_2]_n$ was heated with phen to produce $Ru(CO)_2Cl_2(phen)$. The IR spectra for $[Ru(CO)_2Cl_2]_n$ and $Ru(CO)_2Cl_2(phen)$ are compared in Figure 3.4.1. In Figure 3.4.1(b), peaks are seen at 1973 cm^{-1} and 2054 cm^{-1} for $Ru(CO)_2Cl_2(phen)$. These two peaks are the anticipated symmetric and asymmetric stretching bands for a complex containing two carbonyl groups.

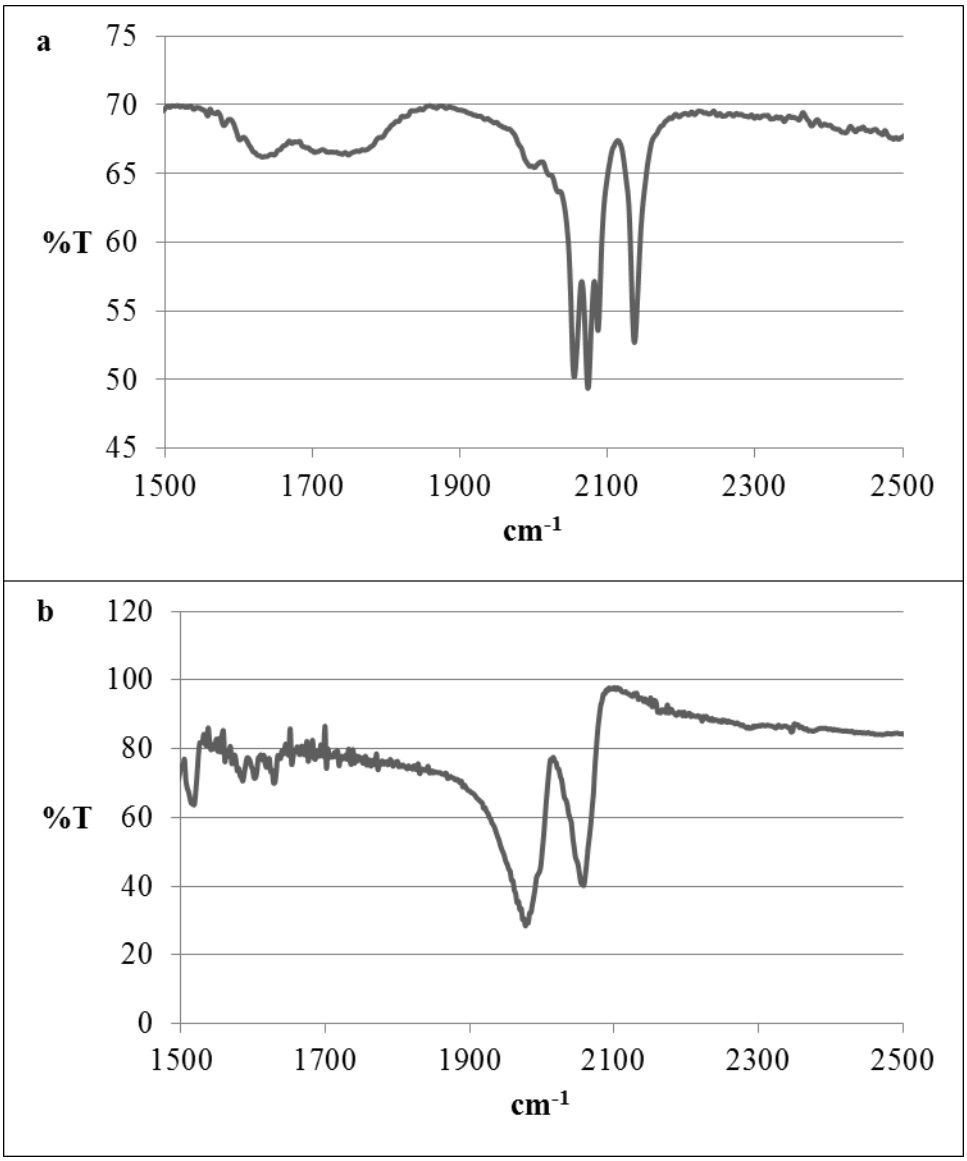

Figure 3.4.1. IR spectra (KBr pellet) comparison for $[Ru(CO)_2Cl_2]_n$ and $Ru(CO)_2Cl_2(phen)$.

The monomeric complexes were synthesized for comparison to the dimeric complexes, so $[Ru(phen)(dpphen)_2](PF_6)_2$, $[Ru(phen)(tmphen)_2](PF_6)_2$, $[Ru(phen)(bpy)_2](PF_6)_2$, and $[Ru(phen)(dmb)_2](PF_6)_2$ were synthesized by heating $Ru(CO)_2Cl_2(phen)$ with the desired ligand.

The products were analyzed using spectroscopic and electrochemical techniques. IR spectra showed the absence of the carbonyl group for $[Ru(phen)(dpphen)_2](PF_6)_2$ and $[Ru(phen)(tmphen)_2](PF_6)_2$. The spectrum for $[Ru(phen)(dpphen)_2](PF_6)_2$ is shown over the range expected for CO bands in Figure 3.4.2.

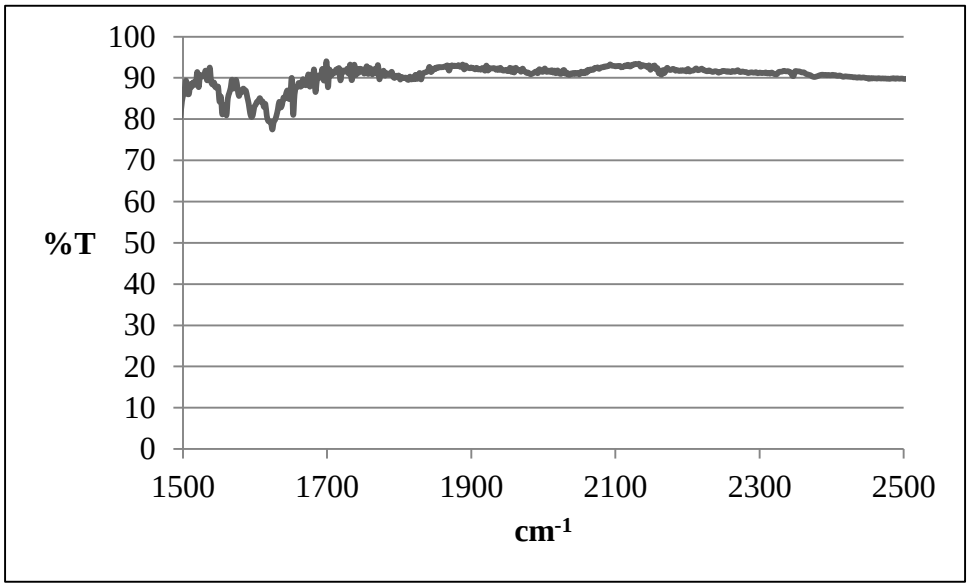

Figure 3.4.2. IR spectrum (KBr pellet) for $[Ru(phen)(dpphen)_2](PF_6)_2$.

IR spectra for $[Ru(phen)(bpy)_2](PF_6)_2$ and $[Ru(phen)(dmb)_2](PF_6)_2$ revealed that there was still a carbonyl group present on some of the product. Figure 3.4.3 is the IR spectrum for $[Ru(phen)(bpy)_2](PF_6)_2$, and a peak at 1963 cm^{-1}. This is band is consistent with symmetric and asymmetric stretching band normally found in complexes containing a carbonyl group.

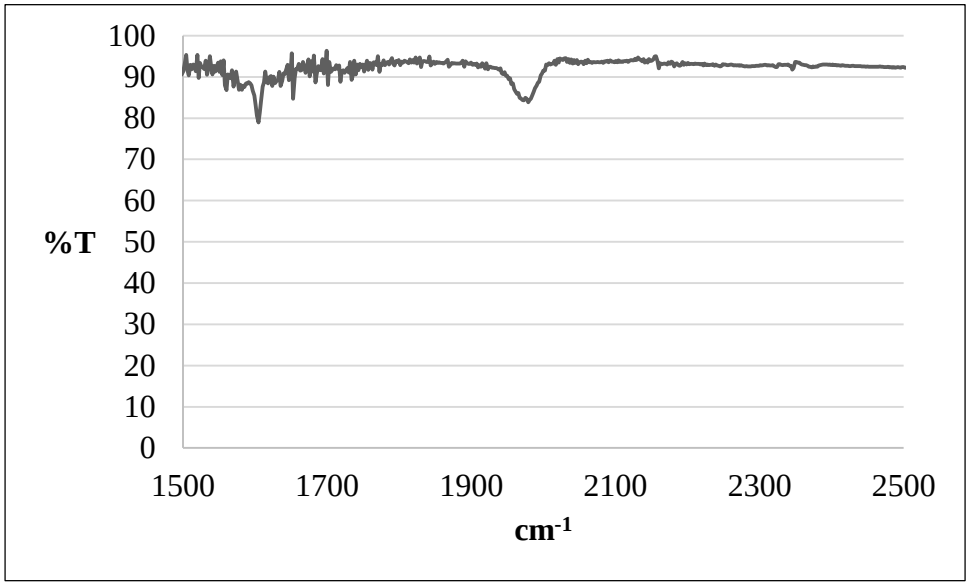

Figure 3.4.3. IR spectrum (KBr pellet) for $[Ru(phen)(bpy)_2](PF_6)_2$.

The UV-vis spectrum for $[Ru(phen)(dpphen)_2](PF_6)_2$ is shown in Figure 3.4.4 and had a λ_{max} at 456 nm. The shift from the $Ru(phen)_3^{2+}$ maxima value of 446 nm is expected due to the added phenyl groups.

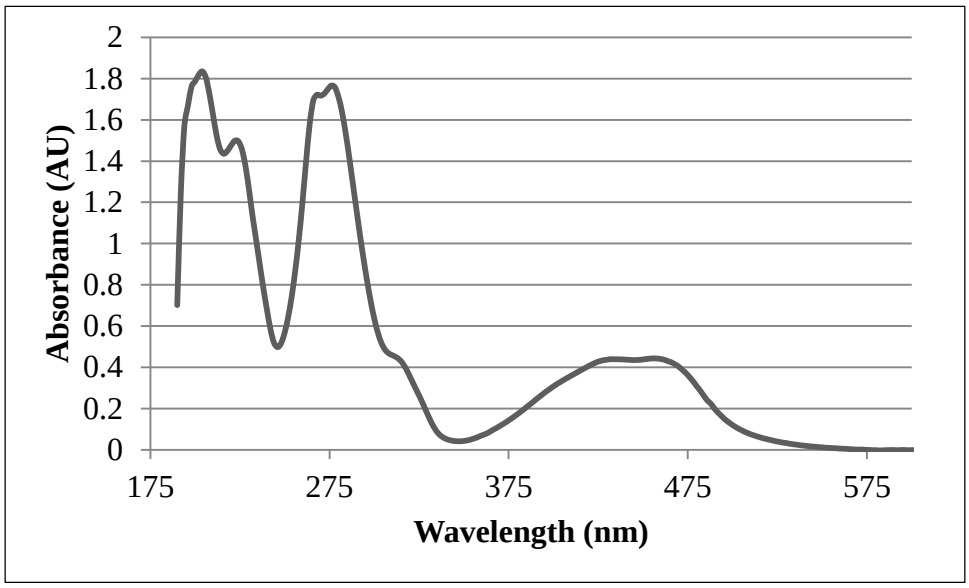

Figure 3.4.4. UV-vis spectrum for $[Ru(phen)(dpphen)_2](PF_6)_2$ in acetonitrile.

The cyclic voltammogram in Figure 3.4.5 for $[Ru(phen)(tmphen)_2](PF_6)_2$ shows an redox potential of 1.107 V vs SCE. This value differs from 1.309 V vs SCE for $Ru(phen)_3^{2+}$, which is expected due to the phenyl groups. Spectrocopic and electrochemical data for all monomeric complexes, including $[Ru(phen)_3](PF_6)_2$, is compiled in Table 3.4.1.

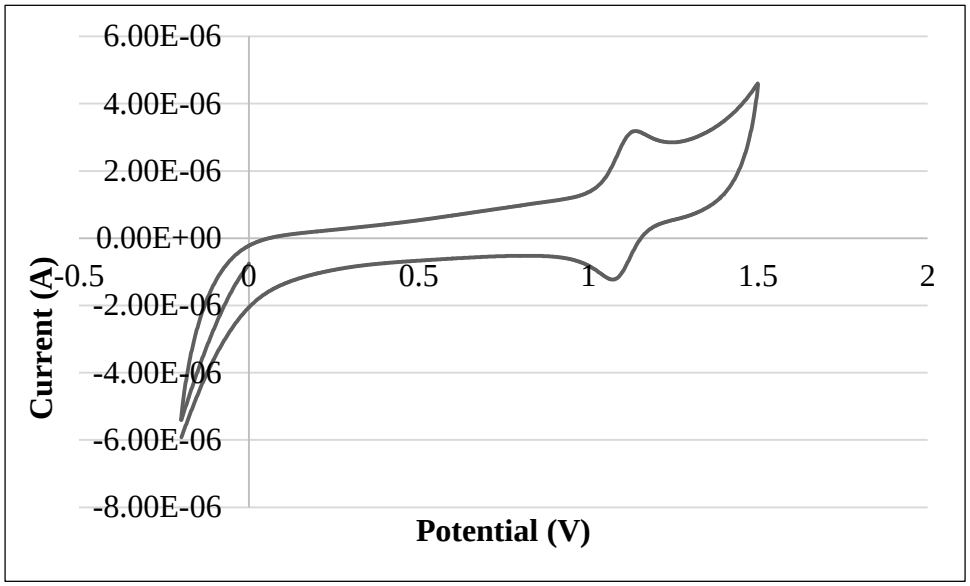

Figure X. Cyclic voltammogram for $[Ru(phen)(tmphen)_2](PF_6)_2$ (0.1M $TBAPF_6$ in acetonitrile, SCE).

Table 3.4.1. Spectroscopic and electrochemical data for ruthenium(II) polypyridine complexes.

Complex	**λ_{max} (nm)**	**2+/3+ vs SCE (V)**	**τ_0 (nsec)**	
			0.5 M H_2SO_4	**CH_3CN**
$Ru(bpy)_3^{2+}$	452	1.29	590	---
$Ru(phen)(bpy)_2^{2+}$	450	1.269	690	---
$(bpy)_2Ru(diphen)Ru(bpy)_2^{4+}$	452	1.297	1000	---
$Ru(phen)(dmb)_2^{2+}$	454	1.161	930	---
$(dmb)_2Ru(diphen)Ru(dmb)_2^{4+}$	458	1.200	1000	---
$Ru(phen)_3^{2+}$	446	1.309	1000	1120
$(phen)_2Ru(diphen)Ru(phen)_2^{4+}$	448	1.308	1470	960
$Ru(phen)(tmphen)_2^{2+}$	427	1.107	1130	---
$(tmphen)_2Ru(diphen)Ru(tmphen)_2^{4+}$	432	1.152	1000	---
$Ru(phen)(dpphen)_2^{2+}$	456	1.236	---	---
$(dpphen)_2Ru(diphen)Ru(dpphen)_2^{4+}$	460	1.282	---	---
$(phen)_2Ru(dpp)Ru(phen)_2^{4+}$	446	1.304	---	---

3.5 Photosubstitution Reactions of Dimeric Ruthenium(II) Polypyridine Complexes

Photochemistry was first carried out using a 300 watt, 120 volt bulb "sunlamp" with no filtering. The photochemical reaction of $[(phen)_2Ru(diphen)Ru(phen)_2](PF_6)_4$ in a solution of dichloromethane and tetrabutylammonium bromide was monitored via UV-vis spectroscopy. The

spectra can be seen in Figure 3.5.1. The peak at 448 nm, which is correlates to the $(phen)_2Ru(diphen)Ru(phen)_2^{4+}$ concentration, decreases over time. This is the expected result of a photosubstitution reaction where a phen ligand on $(phen)_2Ru(diphen)Ru(phen)_2^{4+}$ is removed and replaced by bromines, which decreases the $(phen)_2Ru(diphen)Ru(phen)_2^{4+}$ concentration. The peak in Figure 3.5.1 at 550 nm increases over time. This is also an expected peak due to the photosubstitution reaction. This is consistent with the phen ligand being replaced by bromines, and the concentration of the new product increasing.

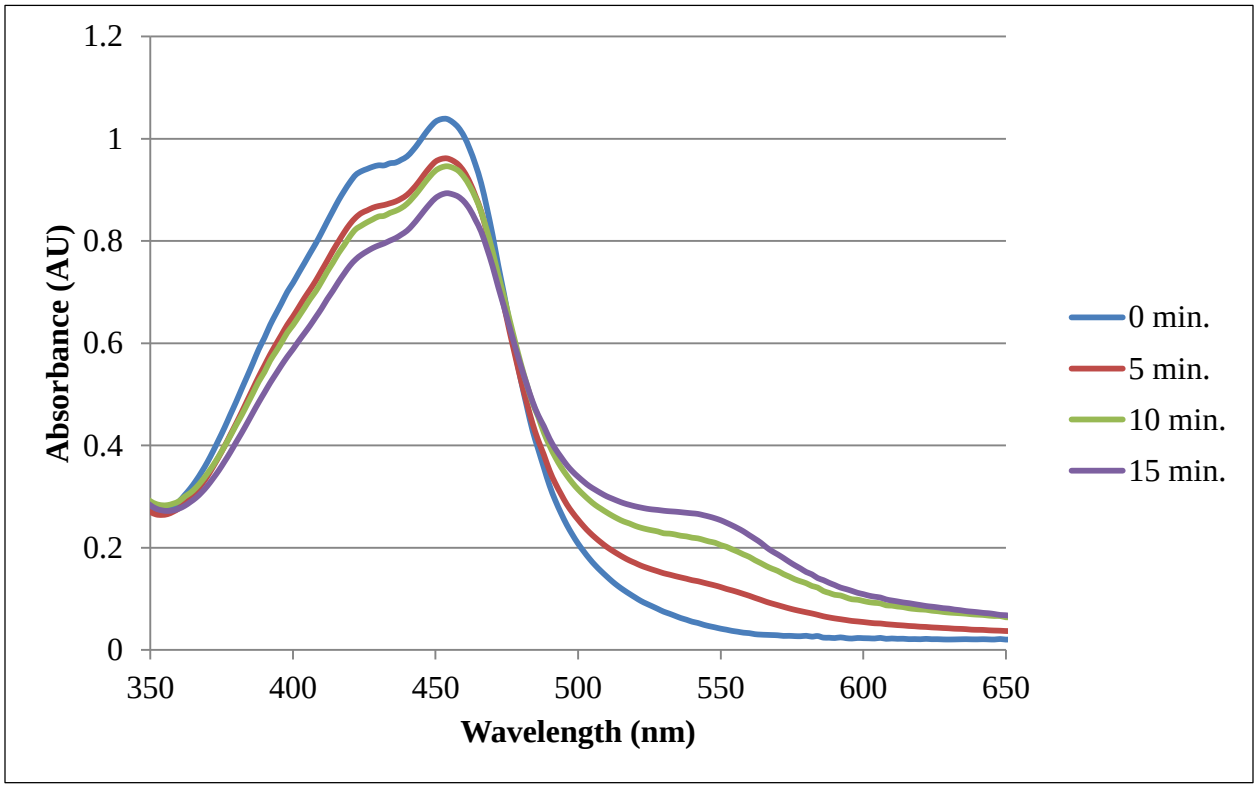

Figure 3.5.1. UV-Vis spectrum for $[(phen)_2Ru(diphen)Ru(phen)_2](PF_6)_4$ taken at intervals during UV irradiation with a 300 watt, 120 volt bulb "sunlamp".

Reproducible results were seen when $[(phen)_2Ru(diphen)Ru(phen)_2]Br_4$ in dichloromethane was irradiated by a 300 watt, 120 volt bulb "sunlamp". The reaction was tracked using UV-vis spectroscopy, which can be seen in Figure 3.5.2. Again, the peak at 448 nm decreases, and the peak at 550 nm increases.

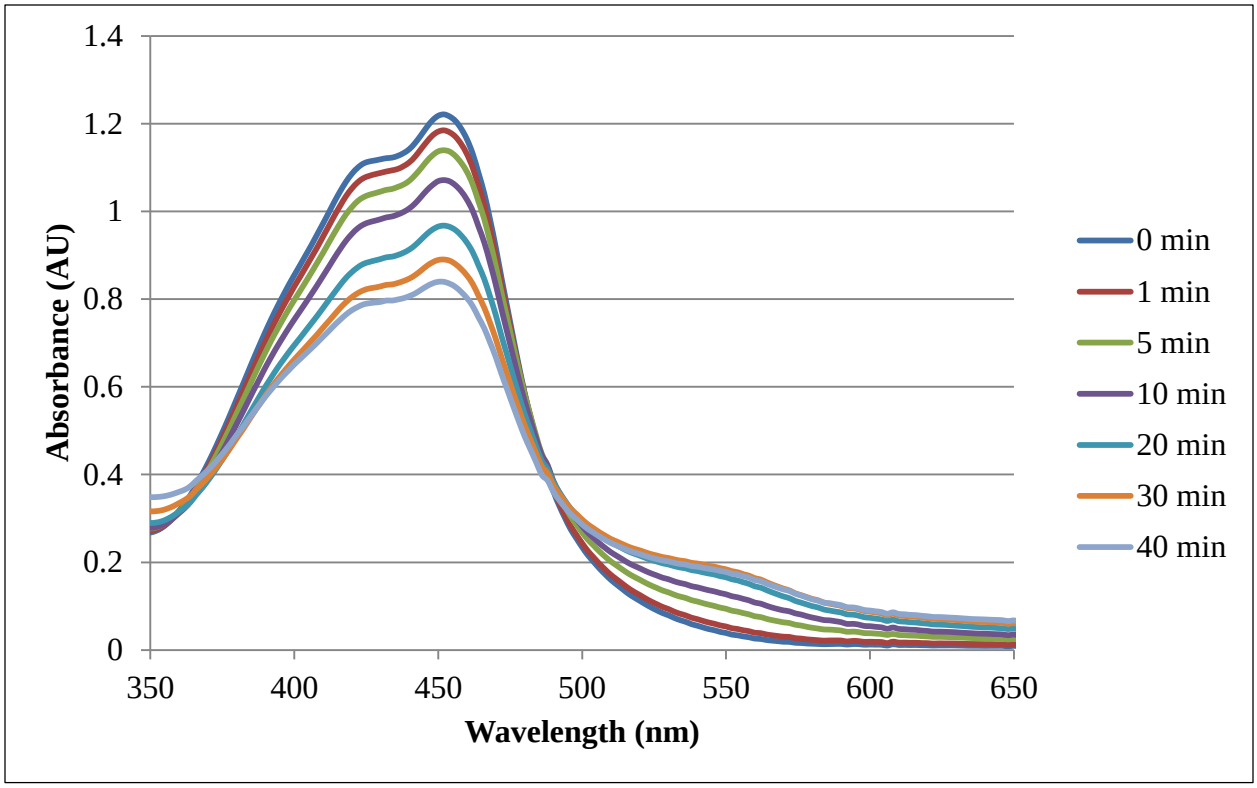

Figure 3.5.2. UV-Vis spectrum for $[(phen)_2Ru(diphen)Ru(phen)_2]Br_4$ taken at intervals during UV irradiation with a 300 watt, 120 volt bulb "sunlamp".

In order to determine the product of the photosubstitution reaction, the product was reacted with water and then the bpy ligand. The series of reactions was monitored using UV-vis spectroscopy and is shown in Figure 3.5.3. As expected, after irradiating $[(phen)_2Ru(diphen)Ru(phen)_2]Br_4$ in dichloromethane, the $(phen)_2Ru(diphen)Ru(phen)_2^{4+}$ peak at 448 nm decreases, and the photosubstitution reaction product peak at 550 nm increases. The dried photosubstitution reaction product was heated in water. The peak at 448 nm stays the same. This indicates that the concentration of $(phen)_2Ru(diphen)Ru(phen)_2^{4+}$ does not change, which was expected. The peak at 550 nm decreases, also as expected, indicating that the bromines on the reaction product are replaced by water. Bpy was then added to the reaction mixture. After heating, The peak at 448 nm increased as predicted with the formation of the expected product

$(phen)_2Ru(diphen)Ru(phen)(bpy)^{4+}$. The resulting product was sent for ESI-MS, but the results were inconclusive.

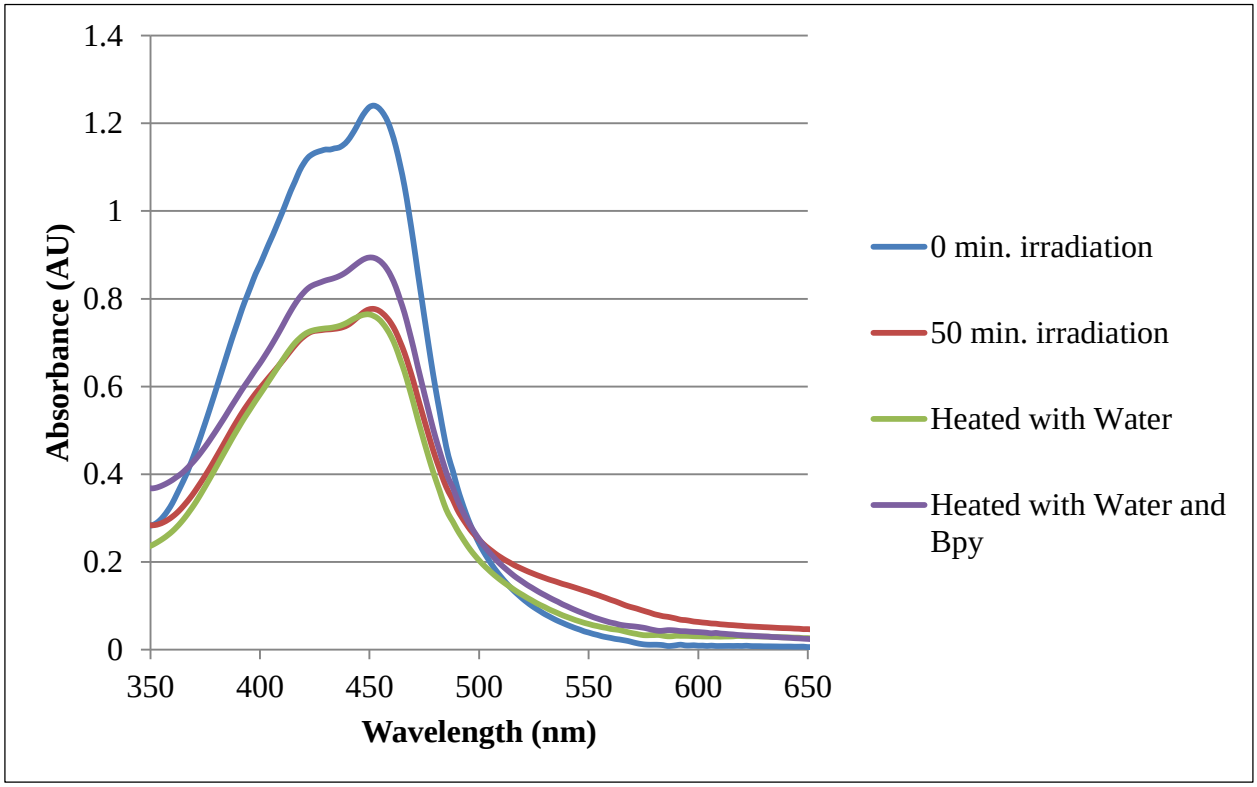

Figure 3.5.3. UV-vis spectrum for a series of reactions starting with $[(phen)_2Ru(diphen)Ru(phen)_2]Br_4$. Irradiation was performed using a 300 watt, 120 volt bulb "sunlamp".

A 1000 watt Xe bulb was also used for photochemical reactions. The reaction mixture consisted of $[(phen)_2Ru(diphen)Ru(phen)_2]Br_4$ in dichloromethane, and the reaction was monitored with UV-vis spectroscopy. Figure 3.5.4 shows the results. The results were not consistent with the usage of the 300 watt, 120 volt bulb "sunlamp. The peak at 448 nm decreases over time, but a distinct peak at 550 nm does not form over time. This is thought to be due to a different reaction taking place and different products being formed due to the increased power of the 1000 watt bulb.

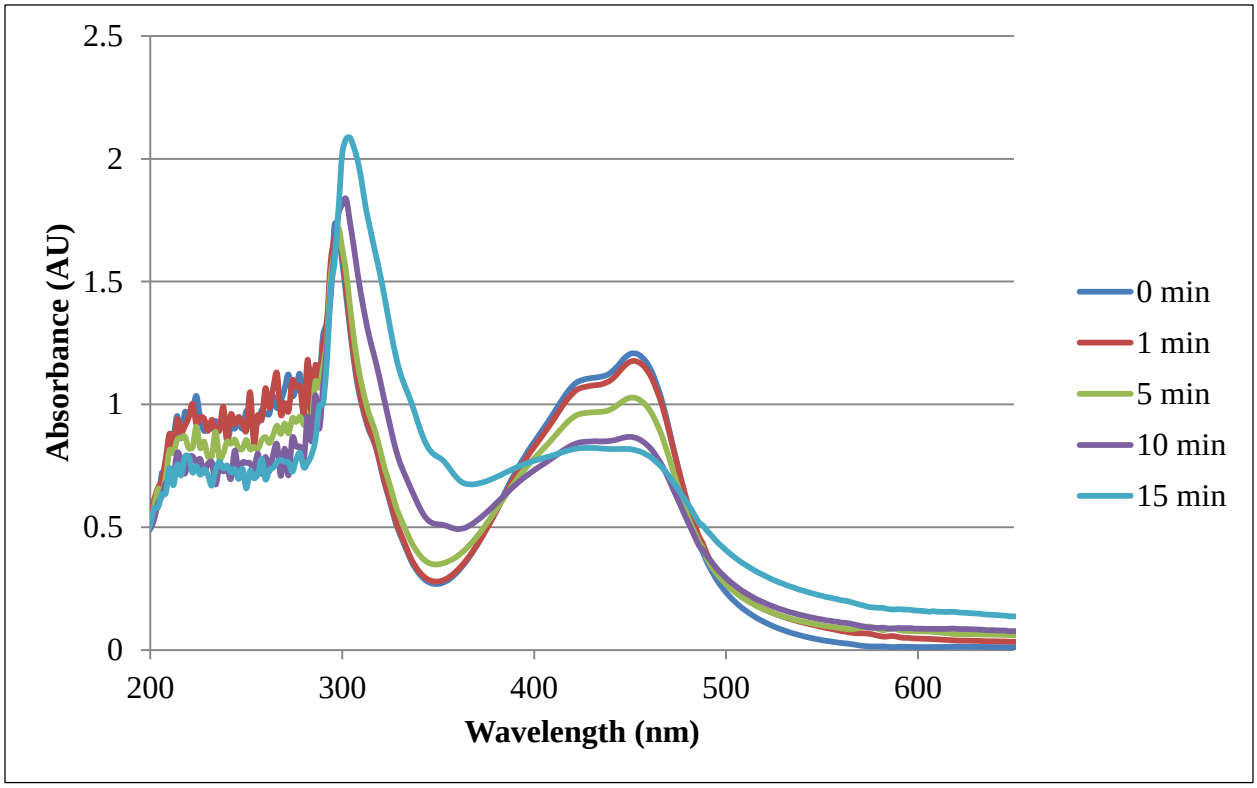

Figure 3.5.4. UV-Vis spectrum for $[(phen)_2Ru(diphen)Ru(phen)_2]Br_4$ taken at intervals during UV irradiation with a 1000 watt Xe bulb.

3.6 Photoredox Reactions of Ruthenium(II) Polypyridine Complexes

In order to investigate the photoredox reactions of the dimeric complexes, a series of quenching reactions were performed. These investigations mirrored previous studies of the monomeric complexes and provided substantial basis for comparison. Again, the focus of the investigation is a comparison of monomers to weakly coupled dimers which should show similar behavior. All of the studies were performed in 0.5 M H_2SO_4 at room temperature.

The impact of the oxidative quencher, Fe^{3+}, on the excited lifetimes of $Ru(bpy)_3^{2+}$, $Ru(phen)(bpy)_2^{2+}$, and $(bpy)_2Ru(diphen)Ru(bpy)_2^{4+}$ was investigated. $Ru(bpy)_3^{2+}$ was included for validation. In the absence of the quencher, the excited state lifetimes were 590, 670, and 1000 nsec, respectively. The Stern-Volmer plots of the relative excited state lifetimes (τ_o/τ) as a

function of quencher concentration were linear over the range 0 – 5 mM Fe^{3+} and relative lifetime of 1 to 12. The Stern-Volmer plots are combined in Figure 3.6.1. The quenching rate constants, τ_o, and relative standard deviation (RSD) are summarized in Table 3.6.1. To get the RSD, the standard deviation of the slope for each set of data was first determined using the Excel "linest" function. This value was then used to find the RSD for the slope by using the equation,

$$RSD = \frac{s}{\bar{x}} * 100$$

where s = standard deviation and $\bar{x}$ = mean. The RSD for all three data sets were low, ranging from 3% to 6%.

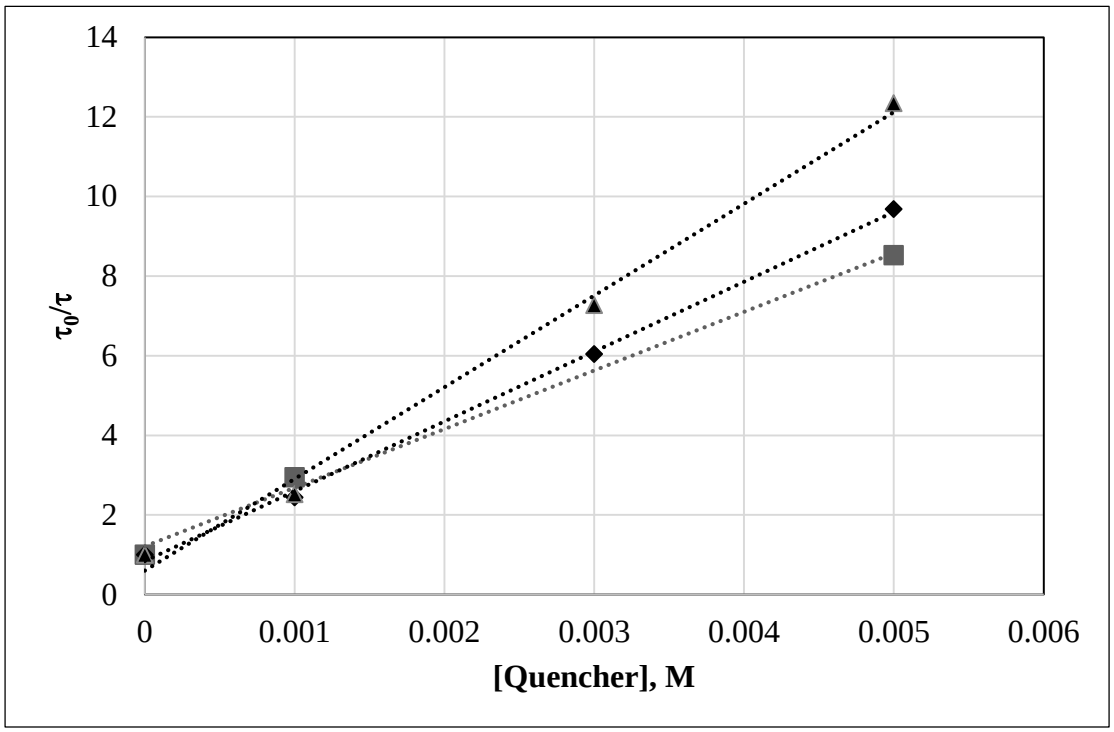

Figure 3.6.1. Stern-Volmer plots for $Ru(bpy)_3^{2+}$ (■), $Ru(phen)(bpy)_2^{2+}$ (♦), and $(bpy)_2Ru(diphen)Ru(bpy)_2^{4+}$ (▲) with Fe^{3+} quencher.

Table 3.6.1. Quenching rate, lifetimes, and error data for $Ru(bpy)_3^{2+}$, $Ru(phen)(bpy)_2^{2+}$, and $(bpy)_2Ru(diphen)Ru(bpy)_2^{4+}$.

Complex	τ_0	k_q	RSD
$Ru(bpy)_3^{2+}$	590 nsec	2.5×10^8 $M^{-1}s^{-1}$	6%
$Ru(phen)(bpy)_2^{2+}$	690 nsec	2.6×10^8 $M^{-1}s^{-1}$	3%
$(bpy)_2Ru(diphen)Ru(bpy)_2^{4+}$	1000 nsec	2.3×10^8 $M^{-1}s^{-1}$	5%

Excited state lifetimes in the absence of quencher were collected for the other complexes, as well. When collected in 0.5 M H_2SO_4, the dimeric complex lifetimes were longer than the monomeric complex lifetimes. This was contrary to the results previously obtained by the group for bpy based complexes, where the monomer lifetimes were longer than the dimer lifetimes. Acetonitrile had been used in those trials, so lifetimes were retaken for $Ru(phen)_3^{2+}$ and $(phen)_2Ru(diphen)Ru(phen)_2^{4+}$. The resulting lifetimes were as expected with 1120 nsec for $Ru(phen)_3^{2+}$ and 960 nm for $(phen)_2Ru(diphen)Ru(phen)_2^{4+}$. These results indicate solvent reorganization is occurring. Excited state lifetime values are shown in Table 3.4.1.

The rate constants for the back reaction that follows the quenching reaction and the yields of oxidized ruthenium complexes were investigated using laser flash photolysis. Cu^{2+} and Fe^{3+} were studied. A representative absorption transient showing the rapid formation of Ru(III) and the subsequent slow back reaction that returns the system to the initial state is shown in Figure 3.6.2. The back reaction follows second order kinetics, and the rate constants are summarized in Table 3.6.2 for Fe^{3+} solutions and Table 3.6.3 for Cu^{2+} solutions. Where possible, comparison of the rate constants with literature values was made and agreement in all cases was excellent.

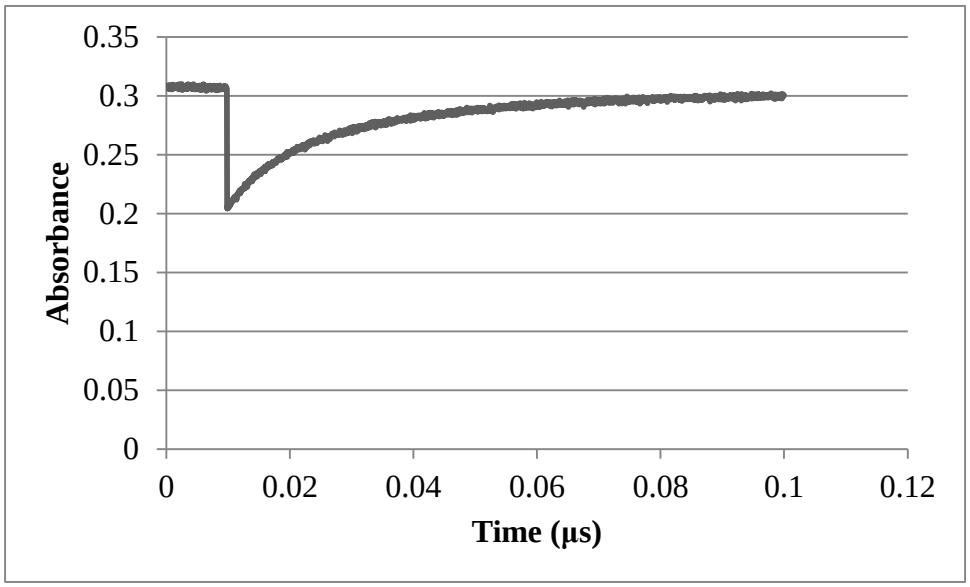

Figure 3.6.2. Representative absorption transient for $Ru(bpy)_3^{2+}$ (50 mM Fe^{3+}).

As expected, the k_{back} values for both 10 mM and 50 mM Fe^{3+} are comparable. This suggests that the monomeric and dimeric complexes act similarly. Values of k_{back} for Cu^{2+} are also as expected and comparable in the data set collected. The cage escape yields were extremely low for both 10 mM and 50 mM Cu^{2+}. It was concluded that the laser system used was not providing enough flux for the quenching reaction, and the Cu^{2+} studies were not analyzed further. The Cu^{2+} data can be seen in Table 3.6.3.

The cage escape percent yields of oxidized ruthenium complexes for the Fe^{3+} quencher were also much lower than expected. Again, this is due to the laser not providing enough flux to excite a majority of the ruthenium complexes. These values can be seen in Table 3.6.2. The efficiency, η, which takes into account that only a fraction of ruthenium centers are excited by the laser, was then determined for $Ru(phen)_3^{2+}$ and $(phen)_2Ru(diphen)Ru(phen)_2^{4+}$ with 50 mM Fe^{3+}. The equation

$$\eta = k_q[Q]/(k_q[Q] + k_0)$$

where k_q = rate constant for excited state quenching, k_0 = rate constant for unquenched decay of excited state, and [Q] = quencher concentration was used (Kalyanasundaram, 1991). For 50 mM Fe^{3+}, the efficiency of $Ru(phen)_3^{2+}$ was 93% and 95% for $(phen)_2Ru(diphen)Ru(phen)_2^{4+}$. The similar efficiency values for the monomer and dimer imply that both ruthenium centers are acting independently.

Table 3.6.2. Back reaction rate constants and yields for ruthenium(II) complexes in 10 mM and 50 mM Fe^{3+} solutions.

	10 mM Fe^{3+}		**50 mM Fe^{3+}**	
Complex	**k_{back}** [a]	**Φ**	**k_{back}**	**Φ**
$Ru(bpy)_3^{2+}$	9.95×10^6 $M^{-1}s^{-1}$	25%	9.95×10^6 $M^{-1}s^{-1}$	32%
$Ru(phen)(bpy)_2^{2+}$	1.08×10^7 $M^{-1}s^{-1}$	30%	1.12×10^7 $M^{-1}s^{-1}$	28%
$(bpy)_2Ru(diphen)Ru(bpy)_2^{4+}$	1.08×10^7 $M^{-1}s^{-1}$	30%	1.11×10^7 $M^{-1}s^{-1}$	30%
$Ru(phen)(dmb)_2^{2+}$	3.00×10^6 $M^{-1}s^{-1}$	37%	2.59×10^6 $M^{-1}s^{-1}$	37%
$(dmb)_2Ru(diphen)Ru(dmb)_2^{4+}$	4.35×10^6 $M^{-1}s^{-1}$	12%	3.16×10^6 $M^{-1}s^{-1}$	21%
$Ru(phen)_3^{2+}$	9.97×10^6 $M^{-1}s^{-1}$	24%	1.27×10^7 $M^{-1}s^{-1}$	22%
$(phen)_2Ru(diphen)Ru(phen)_2^{4+}$	1.17×10^7 $M^{-1}s^{-1}$	15%	1.13×10^7 $M^{-1}s^{-1}$	22%
$Ru(phen)(tmphen)_2^{2+}$	2.70×10^6 $M^{-1}s^{-1}$	30%	8.47×10^6 $M^{-1}s^{-1}$	36%
$(tmphen)_2Ru(diphen)Ru(tmphen)_2^{4+}$	7.83×10^6 $M^{-1}s^{-1}$	13%	2.76×10^6 $M^{-1}s^{-1}$	21%

[a] k_{back} values for the same sample were within 15% of each other.

Table 3.6.3. Back reaction rate constants and yields for ruthenium(II) complexes in 10 mM and 50 mM Cu^{2+} solutions.

	10 mM Cu^{2+}		**50 mM Cu^{2+}**	
Complex	**k_{back}**	**Φ**	**k_{back}**	**Φ**
$Ru(bpy)_3^{2+}$	1.05×10^9 $M^{-1}s^{-1}$	3%	8.53×10^8 $M^{-1}s^{-1}$	9%
$Ru(phen)(bpy)_2^{2+}$	9.80×10^8 $M^{-1}s^{-1}$	4%	1.03×10^9 $M^{-1}s^{-1}$	8%
$(bpy)_2Ru(diphen)Ru(bpy)_2^{4+}$	5.03×10^8 $M^{-1}s^{-1}$	7%	7.69×10^8 $M^{-1}s^{-1}$	8%
$Ru(phen)(dmb)_2^{2+}$	3.83×10^8 $M^{-1}s^{-1}$	8%	2.57×10^8 $M^{-1}s^{-1}$	15%
$(dmb)_2Ru(diphen)Ru(dmb)_2^{4+}$	5.49×10^8 $M^{-1}s^{-1}$	4%	2.47×10^8 $M^{-1}s^{-1}$	9%
$Ru(phen)_3^{2+}$	1.02×10^9 $M^{-1}s^{-1}$	6%	1.03×10^9 $M^{-1}s^{-1}$	8%
$(phen)_2Ru(diphen)Ru(phen)_2^{4+}$	9.47×10^8 $M^{-1}s^{-1}$	3%	9.68×10^8 $M^{-1}s^{-1}$	8%
$Ru(phen)(tmphen)_2^{2+}$	2.60×10^8 $M^{-1}s^{-1}$	10%	1.41×10^8 $M^{-1}s^{-1}$	13%
$(tmphen)_2Ru(diphen)Ru(tmphen)_2^{4+}$	2.46×10^8 $M^{-1}s^{-1}$	3%	4.34×10^7 $M^{-1}s^{-1}$	5%

4.1 Discussion

4.2 Ni(0) Catalyzed Coupling Reaction for Symmetric Dimeric Ruthenium(II) Polypyridine Complexes

When this research project began, a nickel (Ni(0)) catalyzed coupling reaction was used for the synthesis of the symmetric dimeric ruthenium(II) polypyridine complexes. This synthesis had been used regularly for the synthesis of complexes such as $[(bpy)_2Ru(diphen)Ru(bpy)_2](PF_6)_4$ and $[(phen)_2Ru(diphen)Ru(phen)_2](PF_6)_4$. The synthesis is comprised of several steps. The first step was the synthesis of $[Ru(CO)_2Cl_2]_n$ based on the reaction described by Aguirre et al. in 2001. The reaction is shown in Scheme 4.2.1.

$$RuCl_3 + HCl + HCOOH \longrightarrow [Ru(CO)_2Cl_2]_n$$

Scheme 4.2.1. Synthesis of $[Ru(CO)_2Cl_2]_n$ (Aguirre, et al. 2001).

$[Ru(CO)_2Cl_2]_n$ was used without further purification in the synthesis of $Ru(CO)_2Cl_2$(Cl-phen), which is shown in Scheme 4.2.2. This reaction was described by Thomas et al. in 1989.

$$[Ru(CO)_2Cl_2]_n + n(\text{Cl-phen}) \xrightarrow{\text{2-methoxyethanol}} n[Ru(CO)_2Cl_2(\text{Cl-phen})]$$

Scheme 4.2.2. Synthesis of $[Ru(CO)_2Cl_2(Cl\text{-phen})]$ (Thomas, et al. 1989).

$Ru(CO)_2Cl_2$(Cl-phen) was used without further purification for the synthesis of $[Ru(Cl\text{-phen})(phen)_2](PF_6)_2$. This procedure was based on the procedure used by Anderson for $[Ru(Cl\text{-phen})(phen)_2]Cl_2$ with some modifications (Anderson, 2007), (Thomas et al., 1989). The 2-methoxyethanol, $Ru(CO)_2Cl_2$(Cl-phen), phen, and Me_3NO were prepared and heated to reflux for 2 hours, just as outlined in the procedure used by Anderson. However, after heating, 10 mL of saturated NH_4PF_6 aqueous solution were added to the solution. This caused $[Ru(Cl\text{-phen})(phen)_2](PF_6)_2$ to form, and the solution was cooled to RT. The bright orange precipitate was filtered and stored. This synthesis is shown in Scheme 4.2.3.

$$[Ru(CO)_2Cl_2(Cl\text{-}phen)] + 2phen + 2Me_3NO \xrightarrow{2\text{-methoxyethanol}} [Ru(Cl\text{-}phen)(phen)_2]Cl_2 + 2Me_3N + 2CO_2$$

$$[Ru(Cl\text{-}phen)(phen)_2]Cl_2 + 2NH_4PF_6 \xrightarrow{2\text{-methoxyethanol}} [Ru(Cl\text{-}phen)(phen)_2](PF_6)_2 + 2NH_4Cl$$

Scheme 4.2.3. Synthesis of $[Ru(Cl\text{-}phen)(phen)_2](PF_6)_2$ (Thomas et al., 1989).

In this step of the synthesis, $[Ru(Cl\text{-}phen)(phen)_2](PF_6)_2$ was confirmed via ESI-MS. $[Ru(Cl\text{-}phen)(phen)_2](PF_6)_2$ was used without further purification to synthesize $[(phen)_2Ru(diphen)Ru(phen)_2](PF_6)_4$. This was done following the procedure outlined by Toyota et al. in 2005. The general reaction is shown in Scheme 4.2.4.

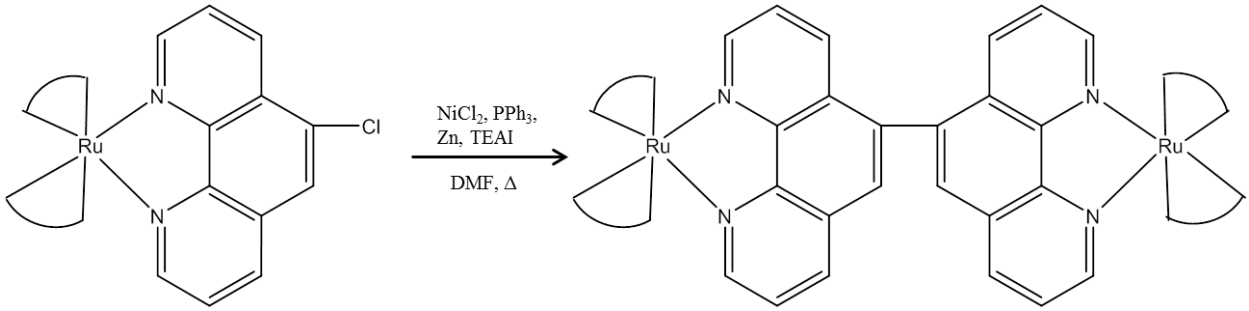

Scheme 4.2.4. General Ni(0) catalyzed coupling reaction for ruthenium(II) dimeric complexes.

The product was confirmed with ESI-MS; however, several drawbacks were found with the synthesis described above. One drawback was found when the synthesis of $(dmb)_2Ru(diphen)Ru(dmb)_2](PF_6)_4$ was attempted using the method described above. The monomeric complex, $[Ru(dmb)_2(Cl\text{-}phen)](PF_6)_2$, was synthesized, and the zinc coupling reaction was carried out. However, the desired dimeric complex was not produced. ESI-MS analysis revealed that the chlorines had, in fact, been removed from the $[Ru(dmb)_2(Cl\text{-}phen)](PF_6)_2$ complex, but the complexes had not coupled.

Another major drawback of the zinc coupling reaction is that monomeric complexes are also present. The dimeric complexes used in this study are very weakly coupled. Thus, the dimeric complexes will have properties that are almost identical to the monomeric complexes

making spectroscopic analysis of only the dimeric complexes in the mixture impossible. It is crucial that only dimeric complexes are present. Due to these drawbacks with the Ni(0) catalyzed coupling reaction for dimeric ruthenium(II) complex synthesis, a new synthesis was developed.

4.3 Synthesis of Symmetric Ruthenium(II) Dimeric Complexes

Several different reactions were explored when searching for an improved synthetic route for synthetic Ruthenium(II) dimeric complexes. The successful route used $[Ru(CO)_2Cl_2]_n$ and diphen as starting materials. $[Ru(CO)_2Cl_2]_n$ was synthesized as previously described in both the "2.5 Syntheses" and the "4.2 Ni(0) Catalyzed Coupling Reaction for Symmetric Dimeric Ruthenium(II) Polypyridine Complexes" sections (Aguirre et al., 2001), (Colton and Farthing, 1967). The synthesis was simple, and had a relatively high yield of 80%. The IR spectrum for $[Ru(CO)_2Cl_2]_n$ shown in Figure 3.2.2 was used for comparison of subsequent reactions. CO stretching peaks are seen at 2053 cm^{-1}, 2075 cm^{-1}, 2088 cm^{-1}, and 2138 cm^{-1}.

Diphen was the second starting material chosen for the dimeric ruthenium(II) complex synthesis. The diphen used in this research was 5,5'-bi-1,10-phenanthroline and was synthesized following a procedure used by the Hu group to synthesize 2,2'-bi-1,10-phenanthroline (Hu et al, 2001). The procedure coupled 5-chloro-1,10-phenanthroline via a Ni(0) catalyzed coupling reaction. There was a moderate average yield of 49%, and the ^1H NMR spectra for the samples were consistent with what is in the literature.

After the starting materials were synthesized, they were reacted to produce $(CO)_2Cl_2Ru(diphen)Ru(CO)_2Cl_2$. $[Ru(CO)_2Cl_2]_n$ and diphen were dissolved separately in 2-methoxyethanol. The two solutions were mixed and boiled for ~7 minutes. The product precipitated out during heating. Initially, the monomer $(CO)_2Cl_2Ru(diphen)$, was also a target

complex. However, after countless trials using different ratios of $[Ru(CO)_2Cl_2]_n$ to diphen, only the dimer was produced.

Absolute confirmation of the expected product $(CO)_2Cl_2Ru(diphen)Ru(CO)_2Cl_2$ was not possible, mostly due to the fact that it had low or no solubility in solvents suitable for UV-vis, ESI-MS, and CV analysis. IR spectroscopy was conducted on the sample, mostly for comparison with the starting material, $[Ru(CO)_2Cl_2]_n$. For $[Ru(CO)_2Cl_2]_n$, peaks due to CO stretching are seen at 2053 cm^{-1}, 2075 cm^{-1}, 2088 cm^{-1}, and 2138 cm^{-1}. Only two peaks are seen for $(CO)_2Cl_2Ru(diphen)Ru(CO)_2Cl_2$, which are at 1987 cm^{-1} and 2058 cm^{-1}. Based on the symmetry of the polymeric material and dimeric complex, these IR spectra results were expected. The IR comparison is shown in Figure 3.2.3.

$(CO)_2Cl_2Ru(diphen)Ru(CO)_2Cl_2$ was then used without further purification. Phen, 1,10-phenanthroline, ligands were added to the complex to yield $[(phen)_2Ru(diphen)Ru(phen)_2](PF_6)_4$. $(CO)_2Cl_2Ru(diphen)Ru(CO)_2Cl_2$, phen, and Me_3NO were heated to reflux for 2 hours in 2-methoxyethanol. The solvent was removed, and water was added to dissolve the remaining oily substance. Saturated NH_4PF_6 aqueous solution was then used to precipitate $[(phen)_2Ru(diphen)Ru(phen)_2](PF_6)_4$.

Various methods were used to identify the product. Figure 3.2.4 shows the IR spectrum for $[(phen)_2Ru(diphen)Ru(phen)_2](PF_6)_4$. The key feature of the IR spectrum is the absence of the CO stretching peaks in the 1900 cm^{-1} to 2200 cm^{-1} range. UV-Vis analysis was also performed on the complex, as shown in Figure 3.2.5. The λ_{max} due to MLCT in the ruthenium dimeric complex is seen at 448 nm. In comparison to an analogous monomeric complex, this is slight shift from the λ_{max} value of 446 nm for $Ru(phen)_3^{2+}$. CV analysis, as shown in Figure 3.2.6,

revealed a redox potential of 1.308 V vs SCE for $[(phen)_2Ru(diphen)Ru(phen)_2](PF_6)_4$. This value was very close to the redox potential of 1.309 V for $Ru(phen)_3^{2+}$.

The product was also confirmed via ESI-MS, as seen in Figures 3.2.7 and 3.2.8. The peak at 321.0 m/z is indicative of $(phen)_2Ru(diphen)Ru(phen)_2^{4+}$. The peak at 321.0 m/z is the expected peak for $(phen)_2Ru(diphen)Ru(phen)_2^{4+}$. There is a peak seen at 427.7 m/z indicating $(phen)_2Ru(diphen)Ru(phen)_2^{3+}$ is present and is due to the ionization technique used. Additional 4^+ and 3^+ species are seen at peaks 338.8 and 358.0 m/z for 4^+ and at 452.0, 475.7, and 500.4 m/z for 3^+. These could be caused by further fragmentation of $(phen)_2Ru(diphen)Ru(phen)_2^{4+}$ and $(phen)_2Ru(diphen)Ru(phen)_2^{3+}$ caused by collision-induced dissociation in the quadrupole system used. Each subsequent peak increases by ~70 g/mol compared to the previous peak. This suggests uniform fragmentation is taking place. The peak indicative of a monomeric complex formed is not seen. The spectroscopic and electrochemical data collected is presented in Table 3.4.1. The scope of the reaction was tested by varying the ligands used.

4.4 Scope of Ligand Addition to $(CO)_2Cl_2Ru(diphen)Ru(CO)_2Cl_2$

To determine the scope of the reaction using $(CO)_2Cl_2Ru(diphen)Ru(CO)_2Cl_2$ to produce symmetric dimers, several ligands were employed. Dpphen, 4,7-diphenyl-1,10-phenanthroline, was reacted with $(CO)_2Cl_2Ru(diphen)Ru(CO)_2Cl_2$ using the same procedure as detailed above for the phen ligand. $[(dpphen)_2Ru(diphen)Ru(dpphen)_2](PF_6)_4$ was first analyzed using IR spectrometry to verify there were no carbonyl ligands on the complex.

The sample was then analyzed using UV-vis spectroscopy. The λ_{max} is was found to be 460 nm, which was a shift from the λ_{max} of 456 nm for $Ru(phen)(dpphen)_2^{2+}$. There was also a shift in the λ_{max} compared to $[(phen)_2Ru(diphen)Ru(phen)_2](PF_6)_4$, which had a λ_{max} of 448 nm. A shift was expected due to the added phenyl groups on the ligand. The sample was also

analyzed with CV. The redox potential obtained was 1.282 V vs SCE for $(dpphen)_2Ru(diphen)Ru(dpphen)_2^{4+}$, which differs slightly from the redox potential of 1.236 V vs SCE for $Ru(phen)(dpphen)_2^{2+}$.

The sample was lastly submitted for ESI-MS analysis, which is shown in Figures 3.2.9 and 3.2.10. A peak at 472.58 m/z due to $(dpphen)_2Ru(diphen)Ru(dpphen)_2^{4+}$ is present. There is also a peak at 333.1 m/z, which is expected for the dpphen free ligand. The ESI-MS spectra are exceptionally clean for the $(dpphen)_2Ru(diphen)Ru(dpphen)_2^{4+}$ sample. All data collected for the complex is shown in Table 3.4.1.

The next ligand used was 3,4,7,8-tetramethyl-1,10-phenanthroline (tmphen), and the procedure used was the same as those used to add the other phen based ligands to $(CO)_2Cl_2Ru(diphen)Ru(CO)_2Cl_2$. The verification of the expected product $(tmphen)_2Ru(diphen)Ru(tmphen)_2^{4+}$ was carried out in the same sequence as the previous dimeric complexes. IR confirmed CO stretching peaks were absent. The UV-vis spectrum revealed the λ_{max} was at 432 nm for $(tmphen)_2Ru(diphen)Ru(tmphen)_2^{4+}$, which was shifted compared to $Ru(phen)(tmphen)_2^{2+}$ with a λ_{max} of 427 nm. There was also a shift due to the added four methyl groups on each ligand compared to $[(phen)_2Ru(diphen)Ru(phen)_2](PF_6)_4$ with a λ_{max} of 448 nm. The CV voltammogram for $(tmphen)_2Ru(diphen)Ru(tmphen)_2^{4+}$ showed a redox potential of 1.152 V vs SCE, which was slightly higher than the redox potential of 1.107 V vs SCE for $Ru(phen)(tmphen)_2^{2+}$.

ESI-MS was the final method used to confirm the identity of the complex, and the spectra can be seen in Figures 3.2.11 and 3.2.12. The peak seen at 376.6 m/z is due to$[(tmphen)_2Ru(diphen)Ru(tmphen)_2^{4+}$. The peak at 501.9 m/z is indicative of

$(tmphen)_2Ru(diphen)Ru(tmphen)_2^{3+}$. Additional peaks seen could be due to continued fragmentation similar to the ESI-MS spectrum for $(phen)_2Ru(diphen)Ru(phen)_2^{4+}$.

As described earlier, the Ni(0) catalyzed coupling reaction failed to yield $[(dmb)_2Ru(diphen)Ru(dmb)_2](PF_6)_4$. Thus, 4,4'-dimethyl-2,2'-dipyridine (dmb) was chosen for use with the new synthesis. Initially the procedure used for the synthesis of $[(dmb)_2Ru(diphen)Ru(dmb)_2](PF_6)_4$ was the same as the method used for the phen based ligands. However, the IR spectrum for the final product of the reaction revealed a single peak at 1977 cm^{-1}. This indicated that there was still one CO group attached to the ruthenium center. From this IR, it was theorized that $[(dmb)_2Ru(diphen)Ru(dmb)(CO)Cl](PF_6)_3$ was present.

To confirm the identity of the product of the synthesis, the sample was submitted for ESI-MS analysis. A peak at 392.4 m/z indicated that $(dmb)_2Ru(diphen)Ru(dmb)(CO)Cl^{3+}$ was present. A peak was also seen at 324.6 m/z, which indicated that $(dmb)_2Ru(diphen)Ru(dmb)_2^{4+}$ was produced as well.

In order to synthesize only $[(dmb)_2Ru(diphen)Ru(dmb)_2](PF_6)_4$, the procedure was modified by adding two portions of Me_3NO. To begin, $(CO)_2Cl_2Ru(diphen)Ru(CO)_2Cl_2$, dmb, and Me_3NO were dissolved in nitrogen purged 2-methoxyethanol. After heating the solution to reflux for 1 hr, additional Me_3NO was added to the solution. The solution was heated for another hr. After cooling and filtering, most of the solvent was removed. The remaining substance was dissolved in H_2O. Saturated NH_4PF_6 solution was used to precipitate the orange product.

The IR spectrum for $[(dmb)_2Ru(diphen)Ru(dmb)_2](PF_6)_4$ confirmed the absence of CO peaks. UV-Vis analysis was also performed on the sample, and the λ_{max} due to MLCT is at 458 nm. This is a slight shift from the λ_{max} value of 454 nm for $Ru(phen)(dmb)_2^{2+}$. CV analysis

showed a redox potential of 1.200 V vs SCE, which is a little higher than the redox potential of 1.161 V vs SCE for $Ru(phen)(dmb)_2^{2+}$.

Lastly, ESI-MS was used to positively identify the product, as seen in Figures 3.2.13 and 3.2.14. The peak at 324.6 m/z indicates $(dmb)_2Ru(diphen)Ru(dmb)_2^{4+}$ was successfully produced. Further fragmentation of the complex is seen, which is similar to results for the previously analyzed complexes. Data collected for both $(dmb)_2Ru(diphen)Ru(dmb)_2^{4+}$ and $Ru(phen)(dmb)_2^{2+}$ is in Table 3.4.1.

Bpy, 2,2'-bipyridine, was also a ligand chosen for the synthesis. The first procedure attempted was the same as the one used to attached the phen based ligands. Just as with the dmb ligand, the IR spectrum for the product showed that there was still one carbonyl group on at least some of the complexes with one peak at 1973 cm^{-1}. It was assumed that $[(bpy)_2Ru(diphen)Ru(bpy)COCl](PF_6)_3$ was present.

To confirm the product identity, ESI-MS analysis was performed. A peak at 364.34 m/z indicated that $(bpy)_2Ru(diphen)Ru(bpy)COCl^{3+}$ was present, a peak at 499.96 m/z showed that $(bpy)COClRu(diphen)Ru(bpy)COCl^{2+}$ was produced, and a peak at 296.5 m/z showed that $(bpy)_2Ru(diphen)Ru(bpy)_2^{4+}$ was also synthesized.

To ensure only $[(bpy)_2Ru(diphen)Ru(bpy)_2](PF_6)_4$ was produced, the modified procedure used to synthesize was $[(dmb)_2Ru(diphen)Ru(dmb)_2](PF_6)_4$ was used. Again, two portions of Me_3NO were added. IR was initially used to confirm the absence of carbonyl groups. The UV-Vis spectrum for $[(bpy)_2Ru(diphen)Ru(bpy)_2](PF_6)_4$ showed the λ_{max} at 452 nm, which matches the value for $Ru(bpy)_3^{2+}$. This value is shifted compared to the λ_{max} at 458 nm for $[(dmb)_2Ru(diphen)Ru(dmb)_2](PF_6)_4$, which was due to the added methyl groups on the dmb ligand. The λ_{max} for $[(bpy)_2Ru(diphen)Ru(bpy)_2](PF_6)_4$ was also shifted compared to the λ_{max}

value of 450 nm of $Ru(phen)(bpy)_2^{2+}$. While the last two procedures presented some difficulties, they have also provided a good means for producing some mixed dimeric complexes by reacting the remaining CO with a different ligand.

CV analysis revealed a redox potential of 1.297 V vs SCE for $[(bpy)_2Ru(diphen)Ru(bpy)_2](PF_6)_4$. This is a slightly higher value than that for both $[(dmb)_2Ru(diphen)Ru(dmb)_2](PF_6)_4$, 1.200 V vs SCE, and $Ru(phen)(bpy)_2^{2+}$, 1.269 V vs SCE. Figures 3.2.15 and 3.2.16 are the ESI-MS spectra for $[(bpy)_2Ru(diphen)Ru(bpy)_2](PF_6)_4$. The peak at 296.5 m/z is as expected for $[(bpy)_2Ru(diphen)Ru(bpy)_2](PF_6)_4$. The peak at 395.7 m/z is expected for $(bpy)_2Ru(diphen)Ru(bpy)_2^{3+}$. Other small peaks could possibly be due to additional fragmentation by the quadrupole system used. Data is shown in Table 3.4.1 for $(bpy)_2Ru(diphen)Ru(bpy)_2^{4+}$ and $Ru(phen)(bpy)_2^{2+}$.

It was determined that the dimeric complexes were free of monomeric complex contamination. In most cases, the dimeric complexes were submitted for ESI-MS analysis before being further purified. Thus, improved purity could have been seen if subsequent ESI-MS analysis was performed. The spectroscopic and electrochemical data collected was in the expected range for the complexes being studied. The five ligands reported above were successfully reacted with $(CO)_2Cl_2Ru(diphen)Ru(CO)_2Cl_2$ to create a symmetric dimeric complex. However, there were additional ligands that were not successfully reacted with $(CO)_2Cl_2Ru(diphen)Ru(CO)_2Cl_2$.

4.5 Failed Ligand Addition to $(CO)_2Cl_2Ru(diphen)Ru(CO)_2Cl_2$

Bpz, 2,2'-bipyrazine was synthesized for use in the newly developed synthetic route for symmetric dimeric complexes. The procedure was rather lengthy, but a better procedure was not found. First, 2-pyrazinecarboxylic acid was dissolved 15 M NH_4OH. The solution dried, and the

solid was dissolved in a saturated copper(II) acetate aqueous solution. It was then stirred for 1 hour without heating. The blue solid was filtered, washed, and dried. A sublimator was used to pyrolize the solid, and the product was collected. The ^{1}H NMR spectrum was in agreement with the literature.

Bpz was then used in the newly developed synthesis for symmetric dimeric complexes. The first procedure employed was the same as the one used to attach the phen based ligands. The Me_3NO was added all in one portion. The largest amount of solid fell out during heating, and it was a black/purple color. Very little solid fell out with addition on saturated NH_4PF_6 solution. It was found via IR spectroscopy that all of the CO groups were not being replaced. The procedure was modified by adding two portions of Me_3NO. Again, the largest amount of solid fell out during heating, and a small amount precipitated with addition of saturated NH_4PF_6 solution. IR spectroscopy again indicated that all of the CO groups were not being replaced. Due to the peaks at 1966 cm^{-1} and 2067 cm^{-1}, it was theorized that (bpz)COClRu(diphen)(bpz)$COCl^{2+}$ was being produced. However, further identification was not pursued since it was not the desired complex.

Bpm, 2,2'-bipyrimidine, was another ligand used in the synthesis. The ^{1}H NMR spectra for bpm samples available in the lab were in agreement with the literature. The procedure followed to react bpm with $(CO)_2Cl_2Ru(diphen)Ru(CO)_2Cl_2$ was the same outlined for the addition of phen based ligands. The behavior of the bpm ligand was very similar to that of the bpz ligand. The largest amount of solid fell out of solution during heating. A very small amount came out with the addition of saturated NH_4PF_6 solution. The reaction was modified by adding two portions of the Me_3NO, but a large amount of solid fell out during heating. Addition of saturated NH_4PF_6 solution precipitated out a very small amount of solid. IR analysis of the product when bpm was used as the ligand resulted in peaks at 2006 cm^{-1} and 2064 cm^{-1}. This

indicated that (bpm)COClRu(diphen)(bpm)COCl^{2+} was produced, but identification was not carried out since it was not the desired complex.

Ethylenediamine (en) was also used as a ligand. The first procedure used was the same as the one used for attaching phen based ligands. The product fell out during heating. IR spectroscopy showed that all of the CO groups were not replaced, so the procedure was modified. Instead of using 2-methoxyethanol as the solvent, ethylenediamine was used as solvent. Most of the product fell out during heating. Again, all of the CO groups were not replaced, as revealed by IR analysis. The peak at 1961 cm^{-1} was indicative of $(en)_2Ru(diphen)Ru(en)(CO)Cl^{3+}$ being synthesized. Product identification was not carried out since it was not the target complex.

One last modification of the procedure was attempted. Since the products of the reaction using bpz, bpm, and en as ligands kept falling out during heating, a solvent with a higher boiling point was used. The hope was that the intermediate would stay in solution long enough to react completely with the ligands. The boiling point of 2-methoxyethanol is 124 °C, so it was replaced with ethylene glycol, which has a boiling point of 197 °C.

Phen was the first ligand used to ensure the reaction would work in ethylene glycol. $(CO)_2Cl_2Ru(diphen)Ru(CO)_2Cl_2$, phen, and Me_3NO were put in nitrogen purged ethylene glycol. The solution was heated for 2 hours, cooled, and filtered. Most of the solvent was removed, and water was added. Saturated NH_4PF_6 solution was used to precipitate out the product. The IR spectrum of $[(phen)_2Ru(diphen)Ru(phen)_2](PF_6)_4$ confirmed that no carbonyl groups were present. UV-vis spectroscopy was performed on the sample, and the λ_{max} at 448 nm was in agreement with values found when 2-methoxyethanol as the solvent.

Based on the success with the phen ligand, the procedure using ethylene glycol as the solvent was used with the bpz ligand. However, the dark purple solid continued to fall out of solution during heating, so the addition of bpz and bpm to $(CO)_2Cl_2Ru(diphen)Ru(CO)_2Cl_2$ was no longer pursued. The scope of the reaction was investigated further by varying the bridging ligand used in the reaction with $[Ru(CO)_2Cl_2]_n$.

4.6 Investigation of Bridging Ligands in Improved Synthetic Route for Dimeric Ruthenium(II) Complexes

The scope of the newly developed synthesis was investigated further by differing the bridging ligand used in the reaction. Dpp, 2,3-bis(2-pyridyl)-pyrazine, was chosen as the second bridging ligand. $[Ru(CO)_2Cl_2]_n$ and dpp were dissolved in 2-methoxyethanol and heated for 20 minutes. The olive green product fell out during heating and was collected by filtering. The product was analyzed using IR. Figure 3.3.1 shows the IR comparison for $[Ru(CO)_2Cl_2]_n$ and $(CO)_2Cl_2Ru(dpp)Ru(CO)_2Cl_2$. Peaks due to carbonyl groups are seen at 2053 cm^{-1}, 2075 cm^{-1}, 2088 cm^{-1}, and 2138 cm^{-1} for $[Ru(CO)_2Cl_2]_n$ and at 2010 and 2065 cm^{-2} for $(CO)_2Cl_2Ru(dpp)Ru(CO)_2Cl_2$. The decrease from four CO stretching bands to two CO stretching bands is consistent with CO groups being replaced during the reaction.

The product was used without further purification and reacted with the phen ligand. The synthesis used was the same as that described for the addition of the phen based ligands to $(CO)_2Cl_2Ru(diphen)Ru(CO)_2Cl_2$. IR spectroscopy was used to confirm the absence of carbonyl groups. UV-vis spectroscopy showed a λ_{max} of 446 nm for $[(phen)_2Ru(dpp)Ru(phen)_2](PF_6)_4$, and the spectrum is shown in Figure 3.3.3. This was a slight shift compared to the λ_{max} of 448 nm for $[(phen)_2Ru(diphen)Ru(phen)_2](PF_6)_4$, but matched the λ_{max} value of $Ru(phen)_3^{2+}$. From the cyclic voltammogram seen in Figure 3.3.4, a redox potential of 1.304 V vs SCE was found. This value

was extremely close to the redox potentials of both $[(phen)_2Ru(diphen)Ru(phen)_2](PF_6)_4$, 1.308 V vs SCE, and $Ru(phen)_3^{2+}$, 1.309 V vs SCE. Data for $[(phen)_2Ru(dpp)Ru(phen)_2](PF_6)_4$ is included in Table 3.4.1.

The reaction involving dpp and $[Ru(CO)_2Cl_2]_n$ to create $(CO)_2Cl_2Ru(dpp)Ru(CO)_2Cl_2$ was successful. Further investigation of bridging ligands was not pursued, but the scope of the reaction involving the use of $[Ru(CO)_2Cl_2]_n$ as a starting material was explored.

4.7 Investigation of Starting Materials in Synthetic Route for Dimeric Ruthenium(II) Complexes

To investigate the range of starting materials $Ru(DMSO)_4Cl_2$ was reacted with diphen with the goal of synthesizing $(DMSO)_2Cl_2Ru(diphen)Ru(DMSO)_2Cl_2$. $Ru(DMSO)_4Cl_2$ samples were synthesized by previous group members. Purity was confirmed via ^1H NMR. $Ru(DMSO)_4Cl_2$ and diphen were heated under nitrogen for 1.5 hr in chloroform. The solution was cooled and a yellow solid was collected. After most of the chloroform was removed via rotavap, the oily substance was dissolved in acetonitrile. A yellow solid was collected via filtration. The filtrate was added drop-wise to ether. A third brownish yellow solid with oily patches and low yield was collected on a filter. The first two solids had identical IR spectra, and both were used in subsequent reactions.

The expected product, $(DMSO)_2Cl_2Ru(diphen)Ru(DMSO)_2Cl_2$, was then used without further purification and reacted with the phen ligand to produce $[(phen)_2Ru(diphen)Ru(phen)_2](PF_6)_4$. After heating under nitrogen for 3 hrs in dry DMF, the solution was cooled. Most of the DMF was removed via rotavap. DI H_2O was used to dissolve the small amount of filtrate, and saturated NH_4PF_6 solution was then added. An orange solid was collected, dissolved in acetonitrile, and then dropped into ether. The final product was collected

via filtration. The product was submitted for ESI-MS analysis. However, $[(phen)_2Ru(diphen)Ru(phen)_2](PF_6)_4$ was not seen on the ESI-MS spectrum. The procedure was attempted several times, but $[(phen)_2Ru(diphen)Ru(phen)_2](PF_6)_4$ was never confirmed. In addition, the yield was low and inconsistent. Thus, the goal of synthesizing $[(phen)_2Ru(diphen)Ru(phen)_2](PF_6)_4$ using $(DMSO)_2Cl_2Ru(diphen)Ru(DMSO)_2Cl_2$ as the starting material was then abandoned.

The most likely route of failure to produce $[(phen)_2Ru(diphen)Ru(phen)_2](PF_6)_4$ was due to $(DMSO)_2Cl_2Ru(diphen)Ru(DMSO)_2Cl_2$ not being produced in the first reaction. $(DMSO)_2Cl_2Ru(diphen)Ru(DMSO)_2Cl_2$ is not detected via ESI-MS, so IR analysis was relied upon to show a change in peaks compared to $Ru(DMSO)_4Cl_2$. A change was seen, so the complex was reacted with phen ligands. When the reaction product was submitted for ESI-MS analysis only complexes containing one ruthenium were detected. Other starting materials were not examined. The newly developed synthesis for dimeric complexes was next applied to the synthesis of monomeric complexes.

4.8 Dimeric Complex Synthesis Applied to Monomeric Complexes

Monomeric analogues of the dimeric complexes were synthesized for comparison. The synthesis developed for the dimeric complexes was used to make the monomeric complexes. $[Ru(CO)_2Cl_2]_n$ was reacted with phen to produce $Ru(CO)_2Cl_2(phen)$. The IR spectrum for the product was obtained to compare to $[Ru(CO)_2Cl_2]_n$. It can be seen in Figure 3.4.1 that $Ru(CO)_2Cl_2(phen)$ has CO stretching peaks at 1973 cm^{-1} and 2054 cm^{-1}, which is consistent with symmetric and asymmetric stretching bands for a complex containing two carbonyl groups.

$Ru(CO)_2Cl_2(phen)$ was used without further purification. Dpphen was reacted with $Ru(CO)_2Cl_2(phen)$ and Me_3NO in 2-methoxyethanol to produce $[Ru(phen)(dpphen)_2](PF_6)_2$. IR

analysis confirmed the absence of carbonyl groups, as can be seen in Figure 3.4.2. UV-vis analysis showed a λ_{max} value of 456 nm, as seen in Figure 3.4.4. The phenyl groups cause a shift compared to $Ru(phen)_3^{2+}$, 446 nm. The redox potential for $[Ru(phen)(dpphen)_2]^{2+}$ was determined to be 1.236 V vs SCE and is slightly lower than 1.309 V vs SCE for $Ru(phen)_3^{2+}$.

Tmphen was the next ligand chosen for the reaction. The reaction was carried out as described above for $[Ru(phen)(dpphen)_2](PF_6)_2$. The $[Ru(phen)(tmphen)_2](PF_6)_2$ sample was first analyze with IR and showed the carbonyl groups were no longer on the complex. The λ_{max} value found via UV-vis spectroscopy was 427 nm. Again, there was a shift due to the methyl groups from the λ_{max} of 446 nm for $Ru(phen)_3^{2+}$. CV analysis showed a redox potential of 1.107 V vs SCE for $[Ru(phen)(tmphen)_2]^{2+}$, as shown in Figure 3.4.5. This value is lower than the redox potential for $Ru(phen)_3^{2+}$, 1.309 V vs SCE.

Bpy was the next ligand reacted with $Ru(CO)_2Cl_2(phen)$. Initially the same procedure used for the dpphen and tmphen ligands was used. However, the IR spectrum revealed that there were still carbonyl groups on the complex, as shown in Figure 3.4.3 with a peak at 1963 cm^{-1} for $[Ru(phen)(bpy)_2](PF_6)_2$. A modified procedure was then adapted to synthesize $[Ru(phen)(bpy)_2](PF_6)_2$. $Ru(CO)_2Cl_2(phen)$ was again heated with bpy and Me_3NO. The procedure was modified by adding more Me_3NO halfway through the reaction time. Unlike with the dimeric ruthenium(II) complexes with dmb and bpy ligands, this procedure was not successful. The IR spectrum showed a CO stretching peak again at 1963 cm^{-1}. From the UV-vis spectrum, the λ_{max} of the sample was determined to be 450 nm. This value is in the expected range and comparable to the $(bpy)_2Ru(diphen)Ru(bpy)_2^{4+}$ λ_{max} of 452 nm. The redox potential of 1.269 V vs SCE was also in the expected range for the complex and close to the value of 1.297 V

vs SCE for $(bpy)_2Ru(diphen)Ru(bpy)_2^{4+}$. The sample was used in further studies as a comparison.

Dmb was the last ligand reacted with $Ru(CO)_2Cl_2(phen)$. The same procedure used with the dpphen and tmphen ligands was first employed. As with the bpy ligand, the IR spectrum showed a carbonyl stretching peak at 1965 cm^{-1}. The modified method used with the bpy ligand was attempted. Again, a carbonyl stretching peak was a seen at 1965 cm^{-1} on the IR spectrum for the sample. The λ_{max} was found to be in the expected range for the complex with a value of 454 nm. The redox potential was 1.161 V vs SCE was also in the expected range for the complex. The product was used as a comparison in subsequent studies. Spectroscopic and electrochemical data collected for the monomeric complexes, including $[Ru(phen)_3](PF_6)_2$, is shown in Table 3.4.1. Photochemical trials were first researched using the dimeric complexes.

4.9 Photosubstitution Reactions of Dimeric Ruthenium(II) Polypyridine Complexes

Preliminary photochemical experiments were performed using $[(phen)_2Ru(diphen)Ru(phen)_2](PF_6)_4$. The first trials were carried out using $[(phen)_2Ru(diphen)Ru(phen)_2](PF_6)_4$ and tetrabutylammonium bromide in dichloromethane. The yellow solution was stirred while being irradiated with a 300 watt, 120 volt bulb "sunlamp" with no filtering. The solution was cooled by using a condenser hooked to a cold water circulator. UV-Vis spectroscopy was performed on the solution at intervals during the irradiation. The solution turned from yellow to a golden color during irradiation. The compiled UV-Vis spectra for $[(phen)_2Ru(diphen)Ru(phen)_2](PF_6)_4$ is shown in Figure 3.5.1.

It can be seen from Figure 3.5.1 that the peak at 448 nm decreases in intensity during irradiation. This peak correlates to the $(phen)_2Ru(diphen)Ru(phen)_2^{4+}$ concentration. After a period of UV irradiation a second peak appears around 550 nm, which indicates a product is

being formed due to a photochemical reaction. The decrease in the peak at 448 nm and appearance and increase over time of the peak at 550 nm is as expected for a photosubstitution reaction where a phen ligand on $(phen)_2Ru(diphen)Ru(phen)_2^{4+}$ is removed and replaced by bromines.

Additional trials were performed on $[(phen)_2Ru(diphen)Ru(phen)_2]Br_4$, which was produced from $[(phen)_2Ru(diphen)Ru(phen)_2](PF_6)_4$ using ion exchange resin. The procedure was the same as with $[(phen)_2Ru(diphen)Ru(phen)_2](PF_6)_4$, only tetrabutylammonium bromide was not added. The results were reproducible when compared to the photochemical reaction using $[(phen)_2Ru(diphen)Ru(phen)_2](PF_6)_4$, and the UV-vis specta for the reaction over time are shown in Figure 3.5.2.

In an attempt to identify the product of the photochemical reaction, the solvent was evaporated from the $[(bpy)_2Ru(diphen)Ru(bpy)_2]Br_4$ solution, and the solid was sent for ESI-MS analysis. ESI-MS analysis was inconclusive. It was thought that the bromine displaced some of the ligands during the photochemical reaction, so several attempts were made to replace the bromines with a ligand that would enable ESI-MS analysis.

One attempt began with evaporating the dichloromethane from the photochemical reaction product and heating the product with water. The progress of the reaction was monitored by UV-vis spectroscopy and is seen in Figure 3.5.3. Upon irradiating $[(phen)_2Ru(diphen)Ru(phen)_2]Br_4$ in dichloromethane, the 448 nm $[(phen)_2Ru(diphen)Ru(phen)_2]^{4+}$ peak decreased, and the product peak at 550 nm appeared and increased. After heating the product with water, the peak at 448 nm did not change, which indicated that the concentration of $[(phen)_2Ru(diphen)Ru(phen)_2]^{4+}$ also did not change. The

peak at 550 nm decreased as expected when the bromines on the reaction product were replaced by water.

Next, bpy was added and the solution was again heated. In Figure 3.5.3, it is seen that after heating with bpy, the peak at 448 nm increased. This indicated that the H_2O ligands were replaced by bpy ligands to form $(phen)_2Ru(diphen)Ru(phen)(bpy)^{4+}$. The sample was sent for ESI-MS analysis, but the results were inconclusive.

A 1000 watt Xe bulb was also used to irradiate a $[(phen)_2Ru(diphen)Ru(phen)_2]Br_4$ sample. Upon irradiation, the peak at 448 nm decreased. However, the peak at 550 nm was not seen. The baseline is raised over time in the 550 nm region, but a distinct peak is not seen. Figure 3.5.4 shows the results. The differing reactions between the 300 watt, 120 volt bulb "sunlamp" and the 1000 watt Xe bulb were more than likely caused by the increased power of the 1000 watt Xe bulb. Due to the inability to easily identify the photosubstitution reaction products for the dimeric complexes further studies were not conducted. The focus then turned to the investigation of the photoredox reactions for the dimeric complexes as compared to the analogous monomeric complexes.

4.10 Photoredox Reactions of Ruthenium(II) Polypyridine Complexes

The photoredox reactions of the dimeric complexes were studied through a series of quenching reactions. The analogous monomeric complexes synthesized in this work were used as comparisons. When possible, the results were compared to literature values. The dimeric complexes used in this study are weakly coupled and should behave similarly to the monomeric complexes.

Fe^{3+} was used as an oxidative quencher, and the excited lifetimes of $Ru(bpy)_3^{2+}$, $Ru(phen)(bpy)_2^{2+}$, and $(bpy)_2Ru(diphen)Ru(bpy)_2^{4+}$ were studied. Solutions were made in 0.5 M

H_2SO_4. The lifetime value in the absence of the quencher, τ_o, was first determined for each complex. The values were determined to be 590 nsec for $Ru(bpy)_3^{2+}$, 690 nsec for $Ru(phen)(bpy)_2^{2+}$, and 1000 nsec for $(bpy)_2Ru(diphen)Ru(bpy)_2^{4+}$. These values are tabulated in Table 3.6.1. Lifetimes for the complexes were then determined for quencher concentrations over a range of 0-5 nM Fe^{3+}. The relative excited state lifetimes, τ_o/τ, were plotted as a function of the quencher concentration, and the resulting linear Stern-Volmer plots can be seen in Figure 3.6.1. The relative standard deviation of the slope, RSD, was determined to be relatively low with values between 3 and 6%.

For each complex, the slope of the line was then divided by the lifetime to find k_q, since slope = $\tau_o k_q$. The k_q value for $Ru(bpy)_3^{2+}$ was 2.5 x 10^8 $M^{-1}s^{-1}$, which was comparable to the k_q values for $Ru(phen)(bpy)_2^{2+}$, 2.6 x 10^8 $M^{-1}s^{-1}$, and $(bpy)_2Ru(diphen)Ru(bpy)_2^{4+}$, 2.3 x 10^8 $M^{-1}s^{-1}$. Thus, the monomeric complexes and the dimeric complexes behave similarly. The k_q values are presented in Table 3.6.1. When possible, the experimental rate constants were compared to values reported in the literature, and the results were in agreement.

Excited state lifetimes in the absence of quencher were obtained and compared for the other complexes. Values collected using 0.5 M H_2SO_4 resulted in higher excited state lifetimes for the dimeric complexes than the monomeric complexes. This was not expected based on previous results for the bpy based complexes obtained by the group. Looking back at the previously obtained data, acetonitrile was used in the trials in which the monomer lifetime was longer than the dimer lifetime. Excited state lifetimes for $Ru(phen)_3^{2+}$ and $(phen)_2Ru(diphen)Ru(phen)_2^{4+}$ were then collected in acetonitrile. As expected, the lifetimes found were 1120 nsec and 960 nsec for $Ru(phen)_3^{2+}$ and $(phen)_2Ru(diphen)Ru(phen)_2^{4+}$, respectively. This difference in lifetimes between solvents indicates there is solvent

reorganization taking place. Excited state lifetime values for the complexes are shown in Table 3.4.1.

Flash photolysis was used to study the back reaction following the quenching reaction and the yields of the oxidized ruthenium complexes. Cu^{2+} and Fe^{3+} in 0.5 M H_2SO_4 were the chosen quenchers. The back reaction follows second order kinetics, and the k_{back} values were determined by fitting the data with the GNOME Gnumeric program. These values are assembled in Table 3.6.2 for the Fe^{3+} solutions and in Table 3.6.3 for the Cu^{2+} solutions. The yields for the oxidized ruthenium complexes are also included in the tables. When possible, values were compared to the literature and were found to be in agreement.

In both 10 mM and 50 mM Fe^{3+}, the k_{back} values are comparable for the same complex. The same is seen for 10 mM and 50 mM Cu^{2+} k_{back} values. For both quenchers, comparison of the k_{back} values between the dimer and the analogous monomer shows the values are similar. This is expected for monomeric and dimeric complexes that are acting similarly.

The cage escape yields are extremely low for both the 10 mM and 50 mM Cu^{2+} solutions. From this it was decided that the laser system could not provide enough flux to allow adequate quenching for the studies. The cage escape yields for Fe^{3+} are increased compared to those for Cu^{2+}, but the values are still lower than expected. Again, this is due to the laser not providing enough flux to excite most of the ruthenium centers.

To account for the inadequate flux, the efficiency, η, was determined for $Ru(phen)_3^{2+}$ and $(phen)_2Ru(diphen)Ru(phen)_2^{4+}$ with 50 mM Fe^{3+}. The efficiency takes into account the fact that only a fraction of the ruthenium centers are being excited by the laser (Kalyanasundaram, 1991). The calculated efficiencies were 93% for $Ru(phen)_3^{2+}$ and 95% for

$(phen)_2Ru(diphen)Ru(phen)_2^{4+}$. The comparable efficiency values for the monomeric and dimeric complexes indicate that both ruthenium centers are acting as independent units.

5.1 Conclusions

An improved synthetic method for dimeric ruthenium(II) polypyridine complexes was developed, and the photochemistry of the complexes was studied. When developing the new synthetic method, the range of reaction was investigated. The first aspect researched was the scope of ligands. Phen, dpphen, tmphen, bpy, and dmb were all successfully reacted with $(CO)_2Cl_2Ru(diphen)Ru(CO)_2Cl_2$ to produce symmetric dimers. Conversely, when bpz and bpm were reacted with $(CO)_2Cl_2Ru(diphen)Ru(CO)_2Cl_2$, the symmetric dimer was not produced. Even after increasing the amount of Me_3NO and trying a different solvent, the bpz and bpm ligands would not replace the last carbonyl group.

The second range of the reaction examined was the bridging ligand. Dpp was successfully reacted with $[Ru(CO)_2Cl_2]_n$ to produce $(CO)_2Cl_2Ru(dpp)Ru(CO)_2Cl_2$, from which $[(phen)_2Ru(dpp)Ru(phen)_2](PF_6)_4$ was synthesized. The third range of the reaction studied was the starting material. $Ru(DMSO)_4Cl_2$ failed to react with diphen to create $(DMSO)_2Cl_2Ru(diphen)Ru(DMSO)_2Cl_2$. The successful complexes with the form $L_2Ru(diphen)RuL_2$ were found to be free from monomeric complex contamination via ESI-MS, and these were chosen for use in photochemical studies.

The improved synthetic method for dimeric complexes was applied to monomeric complexes. Phen was successfully reacted with $[Ru(CO)_2Cl_2]_n$ to create $Ru(CO)_2Cl_2(phen)$. Dpphen, tmphen, bpy, and dmb were then reacted with $Ru(CO)_2Cl_2(phen)$ to create monomeric complexes of the form $Ru(phen)L_2$. The spectroscopic and electrochemical data for the dimers is comparable to the data for the analogous monomers. This implies that the dimeric complexes are weakly coupled and each ruthenium unit is acting independently.

The first photochemical investigation involved photosubstitution reactions. When $(phen)_2Ru(dpp)Ru(phen)_2^{4+}$ was irradiated with a 300 watt, 120 volt bulb "sunlamp", over time a decrease in the reactant peak was seen, as well as the appearance and increase of a product peak. The results were reproducible when using the same lamp. Several failed attempts were made to replace the bromines on the photosubstitution reaction product with ligands that would allow the complex to be detected via ESI-MS. Thus, the photosubstitution product was never successfully identified.

Additional photochemical investigations looked at the photoredox reactions of the dimeric complexes. The influence of the oxidative quencher Fe^{3+} on the lifetime of the dimers and monomers was investigated. The k_q values determined for $Ru(bpy)_3^{2+}$, $Ru(phen)(bpy)_2^{2+}$, and $(bpy)_2Ru(diphen)Ru(bpy)_2^{4+}$ were all comparable. This implies that the dimeric complex is weakly coupled.

The back reaction that takes place after the quenching reaction and the yield of the oxidized ruthenium complexes were studied. Fe^{3+} and Cu^{2+} were the chosen quenchers. The k_{back} values for both quenchers were as expected and comparable among the complexes. This is consistent with the dimeric complexes acting similarly to the monomers. The cage escape yields, however, were much lower than expected due to inadequate flux from the laser used to excite the samples. The efficiencies found for $Ru(phen)_3^{2+}$ and $(phen)_2Ru(diphen)Ru(phen)_2^{4+}$ were similar and support the assertion that both ruthenium centers are acting independently. Thus, it was found that both ruthenium centers in the dimeric complex can be excited and both centers can be oxidized.

6.1 References

1. Aguirre, Pedro, Renato Sariego, and Sergio A. Moya. 2001. Ruthenium (II) complexes in catalytic oxidation. *Journal of Coordination Chemistry* 54 (3-4): 401-13.

2. Ahmed, Hamis M. Younis. 2011. *Investigation of the Photochemical Properties of Ruthenium Polypyridyl Complexes using High Performance Liquid Chromatography*.

3. Akiyama, Minoru, Tomohiro Watanabe, and Masato Kakihana. 1986. Internal rotation of biphenyl in solution studied by IR and NMR spectra. *The Journal of Physical Chemistry* 90 (9): 1752-5.

4. Allsopp, Stephen R., Alan Cox, Terence J. Kemp, and W. John Reed. 1978. Inorganic photophysics in solution. part 1.—Temperature activation of decay processes in the luminescence of tris (2, 2′-bipyridine) ruthenium (II) and tris (1, 10-phenanthroline) ruthenium (II) ions. *Journal of the Chemical Society, Faraday Transactions 1: Physical Chemistry in Condensed Phases* 74 : 1275-89.

5. Amouyal, Edmond. 1995. Photochemical production of hydrogen and oxygen from water: A review and state of the art. *Solar Energy Materials and Solar Cells* 38 (1): 249-76.

6. Anderson, Peter A., Glen B. Deacon, Klaus H. Haarmann, F. Richard Keene, Thomas J. Meyer, David A. Reitsma, Brian W. Skelton, Geoffrey F. Strouse, and Nicholas C. Thomas. 1995. Designed synthesis of mononuclear tris (heteroleptic) ruthenium complexes containing bidentate polypyridyl ligands. *Inorganic Chemistry* 34 (24): 6145-57.

7. Anderson, Thomas J. 2007. *Synthesis of ruthenium and iridium complexes for use as photoinitiators in electron transfer reactions of metalloproteins*ProQuest.

8. Barigelletti, F., A. Juris, V. Balzani, P. Belser, and A. Von Zelewsky. 1987. Influence of the ligand structure on the electrochemical and spectroscopic properties of ruthenium (II)-polypyridine complexes. *Inorganic Chemistry* 26 (24): 4115-9.

9. Barthram, Anita M., Michael D. Ward, Alessandro Gessi, Nicola Armaroli, Lucia Flamigni, and Francesco Barigelletti. 1998. Spectroscopic, luminescence and electrochemical studies on a pair of isomeric complexes [(bipy) 2 ru (AB) PtCl 2][PF 6] 2 and [cl 2 pt (AB) ru (bipy) 2][PF 6] 2, where AB is the bis-bipyridyl bridging ligand 2, 2′: 3′, 2 ″: 6 ″, 2 [triple prime]-quaterpyridine. *New Journal of Chemistry* 22 (8): 913-7.

10. Bechtold, Rolf, Christa Kuehn, Chris Lepre, and Stephan S. Isied. 1986. Directional electron transfer in ruthenium-modified horse heart cytochrome c.

11. Benniston, Andrew C., Anthony Harriman, Peiyi Li, Pritesh V. Patel, James P. Rostron, and Craig A. Sams. 2006. An apparent angle dependence for the nonradiative deactivation of excited triplet states of sterically constrained, binuclear ruthenium (II) bis (2, 2': 6', 2''-terpyridine) complexes. *The Journal of Physical Chemistry A* 110 (32): 9880-6.

12. Benniston, Andrew C., Anthony Harriman, Peiyi Li, Craig A. Sams, and Michael D. Ward. 2004. Orientational control of electronic coupling in mixed-valence, binuclear ruthenium (II)-bis (2, 2': 6', 2"-terpyridine) complexes. *Journal of the American Chemical Society* 126 (42): 13630-1.

13. Cleare, MJ, and WP Griffith. 1969. Halogeno-carbonyl and-nitrosyl complexes of the platinum metals, and their vibrational spectra. *Journal of the Chemical Society A: Inorganic, Physical, Theoretical*: 372-80.

14. Colton, R., and RH Farthing. 1967. Carbonyl halides of the group VIII transition metals. I. dicarbonyldihalogenoruthenium (II) and related compounds. *Australian Journal of Chemistry* 20 (6): 1283-6.

15. Constable, Edwin C., Alexander MW Cargill Thompson, and Stefan Greulich. 1993. Novel synthesis of a doubly cyclometallated diruthenium complex with strongly coupled metal centres. *Journal of the Chemical Society, Chemical Communications*(18): 1444-6.

16. Creutz, Carol, and Norman Sutin. 1976. Electron-transfer reactions of excited states. reductive quenching of the tris (2, 2'-bipyridine) ruthenium (II) luminescence. *Inorganic Chemistry* 15 (2): 496-9.

17. Creutz, Carol, and H. Taube. 1973. Binuclear complexes of ruthenium ammines. *Journal of the American Chemical Society* 95 (4): 1086-94.

18. Creutz, C., and N. Sutin. 1975. Reaction of tris(bipyridine)ruthenium(III) with hydroxide and its application in a solar energy storage system. *Proceedings of the National Academy of Sciences of the United States of America* 72 (8) (Aug): 2858-62.

19. D'Alessandro, Deanna M., and F. Richard Keene. 2006. Current trends and future challenges in the experimental, theoretical and computational analysis of intervalence charge transfer (IVCT) transitions. *Chemical Society Reviews* 35 (5): 424-40.

20. D'Alessandro, Deanna M., Laurence S. Kelso, and F. Richard Keene. 2001. Stereochemical influences on intervalence charge transfer in homodinuclear complexes of ruthenium. *Inorganic Chemistry* 40 (26): 6841-4.

21. De Cola, Luisa, Peter Belser, Frank Ebmeyer, Francesco Barigelletti, Fritz Voegtle, Alex Von Zelewsky, and Vincenzo Balzani. 1990. Mononuclear, dinuclear, and trinuclear ruthenium (II) complexes of a tris (bipyridine) bridging ligand: Syntheses, absorption spectra, redox potentials, and photophysical properties. *Inorganic Chemistry* 29 (3): 495-9.

22. Durham, Bill, Jonathan V. Caspar, Jeffrey K. Nagle, and Thomas J. Meyer. 1982. Photochemistry of tris (2, 2'-bipyridine) ruthenium (2) ion. *Journal of the American Chemical Society* 104 (18): 4803-10.

23. Durham, Bill, and Francis Millett. 2012. Design of photoactive ruthenium complexes to study electron transfer and proton pumping in cytochrome oxidase. *Biochimica Et Biophysica Acta (BBA)-Bioenergetics* 1817 (4): 567-74.

24. Durham, Bill, Jerry L. Walsh, Charles L. Carter, and Thomas J. Meyer. 1980. Synthetic applications of photosubstitution reactions of poly (pyridyl) complexes of ruthenium (II). *Inorganic Chemistry* 19 (4): 860-5.

25. Emeléus, Harry Julius, and Alan G. Sharpe. 1968. *Advances in inorganic chemistry and radiochemistry*. Vol. 10 Academic Press.

26. Fan, Su-Hua, Ke-Zhi Wang, and Wei-Chun Yang. 2009. A Carbazole-Containing difunctional RuII complex that functions as a pH-Induced emission switch and an efficient sensitizer for solar cells. *European Journal of Inorganic Chemistry* 2009 (4): 508-18.

27. Fanni, Stefano, Cinzia Di Pietro, Scolastica Serroni, Sebastiano Campagna, and Johannes G. Vos. 2000. Ni (0) catalysed homo-coupling reactions: A novel route towards the synthesis of multinuclear ruthenium polypyridine complexes featuring made-to-order properties. *Inorganic Chemistry Communications* 3 (1): 42-4.

28. Felix, Franz, James Ferguson, Hans U. Guedel, and Andreas Ludi. 1980. The electronic spectrum of tris (2, 2'-bipyridine) ruthenium (2). *Journal of the American Chemical Society* 102 (12): 4096-102.

29. Grätzel, Michael. 2003. Dye-sensitized solar cells. *Journal of Photochemistry and Photobiology C: Photochemistry Reviews* 4 (2): 145-53.

30. Griffiths, Paul M., Frédérique Loiseau, Fausto Puntoriero, Scolastica Serroni, and Sebastiano Campagna. 2000. New luminescent and redox-active homometallic dinuclear iridium (iii), ruthenium (ii) and osmium (ii) complexes prepared by metal-catalyzed coupling reactionsElectronic supplementary information (ESI) available: Spectral data for 1–4, cyclic voltammogram for 3 and absorption and emission spectra for 1–3. see http://www. rsc. org/suppdata/cc/b0/b006456o. *Chemical Communications*(23): 2297-8.

31. Halpin, Yvonne, Laura Cleary, Lynda Cassidy, Sabine Horne, Danilo Dini, Wesley R. Browne, and Johannes G. Vos. 2009. Spectroelectrochemical properties of homo-and heteroleptic ruthenium and osmium binuclear complexes: Intercomponent communication as a function of energy differences between HOMO levels of bridge and metal centres. *Dalton Transactions*(21): 4146-53.

32. Havens, Jeffrey, Michela Castellani, Thomas Kleinschroth, Bernd Ludwig, Bill Durham, and Francis Millett. 2011. Photoinitiated electron transfer within the paracoccus denitrificans cytochrome bc 1 complex: Mobility of the Iron–Sulfur protein is modulated by the occupant of the qo site. *Biochemistry* 50 (48): 10462-72.

33. Horváth, Ottó, and Kenneth L. Stevenson. 1993. *Charge transfer photochemistry of coordination compounds* VCH New York etc.

34. Hoselton, MA, C-T_ Lin, HA Schwarz, and N. Sutin. 1978. Kinetics and mechanism of the quenching of the emission of substituted polypyridineruthenium (II) complexes. reactions of RuL3 ,* RuL32 , and RuL33 with the copper (I)-copper (II) couple. *Journal of the American Chemical Society* 100 (8): 2383-8.

35. Hu, Yi-Zhen, Qin Xiang, and Randolph P. Thummel. 2002. Bi-1, 10-phenanthrolines and their mononuclear ru (II) complexes. *Inorganic Chemistry* 41 (13): 3423-8.

36. Iyoda, Masahiko, Hiroki Otsuka, Koichi Sato, Nobue Nisato, and Masaji Oda. 1990. Homocoupling of aryl halides using nickel (II) complex and zinc in the presence of et 4 NI. an efficient method for the synthesis of biaryls and bipyridines. *Bulletin of the Chemical Society of Japan* 63 (1): 80-7.

37. Kalyanasundaram, K. 1991. *Photochemistry of polypyridine and porphyrin complexes* Academic Press.

38. Krause, Ronald A., and Kirsten Krause. 1980. Chemistry of bipyridyl-like ligands. isomeric complexes of ruthenium (II) with 2-(phenylazo) pyridine. *Inorganic Chemistry* 19 (9): 2600-3.

39. Kreitner, Christoph, Markus Grabolle, Ute Resch-Genger, and Katja Heinze. 2014. Dual emission and excited-state mixed-valence in a quasi-symmetric dinuclear Ru–Ru complex. *Inorganic Chemistry* 53 (24): 12947-61.

40. Lafferty, John J., and Francis H. Case. 1967. The preparation and properties of certain pyridylpyrimidines and bidiazines as potential chelating agents for iron (II). *The Journal of Organic Chemistry* 32 (5): 1591-6.

41. Lin, CT, W. Böttcher, M. Chou, C. Creutz, and N. Sutin. 1976. Mechanism of the quenching of the emission of substituted polypyridineruthenium (II) complexes by iron (III), chromium (III), and europium (III) ions. *Journal of the American Chemical Society* 98 (21): 6536-44.

42. Maity, Soumitra, Mingzhao Zhu, Ryan Spencer Shinabery, and Nan Zheng. 2012. Intermolecular [3 2] cycloaddition of cyclopropylamines with olefins by Visible-Light photocatalysis. *Angewandte Chemie International Edition* 51 (1): 222-6.

43. Meade, Thomas J., Harry B. Gray, and Jay R. Winkler. 1989. Driving-force effects on the rate of long-range electron transfer in ruthenium-modified cytochrome c. *Journal of the American Chemical Society* 111 (12): 4353-6.

44. Miessler, GL, and DA Tarr. 2004. Inorganic chemistry pearson prentice hall. *Upper Saddle Rive, NJ*.

45. Millett, Francis, and Bill Durham. 2002. Design of photoactive ruthenium complexes to study interprotein electron transfer. *Biochemistry* 41 (38): 11315-24.

46. Nazeeruddin, Md K., A. Kay, I. Rodicio, R. Humphry-Baker, E. Müller, P_ Liska, N. Vlachopoulos, and M. Grätzel. 1993. Conversion of light to electricity by cis-X2bis (2, 2'-bipyridyl-4, 4'-dicarboxylate) ruthenium (II) charge-transfer sensitizers (X= cl-, br-, I-, CN-, and SCN-) on nanocrystalline titanium dioxide electrodes. *Journal of the American Chemical Society* 115 (14): 6382-90.

47. Nelsen, Stephen F. 2000. "Almost delocalized" intervalence compounds. *Chemistry-A European Journal* 6 (4): 581-8.

48. Ngebichie Njabon, Roland. 2013. *An investigation of the electronic coupling in some dimeric ruthenium (II) polypyridine complexes* University of Arkansas.

49. O'Donnell, Ryan M., Patrik G. Johansson, Maria Abrahamsson, and Gerald J. Meyer. 2013. Excited-state relaxation of ruthenium polypyridyl compounds relevant to dye-sensitized solar cells. *Inorganic Chemistry*.

50. Paris, JP, and Warren W. Brandt. 1959. Charge transfer luminescence of a ruthenium (II) chelate. *Journal of the American Chemical Society* 81 (18): 5001-2.

51. Petrov, Vladimir, Joseph T. Hupp, Carolyn Mottley, and Loren C. Mann. 1994. Resonance raman studies in the extended near infrared region: Experimental verification of a three-site mixing mechanism for valence delocalization in the creutz-taube ion. *Journal of the American Chemical Society* 116 (5): 2171-2.

52. Press, William H., Saul A. Teukolsky, William T. Vetterling, and Brian P. Flannery. 1992. Numerical recipes in C: The art of scientific computing. *Cambridge University Press, Cambridge, MA,* 131 : 243-62.

53. Prier, Christopher K., Danica A. Rankic, and David WC MacMillan. 2013. Visible light photoredox catalysis with transition metal complexes: Applications in organic synthesis. *Chemical Reviews* 113 (7): 5322-63.

54. Rillema, D. Paul, G. Allen, TJ Meyer, and D. Conrad. 1983. Redox properties of ruthenium (II) tris chelate complexes containing the ligands 2, 2'-bipyrazine, 2, 2'-bipyridine, and 2, 2'-bipyrimidine. *Inorganic Chemistry* 22 (11): 1617-22.

55. Roundhill, D. Max. 1994. *Photochemistry and photophysics of metal complexes* Plenum Press New York.

56. Sadoski, Robert C., Gregory Engstrom, Hua Tian, Li Zhang, Chang-An Yu, Linda Yu, Bill Durham, and Francis Millett. 2000. Use of a photoactivated ruthenium dimer complex to measure electron transfer between the rieske iron-sulfur protein and cytochrome c 1 in the cytochrome bc 1 complex. *Biochemistry* 39 (15): 4231-6.

57. Schwarz, Oliver, Dietmar van Loyen, Steffen Jockusch, Nicholas J. Turro, and Heinz Dürr. 2000. Preparation and application of new ruthenium (II) polypyridyl complexes as sensitizers for nanocrystalline TiO 2. *Journal of Photochemistry and Photobiology A: Chemistry* 132 (1): 91-8.

58. Scott, Jill R., Anne Willie, Mark McLean, Patrick S. Stayton, Stephen G. Sligar, Bill Durham, and Francis Millett. 1993. Intramolecular electron transfer in cytochrome b5 labeled with ruthenium (II) polypyridine complexes: Rate measurements in the marcus inverted region. *Journal of the American Chemical Society* 115 (15): 6820-4.

59. Seneviratne, Dhehinie S., Md Jamal Uddin, V. Swayambunathan, H. Bernhard Schlegel, and John F. Endicott. 2002. Characteristics and properties of metal-to-ligand charge-transfer excited states in 2, 3-bis (2-pyridyl) pyrazine and 2, 2'-bypyridine ruthenium complexes. perturbation-theory-based correlations of optical absorption and emission parameters with electrochemistry and thermal kinetics and related ab initio calculations. *Inorganic Chemistry* 41 (6): 1502-17.

60. Spiccia, Leone, Glen B. Deacon, and Christopher M. Kepert. 2004. Synthetic routes to homoleptic and heteroleptic ruthenium (II) complexes incorporating bidentate imine ligands. *Coordination Chemistry Reviews* 248 (13): 1329-41.

61. Thomas, Nicholas C., Glen B. Deacon, Antonio Llobet, and Thomas J. Meyer. Tris (bidentate) ruthenium (II) bis [hexafluorophosphate] complexes. *Inorganic Syntheses*: 107-10.

62. Toyota, Shinji, Akito Goto, Keiko Kaneko, and Takumi Umetani. 2005. Syntheses, spectroscopic properties, and CU (I) complexes of all possible symmetric BI-1, 10-phenanthrolines. *Heterocycles* 65 (3): 551-62.

63. Treadway, Joseph A., Barbara Loeb, Rosa Lopez, Peter A. Anderson, F. Richard Keene, and Thomas J. Meyer. 1996. Effect of delocalization and rigidity in the acceptor ligand on MLCT excited-state decay. *Inorganic Chemistry* 35 (8): 2242-6.

64. Treadway, Joseph A., and Thomas J. Meyer. 1999. Preparation of coordinatively asymmetrical ruthenium (II) polypyridine complexes. *Inorganic Chemistry* 38 (10): 2267-78.

65. Van Houten, J., and RJ Watts. 1978. Photochemistry of tris (2, 2'-bipyridyl) ruthenium (II) in aqueous solutions. *Inorganic Chemistry* 17 (12): 3381-5.

66. Van Houten, J., and RJ Watts. 1976. Temperature dependence of the photophysical and photochemical properties of the tris (2, 2'-bipyridyl) ruthenium (II) ion in aqueous solution. *Journal of the American Chemical Society* 98 (16): 4853-8.

67. Wang, Youxiang, Willie J. Perez, Greg Y. Zheng, D. Paul Rillema, and Connie L. Huber. 1998. Preparation, purification, and characterization of binuclear ruthenium (II) complexes: Bridging ligands based on diazafluorenes. *Inorganic Chemistry* 37 (9): 2227-34.

68. Wenger, Oliver S. 2009. Long-range electron transfer in artificial systems with d^6 and d^8 metal photosensitizers. *Coordination Chemistry Reviews* 253 (9): 1439-57.

69. Zaslavsky, Dmitry, and Robert B. Gennis. 2000. Proton pumping by cytochrome oxidase: Progress, problems and postulates. *Biochimica Et Biophysica Acta (BBA)-Bioenergetics* 1458 (1): 164-79.

70. Zaslavsky, Dmitry, Robert C. Sadoski, Kefei Wang, Bill Durham, Robert B. Gennis, and Francis Millett. 1998. Single electron reduction of cytochrome c oxidase compound F: Resolution of partial steps by transient spectroscopy. *Biochemistry* 37 (42): 14910-6.